Theoretical Issues in Quantum Computation: Spin Bus, Exchange Only Qubit and Separability Probability

by

Jianjia Fei

A dissertation submitted in partial fulfillment of
the requirements for the degree of

Doctor of Philosophy
(Physics)

at the
University of Wisconsin – Madison
2014

Defended on September 8 2014
Dissertation approved by the following members of the Final Oral Committee:

Mark G. Friesen · Senior Scientist of Physics
Robert J. Joynt · Professor of Physics
Susan N. Coppersmith · Professor of Physics
Robert F. McDermott · Associate Professor of Physics
Mark A. Eriksson · Professor of Physics
Materials Science and Engineering

Abstract

This thesis explores several different aspects in theoretical quantum computing, including problems in application, implementation and fundamental theories.

First, we investigate the spin bus problem. We primarily focus on the non-local multi-qubit entanglement state generation and unitary gate construction using the new type of gates we proposed, the mediated gates. We build a complete set of toolbox to solve and optimize this problem using all the different mediated gates spin bus could offer. Specifically, we compare the quantum circuit efficiency with the conventional serial gate implementation method using a nearest-neighbor SWAP gate and demonstrate that in most cases, using mediate gates through a spin bus will provide a significant improvement in terms of circuit depth. As a consequence, it provides a viable and robust solution to the challenges we face when considering scalability in quantum circuits.

We then turn our attention to a specific implementation of encoded logical qubit, the exchange-only qubit in a semiconductor triple quantum dot. It has plenty of advantages compare to other encoded qubit, such as fast gate operations via pure electrical control, and robustness against global magnetic noise when encoding happens in decoherence free subspace, etc. We show that there are more things we could do to further improve the quality of gate operations on such encoded logical qubits. The general idea is similar as in the context of singlet-triplet qubits and hybrid qubits. One thing is to take full advantage of the true "sweet spot" of its energy level diagram as the optimal working point, which provides protection against charge noise. The other is that we could optimize the tunnable parameters in the pulse sequence by taking into account the knowledge we have about the device, such as the strength of nuclear field bath (for GaAs triple quantum dot) and the dephasing rate. Our result shows the upper bounds you could anticipate for specific gate operations using DC pulse sequences.

Finally, we discuss a more theoretically fundamental problem in quantum computation, the property of two partite entanglement space. We calculate the separability probability in the high dimensional space of two rebits, two qubits, and two quaterbits using Monte

Carlo Sampling methods. Our results match the analytical conjecture almost perfectly for such three systems. Our method of probing such problems provides a simple but efficient way to explore the geometrical structure of high dimensional two partite system, such as the distribution of physical, separable and entanglement states. And the connection between our numerical simulations and the analytical conjecture proposed earlier might imply something more fundamental yet to be uncovered.

Acknowledgements

My journey in graduate school is a long and fruitful one. This thesis would not have been possible without the countless help I received in this process. I am deeply grateful and honored to have such a chance to live and work around so many amazing people.

Firstly, I would like to thank my advisors, Dr. Mark Friesen and Prof. Robert Joynt for their support and guildance over the years. From them, I learned how to conduct scientific research. I learned to always keep a big picture in mind, meanwhile pay attention to details. These will be invaluable assets to me for my entire life. Especially, I would like to express my gratitude for their tremendous amount of patience. They are probably the nicest people and advisors any PhD student could ever ask for, for which I feel so blessed.

Sincerely, I would like to thank Prof. Xuedong Hu of University at Buffalo, The State University of New York. It's a nice and pleasant collaboration with the Buffalo team, and it's definitely a fruitful one. From Xuedong, I know I could always expect opinions and suggestions of an expert. Discussion with him is always inspirational and rewarding.

I would also like to express my appreciation to Prof. Mark Eriksson and Prof. Susan Coppersmith for all the advice and guidance, particularly for their suggestions on how to give great presentations.

I consider myself an extremely lucky person to be surrounded by so many caring, loving and talented friends during my years in Madison. Tech Seng Koh, Dong Zhou, Yun-Pil Shim, HyungJun Lim, Kenneth Rudinger, John Gamble, they were my constant source of help. I learned so much from each of them, and I appreciate it deeply. I also thank Zhan Shi and Xian Wu for their input from an experimental point of view.

Special thanks to all my committee members, Dr. Mark Friesen, Prof. Robert Joynt, Prof. Susan Coppersmith, Prof. Robert McDermott, and Prof. Mark Eriksson, for their time and effort on my thesis and my defense.

Finally, I would like to thank my family for their unconditional love and support over the years. To my parents, Baolai Fei and Jiling Tian, thank you for raising me up and encouraging me through the hard times. To my wife, Chuanzi OuYang, thank you for

being with me all these years, up and down. Your support and love will always be my motivation to be brave and to be better.

I dedicate this thesis to my parents

for their unconditional love.

Contents

List of Figures

List of Tables

Chapter 1

Introduction

The last twenty years have witnessed the rapid advancement of computation powers, based upon the traditional electrical and computer engineering. Along with that, is the fast development of microprocessing techniques towards the nanometer scales, which set the bigger stage for quantum mechanics to reach its potential.

Utilizing the power of quantum mechanics to store, process and transfer information has long been an intriguing and promising idea [1]. A quantum computer, if realized, is expected to speed up certain types of computations exponentially [2]. A huge amount of effort has been devoted into relevant research of a quantum computer on multiple different levels. On the hardware side, several different implementations have made spectacular progress towards the goal of building a working quantum computer [3], such as in photons [4, 5], trapped atoms [6], superconductors [7] and quantum dots [8, 9]. On the software side, multiple quantum algorithms have been proposed that could offer significant speed up to solve some of the most difficult problems when compared to their classical counterparts, such as Shor's factorization algorithm [2], Grover's searching algorithm [10] and algorithms on graph isomorphism problems [11, 12].

With the maturity of modern technology, the ability to control and manipulate multiple qubits simultaneously is already within reach, which poses challenges along with the excitement. Large-scale quantum computing is challenging in any qubit implementation.

So, scalability issue is definitely a key factor that needs to be thoroughly considered for any implementations to be practically meaningful.

The recent growing and development on experimental quantum computing also provides us an unforeseen testbed to study fundamental theories in quantum mechanics. Quantum mechanics, over the course of more than a hundred years history, still has plenty open questions need to be answered. One such example is quantum entanglement [13]. It's one of the most peculiar phenomenon in quantum mechanics that lacks a classical counterpart, which we still don't fully understand.

In this thesis, we present our attempt and effort to attack several interesting problems of the type described above.

1.1 Thesis outline

This thesis is an attempt to give a comprehensive overview of all the work I've been involved during my graduate school. It is organized as follows.

First, in chapter 2, we show the application of spin bus in non-proximal quantum entanglement state generation and unitary gate construction on multiple qubits. We particularly emphasize the aspect of efficiency comparison between the spin bus based protocols versus the conventional swap gate based serial protocols. In order to address such problem, we develop a complete numerical solver to try to find the optimal solution. We utilize a mix of different optimization methods, including both global (genetic algorithm, clustering algorithm) and local (Nelder-Mead downhill simplex search) optimization methods. We provide example solution for such problems in the generation of some of the most important resources for quantum computation, such as entanglement state as Bell state, W state, GHZ state, and also gates as CNOT and Toffoli. We demonstrate that in most cases, "mediated gates" protocol through a spin bus is indeed superior than conventional swap gate based methods, and more so when we scale up the computation. We list the comparison as benchmarks.

Second, in chapter 3, we zoom in onto the microscopic level. We study one particular

implementation of encoded logical qubit, the exchange-only qubit in a triple quantum dot. We simulate the dynamic evolution process for such logical qubit under DC pulsed gate, in a full set of relevant basis states. There are multiple sources of errors that are associated with such evolution, including both leakage and dephasing. We use the master equation method the primary tool to model such a process, specifically for Z and X logical qubit rotations. Knowledges and parameter settings of the device are taken into full account during the simulation. We show that by operating the qubit at its "sweet spot" in the energy level diagram and optimizing the pulse parameters, we could achieve reasonably high fidelities for logical qubit rotations.

The last topic we delve into details is presented in chapter 4. We study the more fundamental problem about quantum computation, the entanglement and its geometrical properties for general two partite systems. There's this very intriguing analytical conjecture proposed to predict the separability probability in two partite systems, which we showed previously that it works very well for qubit systems. Now we expand our work into rebit and quaterbit systems, and test the conjecture again using Monte Carlo Simulations. Our result still strongly supports the correctness of the conjecture.

Finally, in chapter 5 we provide a brief conclusion for the whole thesis.

We put most of our calculation details into the supplemental materials, which are presented in the corresponding order.

1.2 Publications List

Each of the three main chapters in this thesis is based on either published work or work to be submitted. Here, I list all the relevant publications for the results presented.

Chapter 2 is based on Ref. [14], titled *Mediated gates between spin qubits*, which I completed with Dr. Dong Zhou, Dr. Yun-Pil Shim, Dr. Sangchul Oh, Prof. Xuedong Hu and Dr. Mark Friesen. Other closely related work that I've contributed to are Ref. [15, 16, 17, 18, 19].

Chapter 3 is based on our work to be submitted, titled *Characterizing gate operations*

near the sweet spot of an exchange-only qubit, which I completed with Jo-Tzu Hung, Dr. Teck Seng Koh, Dr. Yun-Pil Shim, Prof. Susan Coppersmith, Prof. Xuedong Hu, and Dr. Mark Friesen. Other closely related work that I've contributed to is Ref. [20].

Chapter 4 is based on our work to be submitted, titled *Numerical Computations of Separability Probabilities*, which I completed with Prof. Robert Joynt. Other closely related work that I've contributed to is Ref. [21].

Chapter 2

Spin Bus

2.1 Introduction

Quantum dot spin qubits are promising candidates for quantum computing because of their long decoherence times and their potential to leverage existing semiconductor technologies [22, 23]. The exchange coupling is a desirable tool for mediating interactions between spin qubits, because it can be controlled electrostatically and it is typically very fast [9]. In combination with arbitrary single-qubit operations, the exchange coupling enables universal quantum computation [8]. When logical qubits consist of two [24] or three [25] physical qubits in a decoherence-free subsystem, the exchange coupling alone is universal for quantum computation. On the other hand, the intrinsic short-range nature of the exchange coupling (typically tens of nanometers) imposes strong constraints on the physical architecture of the spin qubits. These constraints present a significant challenge to scalability during quantum error correction, particularly for linear qubit architectures, which are typical for quantum dot spin qubits [26]. Indeed, large-scale quantum computing is challenging in any qubit implementation, and the complexity of a given quantum circuit could, to a large extent, determine its success.

In a number of qubit systems, such as nuclear magnetic resonance (NMR), the physical interactions may be constant or "always on." This is not necessarily a disadvantage. For

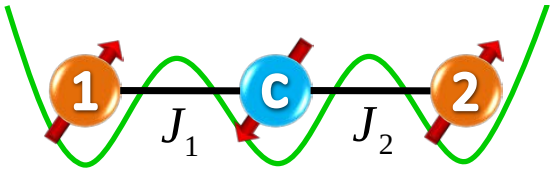

Figure 2.1: A linear triple-quantum-dot geometry with three electrons. Mediated gates can be achieved between qubit 1 and qubit 2 by applying simultaneous exchange couplings, with $J_1 = J_2$. At the end of the operation, the ancilla qubit c is restored to its initial state.

example, it has been shown that simultaneous, multiqubit couplings can be used to enable quantum state transfer [27, 15], and other rudimentary quantum gates [28]. Similar considerations apply to quantum dot spin systems with Heisenberg couplings [29]. Quantum dots provide unique opportunities for controlling the nature of the interactions. For example, simultaneous, multiqubit couplings could provide a potential route for enhancing the effective range of the coupling, in analogy with the Ruderman-Kittel-Kasuya-Yosida (RKKY) interaction [30, 31, 32]. When these couplings are arranged into nontrivial topologies, such as rings, a rich spectrum of quantum gates emerges [33, 34, 35]. However, even simple topologies, like those considered here, can produce entangling gates that differ from the existing two-qubit gates in spin qubits [36, 37, 38].

In this paper, we show how to control such simultaneous, multiqubit couplings. The result is a class of "mediated" quantum gates. We focus primarily on the three-qubit geometry shown in Fig. 2.1, due to recent experimental progress on triple quantum dots [39, 40, 41]. In this arrangement, the mediated gate acts on the nonproximal qubits 1 and 2, leaving the ancilla or central qubit c unaffected, at the end of the operation. We characterize this well-defined gate operation, $\mathbb{U}_2$, and show how arbitrary two-qubit states and gates can be generated using $\mathbb{U}_2$ as the sole entangling resource. We also compare the circuit depth of these mediated gate protocols to more conventional SWAP-based protocols. Finally, we explain how long-range mediated gates can be attained by replacing qubit c with a spin bus.

2.2 Two-Qubit Mediated Gate, $\mathbb{U}_2$

Mediated gate, $\mathbb{U}_2$

We begin by characterizing the mediated gate $\mathbb{U}_2$. The effective spin Hamiltonian for the quantum dot geometry in Fig. 2.1 derives from the exchange interaction and takes the form of nearest-neighbor Heisenberg couplings [8], given by

$$H = J_1 \mathbf{s}_1 \cdot \mathbf{s}_c + J_2 \mathbf{s}_2 \cdot \mathbf{s}_c, \tag{2.1}$$

where $\mathbf{s}_j$ are spin operators. In typical experiments, the coupling constants J_1 and J_2 are controlled by detuning the local electrostatic potentials in a given dot [9]. J_1 and J_2 can usually be varied independently as a function of time [39, 40]. For mediated gates, however, we assume that both couplings are turned on and off simultaneously.

The Hamiltonian H induces three-spin dynamics according to the time evolution operator $U(t) = e^{-iHt}$, where we set $\hbar = 1$. However, the mediated gate we seek has the special form $U = \mathbb{U}_2 \otimes I$, where $\mathbb{U}_2$ acts on qubits 1 and 2, and the identity operator I acts on the ancilla qubit c. In Appendix A, we prove that only one nontrivial mediated gate exists for the geometry in Fig. 2.1, corresponding to the unique parameter combination $J_1 = J_2 = J$ and the special evolution period $T_g = 4\pi/3J$ (with periodic recurrences [42]). The gate is robust against control errors, similarly to conventional two-qubit exchange gates. For example, if $J_2 = J_1(1+\delta)$ results in the gate $U(\delta)$, where $U(0)$ is the desired gate, and if the fidelity is defined as [43] $F = |\mathrm{Tr}[U(\delta)^\dagger U(0)]|/\mathrm{Tr}[U(0)^\dagger U(0)]$, then we obtain a quadratic error in the fidelity: $1 - F \simeq 0.97\delta^2$ when $\delta \leq 0.4$.

Any unitary two-qubit operator $U_2 \in \mathrm{SU}(4)$, including $\mathbb{U}_2$, can be expressed in the form of a Cartan decomposition, given by [44, 45]

$$U_2 \overset{\text{l.u.}}{=} e^{\frac{i}{2}(c_1 \sigma_x \otimes \sigma_x + c_2 \sigma_y \otimes \sigma_y + c_3 \sigma_z \otimes \sigma_z)}, \tag{2.2}$$

where $\sigma_x, \sigma_y, \sigma_z$ are the Pauli matrices, and $\mathbf{s} = \sigma/2$ in spinor notation. Here, the relation $\overset{\text{l.u.}}{=}$ means "equal, up to local unitary gates," where the latter may be applied before and/or after the nonlocal operator. The decomposition is unique when the parameters (c_1, c_2, c_3)

are restricted to the tetrahedron $\pi - c_2 \geq c_1 \geq c_2 \geq c_3 \geq 0$, known as the Weyl chamber. (Note that special considerations apply to the base of the tetrahedron [45].) There is a one-to-one mapping between the Weyl chamber and the Makhlin invariants [46], which provides an alternative representation of the nonlocal properties of $U_2 \in \mathrm{SU}(4)$ (except on the bottom surface of the chamber). The Cartan decomposition for our two-qubit mediated gate is given by $(c_1, c_2, c_3) = (2, 1, 1)(\pi/3)$ and it has the explicit form (see Appendix A for details)

$$\mathbb{U}_2 = -\begin{pmatrix} \frac{1}{2}(1+i\sqrt{3}) & 0 & 0 & 0 \\ 0 & \frac{1}{4}(-1+i\sqrt{3}) & \frac{1}{4}(3+i\sqrt{3}) & 0 \\ 0 & \frac{1}{4}(3+i\sqrt{3}) & \frac{1}{4}(-1+i\sqrt{3}) & 0 \\ 0 & 0 & 0 & \frac{1}{2}(1+i\sqrt{3}) \end{pmatrix}. \tag{2.3}$$

The position of $\mathbb{U}_2$ in the Weyl chamber is shown in Fig. 2.2, along with several other common two-qubit gates.

The gating capabilities of $U_2 \in \mathrm{SU}(4)$ derive from its entangling properties, which can be characterized in part by its position in the Weyl chamber. The operators known as "perfect entanglers" lie inside a polyhedron, which fills half of the chamber [45], as shown in Fig. 2.2. Combined with local unitaries, a perfect entangler can generate a maximally entangled state from a separable state. For example, if we quantify two-qubit entanglement in terms of the "concurrence" measure C [47, 48], then a separable state exhibits no entanglement, with $C = 0$, while a highly nonlocal state like the singlet Bell state $|\Psi^-\rangle = \frac{1}{\sqrt{2}}(|01\rangle - |10\rangle)$ exhibits maximal entanglement, with $C = 1$. Thus, for some initial two-qubit state with $C = 0$, one application of a perfect entangler produces a state with $C = 1$. The standard CNOT gate is known to be a perfect entangler [45], as indicated in Fig. 2.2. However, CNOT does not arise naturally from the exchange interaction between spin qubits; it must be constructed from more basic gates [8]. In contrast, the mediated gate $\mathbb{U}_2$ does arise naturally in many-body spin systems as we have shown; however, its location in the Weyl chamber indicates that it is not a perfect entangler. Using the methods of [44], we find that $\mathbb{U}_2$ achieves a maximum concurrence of $C_{\max} = \sqrt{3}/2 < 1$, when acting on a separable state.

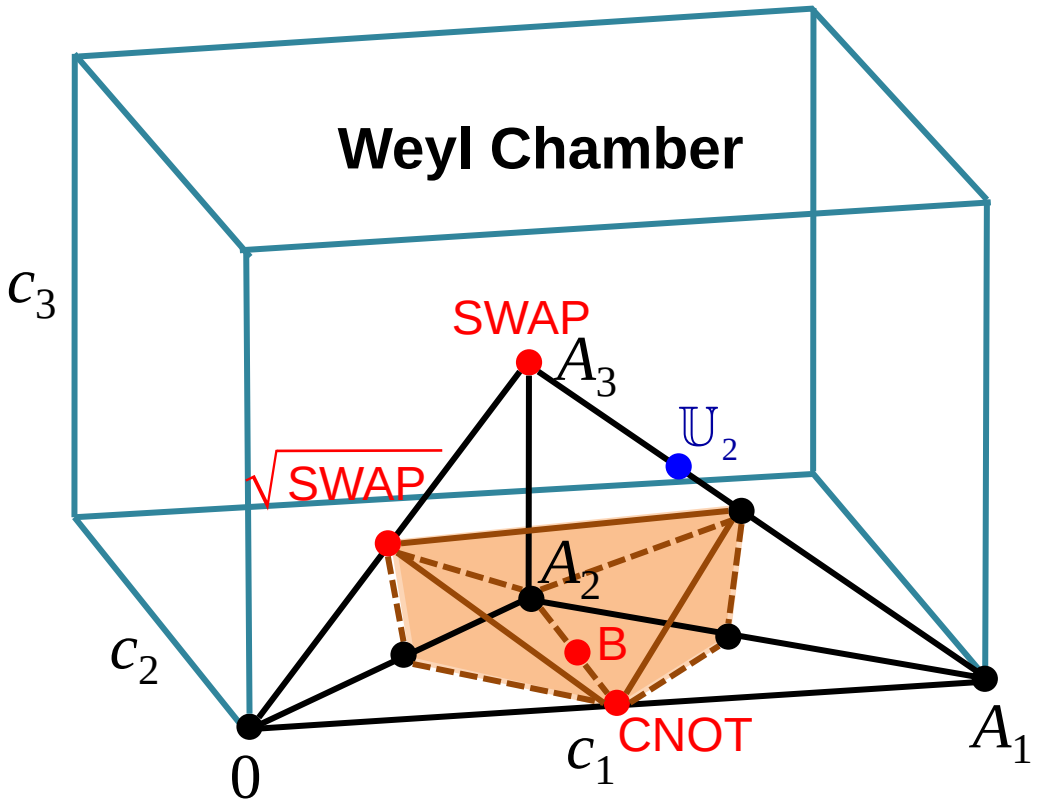

Figure 2.2: A geometric representation of two-qubit SU(4) gate operations. Axes c_1, c_2, and c_3 are defined in Eq. (2.2). The Weyl chamber corresponds to the tetrahedron 0-A_1-A_2-A_3, while the gates known as perfect entanglers lie inside the shaded region [45]. The coordinates for other special gates are given by B $= (\frac{\pi}{2}, \frac{\pi}{4}, 0)$, CNOT $= (\frac{\pi}{2}, 0, 0)$, SWAP $= (\frac{\pi}{2}, \frac{\pi}{2}, \frac{\pi}{2})$, and $\sqrt{\text{SWAP}} = (\frac{\pi}{4}, \frac{\pi}{4}, \frac{\pi}{4})$.

A universal quantum processor must be able to generate arbitrary entangled states or implement arbitrary quantum circuits. For example, CNOT gates combined with single-qubit unitaries are known to be universal [49, 50, 51]. Any two-qubit entangling gate U_2 can replace CNOT in this scheme [52], although the entangling capabilities of the gate will affect the overall circuit depth. In the remainder of this section, we explore methods for generating arbitrary entangled states and entangling gates using the mediated gate $\mathbb{U}_2$, and we determine the circuit depth of such protocols.

Generation of arbitrary states

Our goal here is to construct arbitrary, two-qubit, entangled pure states between qubit 1 and qubit 2 in the geometry shown in Fig. 2.1, using the mediated gate $\mathbb{U}_2$ as our nonlocal entangling resource. Allowing for local operations and classical communication (LOCC), it is possible to transform maximally entangled states, such as Bell states, into arbitrary pure states [53]. We therefore focus on using $\mathbb{U}_2$ to generate Bell states. For simplicity, we ignore global phase factors throughout this paper.

The strategy we adopt is to apply $\mathbb{U}_2$ repeatedly, assisted by single-qubit unitary rotations U_1, as needed:

$$|\psi\rangle = (U_1 \otimes U_1)[\mathbb{U}_2(U_1 \otimes U_1)]^n|00\rangle. \tag{2.4}$$

Note that each application of U_1 here represents an arbitrary rotation, and that, in general, the rotations can all be different.

We would like to be able to compare the speed or efficiency of disparate gating protocols, particularly between mediated and conventional gates. The most convenient measure of this efficiency is the "circuit depth," which we define here as the total number of exchange gates. For example, in Eq. (2.4), the circuit depth is equal to n. For conventional quantum dot circuits, there may be cases where it is possible to implement gates between different pairs of qubits simultaneously, due to physical separation. We define the circuit depth of such parallel gates to be 1, since they occur simultaneously. On the other hand, conventional circuits typically require intermediate SWAP gates to be applied sequentially when the qubits are nonproximal, causing the circuit depth to increase by 1 with each SWAP application. This notion of circuit depth plays an important role in the gate times and fidelities of quantum circuits, and we speak of circuit depth throughout the following discussion. To conclude, we note that since $\mathbb{U}_2$ is not a perfect entangler, the value of n in Eq. (2.4) must be greater than 1 when we generate a Bell state.

We have solved Eq. (2.4) numerically, obtaining several two-qubit states of interest. Our procedure involves maximizing the state fidelity, $f = |\langle\psi_{\text{des}}|\psi_{\text{actual}}\rangle|^2$, where $|\psi_{\text{actual}}\rangle$ is the outcome of Eq. (2.4), and $|\psi_{\text{des}}\rangle$ is the desired outcome. The two-qubit mediated gate used

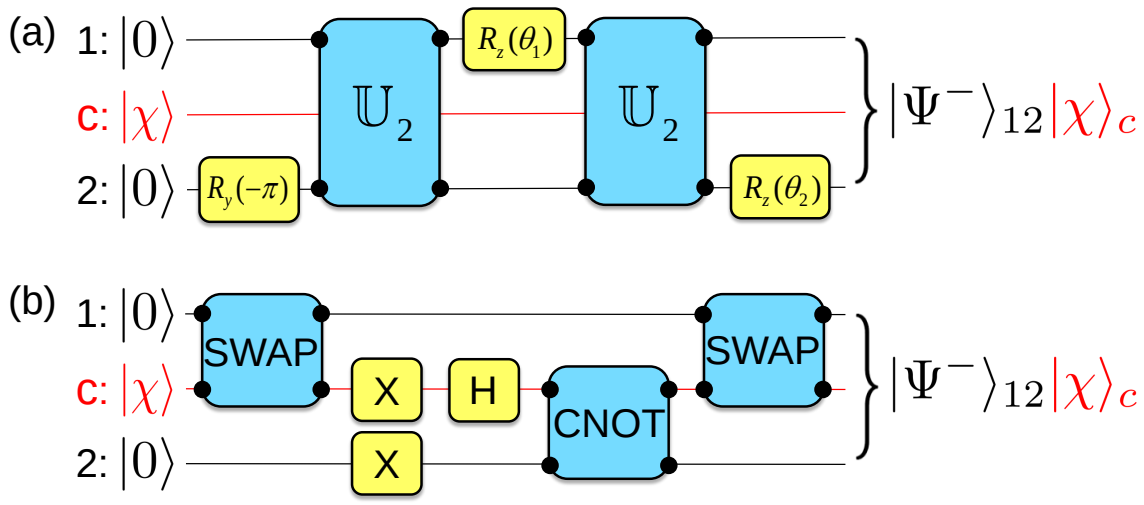

Figure 2.3: Quantum circuit for Bell state generation. (a) A quantum circuit for generating the singlet Bell state $|\Psi^-\rangle = \frac{1}{\sqrt{2}}(|01\rangle - |10\rangle)$ (up to a global phase), using the mediated gate $\mathbb{U}_2$, given in Eq. (2.3). Here, the single qubit rotations are defined as $R_\alpha(\theta) = e^{-\frac{i}{2}\theta\sigma_\alpha}$, where $\alpha = x, y, z$. The rotation angles are given by $\theta_1 = -\arccos(\frac{1}{3})$, $\theta_2 = -\frac{1}{6}\pi - \arctan\frac{4\sqrt{2}-3\sqrt{3}}{5}$. (b) An efficient Bell-state protocol between nonproximal qubits, based on nearest-neighbor, pairwise gates. Here, H is the Hadamard gate and X is the Pauli gate σ_x, corresponding to a π rotation about the x axis of the Bloch sphere (up to a global phase). In this figure, and several other subsequent figures, we note that the central ancilla spin c mediates the multi-qubit gates. The initial state of the ancilla $|\chi\rangle$ is arbitrary, and it returns to its initial state at the end of the operation. For completeness, we include c in these circuit diagrams and use filled circles to indicate the qubits being acted on.

in the simulations is given by Eq. (2.3), and the individual single-qubit rotations U_1 are determined using global optimization methods, as described in Appendix B. In principle, we could also allow the circuit depth n to vary. However, we find that maximally entangled Bell states can already be obtained when $n = 2$. The resulting circuit for the singlet Bell state $|\Psi^-\rangle = \frac{1}{\sqrt{2}}(|01\rangle - |10\rangle)$ is shown in Fig. 2.3(a). Other Bell states can be generated in a similar fashion.

We can compare our mediated gate protocol to the conventional Bell-state protocol based on nearest-neighbor gates, as shown in Fig. 2.3(b). In the latter case, CNOT is used to generate the Bell state, while the SWAP gates are used to make the qubits proximal. The minimal circuit depth needed to construct CNOT is 2 [8]. Comparing Figs. 2.3(a) and 2.3(b), we obtain an exchange gate circuit depth of $n = 2$ for the mediated gate protocol and $n = 4$

for the SWAP-based protocol. The mediated gate therefore offers distinct advantages for generating arbitrary states.

Experimental proposal for a triple quantum dot

Triple quantum dots have been investigated in several laboratories [40, 41]. Here, we suggest a specific protocol for generating a Bell state in a triple quantum dot, using the mediated gate protocol in Fig. 2.3(a). Our proposal includes the supporting initialization and verification steps, and it is based on existing experimental methods. We note that Bell states can also be produced via standard, conventional (*i.e.*, nonmediated) techniques [9]. The purpose of this section is simply to outline a proof-of-principle experiment that employs mediated gates.

To generate a Bell state using mediated gates, we must first initialize the triple dot into the separable state $|0\rangle_1|\chi\rangle_c|0\rangle_2$, as shown on the left in Fig. 2.3(a). There are two common procedures for initializing quantum dot spin qubits: the preferential loading of single-electron spin ground states ($|0\rangle_1$ and $|0\rangle_2$) in a large magnetic field [54], and the preferential loading of a two-electron singlet state ($|S\rangle_1$) [9]. The latter can be transformed into the spin ground state of a double quantum dot ($|0\rangle_1|0\rangle_c$) by adiabatically detuning the double dot in a moderate magnetic field [9]. Both of these methods require a magnetic field, and we have confirmed that the protocol shown in Fig. 2.3(a) is unaffected by a uniform field, up to an overall phase factor. For the singlet loading method, the desired initial state is achieved, finally, by performing a SWAP operation between qubit c and qubit 2. Once the triple dot has been initialized, the mediated gate protocol is implemented as shown in Fig. 2.3(a), giving the result $|\Psi^-\rangle_{12}|\chi\rangle_c$.

The verification step is performed most conveniently via spin-to-charge conversion, using a singlet projection procedure [9]. We first perform a SWAP operation between qubit c and qubit 2, so the two spins in the singlet state become proximal: $|\Psi^-\rangle_{12}|\chi\rangle_c \rightarrow |\Psi^-\rangle_{1c}|\chi\rangle_2$. Dots 1 and c are then detuned, so that the electron in dot c tunnels to dot 1 only if the two electrons form a singlet, due to the large singlet-triplet energy splitting in a single quantum

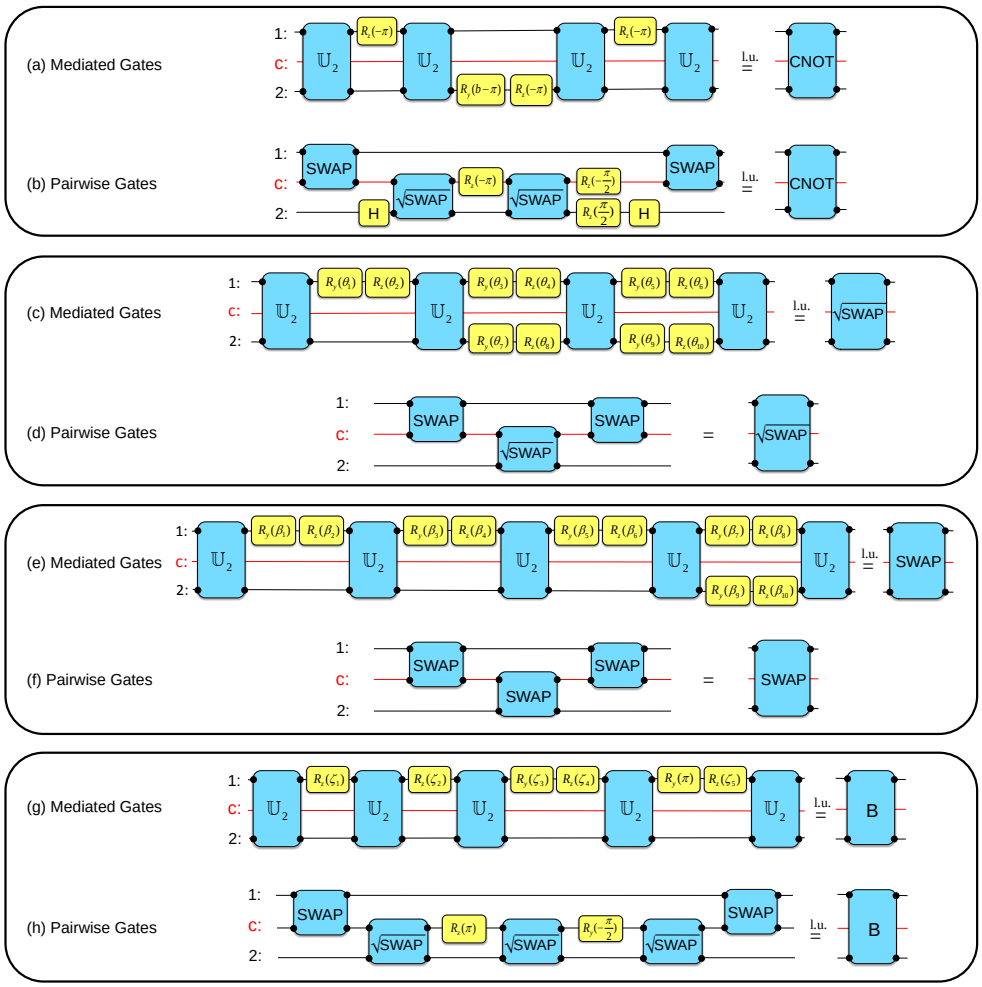

Figure 2.4: A comparison of circuits used to construct some common quantum gates. Each case presents two results: a mediated gate construction, obtained using global optimization methods (as described in Appendix B), and a "conventional" circuit, based on nearest-neighbor, pairwise gates. The pairwise gates require extra SWAP operations when the qubits being acted on are not proximal. In the cases shown here, the qubits (1 and 2) are separated by one ancilla (c). (a), (b) CNOT gates. For the mediated gate circuit, we have $b = -\arccos(-1/3)$. The pairwise gate circuit is given in [8]. (c), (d) $\sqrt{\text{SWAP}}$ gates. For the mediated gate circuit, we have $\theta_1 = 0.524\pi$, $\theta_2 = 0.549\pi$, $\theta_3 = 1.015\pi$, $\theta_4 = 0.100\pi$, $\theta_5 = 0.392\pi$, $\theta_6 = -0.305\pi$, $\theta_7 = -0.437\pi$, $\theta_8 = 0.626\pi$, $\theta_9 = -0.906\pi$, and $\theta_{10} = -0.174\pi$. (These parameters can be obtained up to machine precision. Here, and elsewhere throughout the paper, we halt the optimization procedure when the objective function is smaller than 10^{-14}.) For the pairwise gate circuit, we note that SWAP and $\sqrt{\text{SWAP}}$ are "natural" gates for spin qubits, whose interactions are of the isotropic Heisenberg type. As a result, the pairwise gate circuits for SWAP and $\sqrt{\text{SWAP}}$ are very simple. (e), (f) SWAP gates. For the mediated gate circuit, we have $\beta_1 = -0.737\pi$, $\beta_2 = -0.465\pi$, $\beta_3 = -0.543\pi$, $\beta_4 = 0.700\pi$, $\beta_5 = 0.807\pi$, $\beta_6 = 0.009\pi$, $\beta_7 = -0.278\pi$, $\beta_8 = 0.369\pi$, $\beta_9 = 0.274\pi$, and $\beta_{10} = -0.325\pi$. (g), (h) B gates. For the mediated gate circuit, we have $\zeta_1 = 0.297\pi$, $\zeta_2 = 0.788\pi$, $\zeta_3 = 0.660\pi$, $\zeta_4 = -1.092\pi$, and $\zeta_5 = 0.579\pi$. For the pairwise gate circuit, the circuit was constructed by first solving for the B gate in terms of $\sqrt{\text{SWAP}}$ gates, using the global optimization methods described in Appendix B. SWAP gates were then applied, to make the qubit states proximal.

dot. This projection technique requires a moderate (not too large) magnetic field, so that the singlet remains the ground state of the two-electron dot.

Construction of arbitrary gates

We now consider protocols for generating arbitrary two-qubit gates, using the mediated gate $\mathbb{U}_2$ as an entangling resource, in combination with arbitrary single-qubit gates U_1. We adopt a strategy analogous to Eq. (2.4), given by

$$U_2 = (U_1 \otimes U_1)[\mathbb{U}_2(U_1 \otimes U_1)]^n. \tag{2.5}$$

As before, we solve this equation using global optimization techniques, as described in Appendix B. The results for some familiar gates are shown in Figs. 2.4(a), 2.4(c), 2.4(e), and 2.4(g). These results appear to have the smallest possible circuit depth, based on exhaustive searches. None of the gates requires more than five applications of $\mathbb{U}_2$.

Our result for CNOT is indicated in Fig. 2.4(a). This mediated gate circuit employs four $\mathbb{U}_2$ gates. The corresponding circuit for conventional, pairwise gate operations employs two $\sqrt{\text{SWAP}}$ gates when the qubits are proximal [8]. When the qubits are nonproximal, additional SWAP gates are needed, as indicated in Fig. 2.4(b). Thus, for the second-nearest-neighbor geometry shown in Fig. 2.1, the mediated and conventional CNOT circuits have equal circuit depths, with $n = 4$.

Figure 2.4 also shows mediated gate results for several other types of gates, as well as the corresponding conventional, pairwise gate circuits. For the examples shown here, the mediated gate method has equal or larger circuit depths compared to the pairwise gate method. The examples where the pairwise gate method is more efficient fall into the SWAP family, which is the "natural" gate for spin qubits, since it is generated by the isotropic Heisenberg interaction. There are other, less familiar gates for which the mediated gate circuit is more efficient; the gate $\mathbb{U}_2$ is an obvious example. Generally, we expect that the mediated gate method should be more likely to improve the circuit depth of larger gates (*e.g.*, Toffoli) when multiqubit entangling gates like $\mathbb{U}_3$ are available, or when the central spin can be replaced with a spin bus. We discuss both of these examples below.

There are several well-known techniques for constructing arbitrary two-qubit gates, which can be adapted for mediated gates. The most efficient method involves the so-called B gate [55], which is defined as the only two-qubit gate that can generate generic two-qubit operations from two successive applications. Figure 2.4(g) shows our globally optimized circuit for a B gate, which employs five $\mathbb{U}_2$ gates. This result (together with [55]), constitutes a formal proof that $n \leq 10$ for a mediated gate with optimal circuit depth, as described in Eq. (2.5). It also forms a constructive protocol for generating an arbitrary two-qubit gate using 10 $\mathbb{U}_2$ gates. However, we note that the bound $n \leq 10$ does not appear to be tight, since none of the gates we have solved requires more than five applications of $\mathbb{U}_2$.

To conclude this section, we consider the scaling properties of the two-qubit mediated gate scheme for a spin bus geometry [42]. Specifically, we consider an odd-size spin chain of length N, and two external qubits. When the bus is constrained to its ground-state energy manifold, it can be treated as a spin-1/2 pseudospin [42]. The effective interaction between the qubits and the bus pseudospin has a Heisenberg form [56, 15], with an effective coupling constant $J^* \propto J/\sqrt{N}$ [42]. We can immediately apply all our three-qubit protocols, simply by replacing the central qubit in Fig. 2.1 with a bus and replacing J with J^* when we calculate the gate period T_g. The resulting bus gate $\mathbb{U}_2$ is identical to the two-qubit mediated gate, and the protocols proceed as before, except that the qubits can now be far apart. The exchange gate circuit depth for the bus protocol is the same as that for mediated gates. Specifically, it is independent of N. The gate period T_g scales as $\sqrt{N}$, however, since $T_g \propto 1/J^*$. In contrast, the circuit depth of a conventional gate protocol, based on pairwise SWAP gates, is proportional to N, while T_g is independent of N for a given pairwise operation. Thus, the spin bus architecture has much better scaling properties than the conventional gate protocol, in terms of both total gate time [$O(\sqrt{N})$ *vs.* $O(N)$] and circuit depth [$O(1)$ *vs.* $O(N)$], with immediate consequences for quantum error correction [26].

2.3 Three-Qubit Mediated Gate, $\mathbb{U}_3$

Mediated gate, $\mathbb{U}_3$

We now consider the mediated gate geometry shown in Fig. 2.5(a), with three qubits coupled through a single mediating spin, c. The system Hamiltonian is given by

$$H = J_{1c}\mathbf{s}_1 \cdot \mathbf{s}_c + J_{2c}\mathbf{s}_2 \cdot \mathbf{s}_c + J_{3c}\mathbf{s}_3 \cdot \mathbf{s}_c, \tag{2.6}$$

and the time evolution operator is given by $U(t) = e^{-iHt}$. If qubits 1–3 are arranged in a linear geometry rather than the "star" geometry shown in Fig. 2.5, then an effective star geometry can still be achieved by introducing a spin bus architecture [42], where c is an odd-size bus.

For larger geometries, the group theoretical methods described in Appendix A become cumbersome. However, for the special case of equal couplings, $J = J_{1c} = J_{2c} = J_{3c}$, we can still obtain mediated gates analytically. We do this by computing $U(t)$ in the angular momentum basis, where it is diagonal [42]. We then transform it to the computational basis and identify the gate periods $t = T_g$ for which the special decomposition $U = \mathbb{U}_3 \otimes I$ is satisfied. Here, $\mathbb{U}_3$ is the mediated gate acting on qubits 1–3, while I is the single-qubit identity operator acting on spin c. This procedure produces four different mediated gates [42]. The first gate is the trivial identity operator, obtained at the gate periods $T_g = (8m)\pi/J$ (m is an integer). The second gate occurs at the gate periods $T_g = (8m+2)\pi/J$, and takes the form

$$\mathbb{U}_3 = i \begin{pmatrix} 1 & 0 & 0 & 0 & 0 & 0 & 0 & 0 \\ 0 & -1/3 & 2/3 & 0 & 2/3 & 0 & 0 & 0 \\ 0 & 2/3 & -1/3 & 0 & 2/3 & 0 & 0 & 0 \\ 0 & 0 & 0 & -1/3 & 0 & 2/3 & 2/3 & 0 \\ 0 & 2/3 & 2/3 & 0 & -1/3 & 0 & 0 & 0 \\ 0 & 0 & 0 & 2/3 & 0 & -1/3 & 2/3 & 0 \\ 0 & 0 & 0 & 2/3 & 0 & 2/3 & -1/3 & 0 \\ 0 & 0 & 0 & 0 & 0 & 0 & 0 & 1 \end{pmatrix}. \tag{2.7}$$

The third gate occurs at the gate periods $T_g = (8m+4)\pi/J$, and is given by $\mathbb{U}_3^2 = -I$. The fourth gate occurs at the gate periods $T_g = (8m+6)\pi/J$, and is given by $\mathbb{U}_3^3 = -\mathbb{U}_3$.

Generation of arbitrary states

The methods used to generate two-qubit states and gates can also be extended to three-qubit problems. However, three-qubit protocols are slightly more complicated because they can involve two-qubit gates, three-qubit gates, or both. The most general scheme for generating a three-qubit state is shown in Fig. 2.6(a). We note that higher order gates such as the three-qubit mediated gate $\mathbb{U}_3$ can potentially achieve shorter circuit depths, because they are more parallel than two-qubit gates. The global optimization techniques used to solve Eq. (2.4) can also be applied to Fig. 2.6(a).

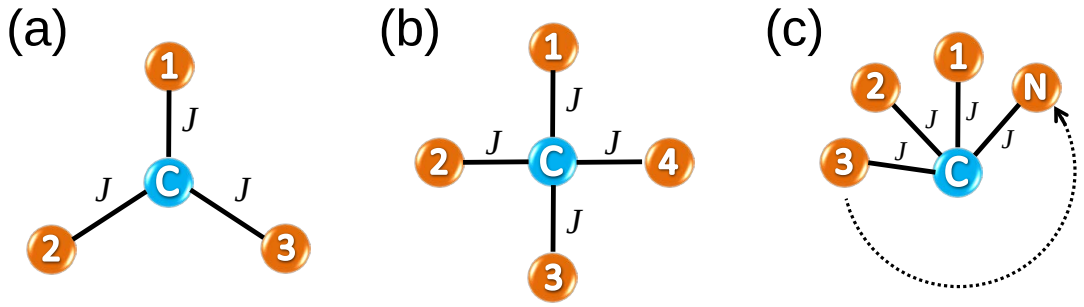

Figure 2.5: Multiqubit "star" geometries for implementing mediated gates. Here, the qubits are labeled with numbers and the ancilla spins labeled c mediate the gates. (a) The $\mathbb{U}_3$ gate acts on qubits 1–3 when the three qubit couplings J are equal. (b) To generate the four-qubit cluster state $|C_4\rangle$, we implement three-qubit mediated gates $\mathbb{U}_3$ by turning on the couplings to three of the qubits at a time. (c) To generate a W_N state, we consider N qubits connected simultaneously to the ancilla spin c, with equal couplings J. In each of these geometries, the ancilla spin can be replaced with an odd-size spin bus. In this case, c represents the pseudospin of the bus ground state [42].

There are known to be two nonfungible forms of entanglement for three qubits [57]: the W-state family, characterized by the symmetric form

$$|W_3\rangle = \frac{1}{\sqrt{3}}(|001\rangle + |010\rangle + |100\rangle), \tag{2.8}$$

and the Greenberger-Horne-Zeilinger (GHZ)-state family [58], characterized by the sym-

metric form

$$|\mathrm{GHZ}_3\rangle = \frac{1}{\sqrt{2}}(|000\rangle + |111\rangle). \tag{2.9}$$

The GHZ state is understood to be maximally entangled for three qubits.

We have applied global optimization methods to obtain $|\mathrm{GHZ}_3\rangle$ and $|W_3\rangle$, obtaining the results shown in Figs. 2.6(b)-2.6(d). For $|W_3\rangle$, we provide two different strategies. One uses a combination of $\mathbb{U}_2$ and $\mathbb{U}_3$; the other uses $\mathbb{U}_3$ only. They both have the same circuit depth, $n = 2$. Remarkably, we find that the GHZ state can be attained using $\mathbb{U}_3$ as the only entangling resource with just a single application:

$$|\mathrm{GHZ}_3\rangle = (U_1 \otimes U_1 \otimes U_1)\mathbb{U}_3(U_1 \otimes U_1 \otimes U_1)|000\rangle. \tag{2.10}$$

The circuit is optimal ($n = 1$), indicating that $\mathbb{U}_3$ is a perfect entangler for the three-qubit GHZ state family [57]. We can compare this result to the conventional, pairwise gating circuit for $|\mathrm{GHZ}_3\rangle$, which uses two CNOT gates [59]. In a quantum dot quantum computer, this would require at least four exchange gate operations, or $n = 4$. It is interesting to note that $\mathbb{U}_3$ is locally equivalent to the time evolution operator describing the three-qubit triangular geometry (evaluated at a special time) [60]. The latter gate is also capable of generating $|\mathrm{GHZ}_3\rangle$ in a single time step.

Although $\mathbb{U}_3$ acts on just three qubits at a time, it is interesting to note that it can also be used as an entangling resource for larger systems. For example, we can consider cluster states, which represent an important entanglement family used for one-way quantum computing [61, 62]. The four-qubit cluster state $|C_4\rangle$ is defined as

$$|C_4\rangle \overset{\text{l.u.}}{=} \frac{1}{2}(|0000\rangle + |0011\rangle + |1100\rangle - |1111\rangle). \tag{2.11}$$

We have solved $|C_4\rangle$ numerically, for the geometry shown in Fig. 2.5(b). Here, the ancilla spin c can be connected to each of the four qubits. However, we assume that only three of the couplings are turned on at a time. For example, $\mathbb{U}_3(1, 2, 3)$ indicates that the couplings between c and qubits 1–3 are turned on, thus implementing the gate $\mathbb{U}_3$ between

those three qubits. Hence, we obtain a numerical solution for $|C_4\rangle$ of the form

$$\begin{aligned}|C_4\rangle =& U_1^{\otimes 4}\mathbb{U}_3(1,2,3)U_1^{\otimes 4}\mathbb{U}_3(1,2,4)U_1^{\otimes 4}\mathbb{U}_3(1,2,3)\\ &\times U_1^{\otimes 4}\mathbb{U}_3(2,3,4)U_1^{\otimes 4}|0000\rangle.\end{aligned} \tag{2.12}$$

Here, $U_1^{\otimes 4}$ represents arbitrary single-qubit rotations acting on each of the four qubits. According to our definition of circuit depth, this protocol corresponds to $n = 4$.

We can compare our mediated gate solution to a conventional sequence for generating $|C_4\rangle$, based on nearest-neighbor pairwise gates. The conventional scheme involves three sequential applications of the phase gate $\mathrm{diag}(1, 1, 1, -1)$, in addition to single-qubit rotations [61, 62]. Since the phase gate is locally equivalent to CNOT, it can be decomposed into two exchange gates plus single-qubit rotations. The resulting circuit depth for the conventional protocol is therefore $n = 6$. Thus, again, we find that mediated gates offer a considerable improvement in terms of circuit depth.

Construction of arbitrary gates

We now turn to the construction of three-qubit quantum gates using $\mathbb{U}_3$. As an example, we determine an explicit gate sequence for generating the Toffoli gate, defined as

$$U_T = \begin{pmatrix} 1 & 0 & 0 & 0 & 0 & 0 & 0 & 0 \\ 0 & 1 & 0 & 0 & 0 & 0 & 0 & 0 \\ 0 & 0 & 1 & 0 & 0 & 0 & 0 & 0 \\ 0 & 0 & 0 & 1 & 0 & 0 & 0 & 0 \\ 0 & 0 & 0 & 0 & 1 & 0 & 0 & 0 \\ 0 & 0 & 0 & 0 & 0 & 1 & 0 & 0 \\ 0 & 0 & 0 & 0 & 0 & 0 & 0 & 1 \\ 0 & 0 & 0 & 0 & 0 & 0 & 1 & 0 \end{pmatrix}. \tag{2.13}$$

Our strategy is analogous to the state-generating circuit in Fig. 2.6(a), where we interspersed $\mathbb{U}_2$ or $\mathbb{U}_3$ gates with arbitrary single-qubit rotations. Our best result for constructing the Toffoli gate by this method is a gate sequence containing five $\mathbb{U}_2$ gates and seven $\mathbb{U}_3$ gates, giving a total exchange-gate circuit depth of $n = 12$.

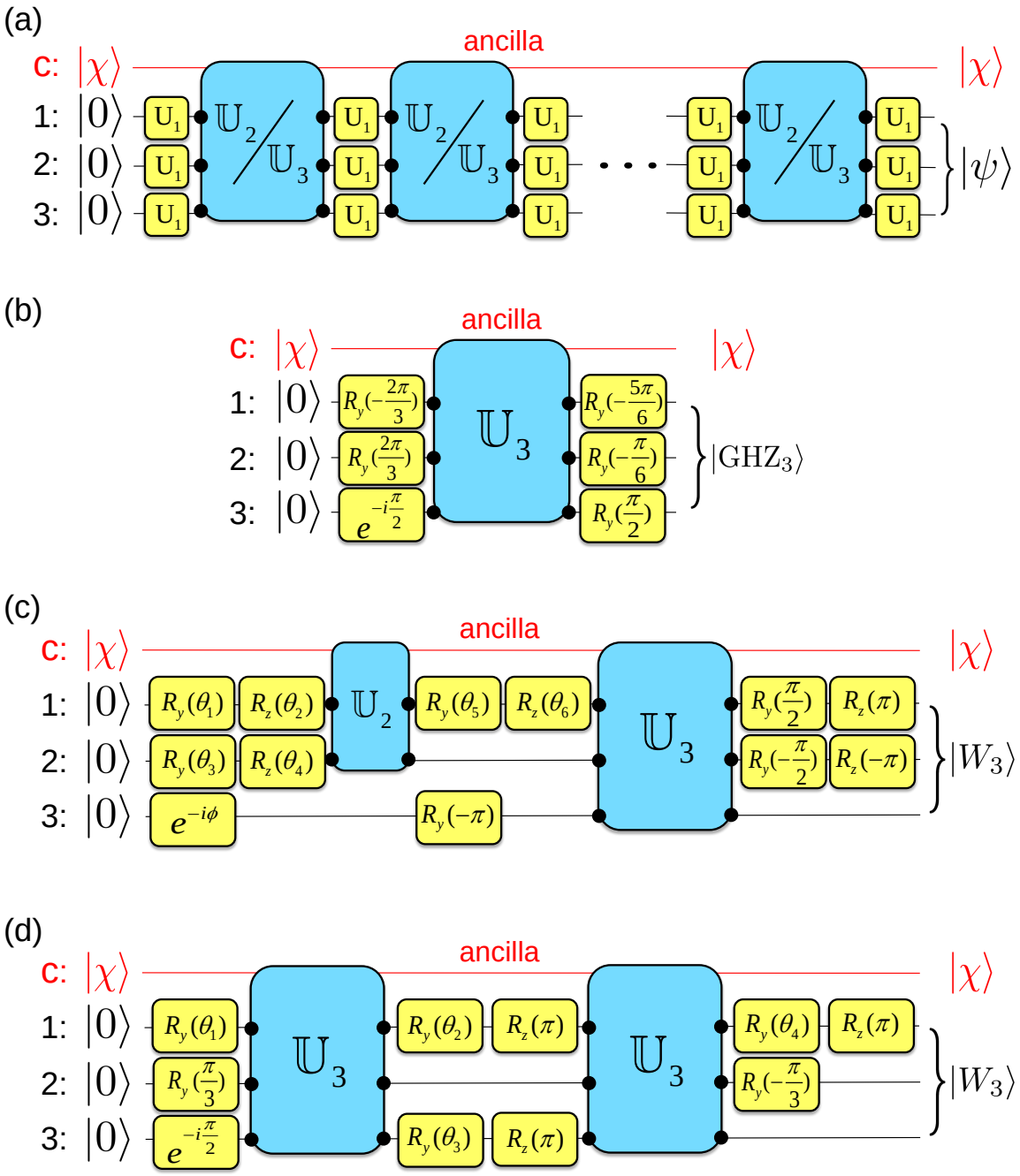

Figure 2.6: Circuits for 3-qubit entanglement state generation with mediated gates. (a) A general circuit for generating an arbitrary three-qubit state, using $\mathbb{U}_2$ and/or $\mathbb{U}_3$ gates. Note that $\mathbb{U}_2$ can act on different pairs of qubits. (b) A circuit for generating a $|\mathrm{GHZ}_3\rangle$ state, using the three-qubit mediated gate $\mathbb{U}_3$. (c) A circuit for generating a $|W_3\rangle$ state, using both $\mathbb{U}_2$ and $\mathbb{U}_3$ gates, with $\theta_1 = -0.262\pi$, $\theta_2 = 0.730\pi$, $\theta_3 = -1.356\pi$, $\theta_4 = 0.349\pi$, $\theta_5 = 1.193\pi$, $\theta_6 = 0.270\pi$, and $\phi = 1.299\pi$. (d) An alternative circuit for generating a $|W_3\rangle$ state, using only $\mathbb{U}_3$ gates, with $\theta_1 = 0.529\pi$, $\theta_2 = 0.725\pi$, $\theta_3 = -0.608\pi$, and $\theta_4 = -0.137\pi$.

We can compare our mediated gate solution to a conventional Toffoli gate construction. A Toffoli circuit using CNOT gates as the entangling resource has been presented in [50] and [63]; it consists of six sequential CNOT gates. We can decompose this into a sequence of nearest-neighbor exchange gates, including intermediate SWAP gates when necessary. After identifying the exchange gates that can be performed in parallel, this procedure gives a circuit depth of $n = 16$. Alternatively, if we allow other two-qubit gates in this procedure, in addition to CNOT, it can be shown that five sequential two-qubit gates are necessary and sufficient for implementing a Toffoli gate [64]. However, some of these gates are decomposed into exchange gate sequences with $n > 2$. Based on such considerations, it appears that the mediated gate circuit with a circuit depth of $n = 12$ for constructing a Toffoli gate is always more efficient than a conventional gate circuit.

2.4 Mediated Gates, $\mathbb{U}_{2N+1}$ $(N > 1)$

The previous approach to state generation and gate construction using mediated gates can be extended to systems with more than three qubits. There are many qubit architectures of interest. Here, we consider the "star" geometry shown in Fig. 2.5(c). In cases where it is experimentally challenging to fabricate a star geometry, due to physical constraints, it may be convenient to replace the central spin c with an odd-size spin bus [42]. In this case, nontrivial mediated gates can be obtained when an odd number of qubits is simultaneously coupled to the bus. These multiqubit mediated gates, $\mathbb{U}_{2N+1}$, are highly parallel and potentially very efficient.

Here, we demonstrate that multiqubit W states can be generated using mediated gates, with very small circuit depths. The N-qubit W state is defined as

$$|W_N\rangle = \frac{1}{\sqrt{N}}(|00\ldots01\rangle + |00\ldots10\rangle + \ldots + |10\ldots00\rangle). \tag{2.14}$$

In Figs. 2.6(c) and 2.6(d) we indicate two methods for generating $|W_3\rangle$. An alternative method is shown in Fig. 2.7. This circuit requires a maximally entangled Bell state, $|\Psi^-\rangle$, as input. The total circuit depth for this solution ($n = 3$) is larger than in Figs. 2.6(c) and

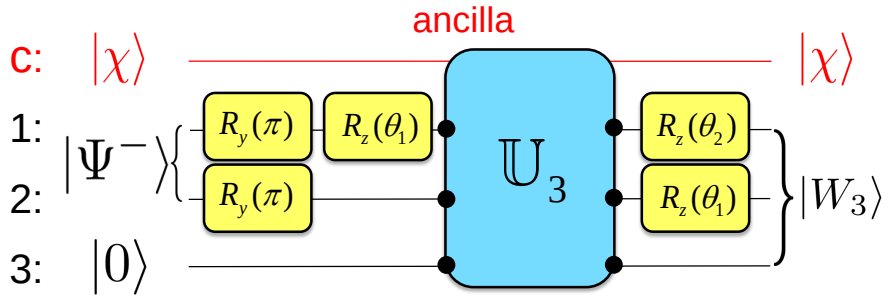

Figure 2.7: A mediated gate circuit for generating $|W_3\rangle$ using a Bell state as input. Here, $\theta_1 = -\theta_2 = \arccos(1/4)$.

2.6(d) because the circuit depth for generating $|\Psi^-\rangle$ is $n = 2$. However, the scheme has the advantage that it may be scalable for odd-size W states.

For the cases $N = 1$–3, we have numerically verified the result that

$$|W_{2N+1}\rangle = (U_1 \otimes U_1)\mathbb{U}_{2N+1}(U_1 \otimes U_1)|\Psi^-\rangle|0\rangle^{\otimes(2N-1)}, \tag{2.15}$$

which includes the result in Fig. 2.7 for the case $N = 1$. For all cases, we note that the single-qubit rotations are applied only to qubits 1 and 2 (the qubits in the Bell state). For the cases of $N = 2, 3$, the generating circuits are similar to Fig. 2.7, but with different angles θ_1 and θ_2. For each of these cases, the circuit depth is given by $n = 3$.

A related, probabilistic scheme can be used to generate the even-size W states. We first generate the odd-size W state, as described above. This state can be expressed as

$$|W_{2N+1}\rangle = \frac{1}{\sqrt{2N+1}}|0\rangle^{\otimes 2N}|1\rangle + \sqrt{\frac{2N}{2N+1}}|W_{2N}\rangle|0\rangle. \tag{2.16}$$

Hence, if one of the qubits is measured in the z basis, with outcome 0, then the state of the remaining qubits will collapse to $|W_{2N}\rangle$. When N is large, this protocol is successful with a high probability, $P = 2N/(2N+1)$.

2.5 Summary and Conclusions

In this paper, we developed the concept of a *mediated gate* between nonproximal qubits. This gate is implemented by coupling the qubits simultaneously through a central, ancilla

Table 2.1: Schemes we consider here are based on (i) mediated gates (as described in this paper), or (ii) conventional pairwise gates. The pairwise gating method requires extra SWAP gates when the qubits being acted on are not proximal. (A useful reference for the scaling of $|W_N\rangle$ state using pairwise gates is [65].)

State or gate	No. mediated gates	No. pairwise gates
$\|\Psi^-\rangle$	2	4
$\|W_3\rangle$	2	2
$\|W_N\rangle$	3	$N-1$
$\|\mathrm{GHZ}_3\rangle$	1	4
$\|C_4\rangle$	4	6
CNOT	4	4
$\sqrt{\text{SWAP}}$	4	3
SWAP	5	3
B	5	5
Toffoli	12	16

qubit, which is restored to its initial state at the end of the operation. We have focused on two and three-qubit gates, although higher dimensional gates can be obtained in similar fashion. We investigated protocols, based on global optimization techniques, for generating arbitrary states and gates, using mediated gates as the sole entangling resource.

Several promising results were obtained using mediated gates, as summarized in Table I. We showed that a maximally entangled Bell state can be achieved with just two applications of a mediated gate $\mathbb{U}_2$, and we proposed an experimental protocol for implementing this procedure in a triple quantum dot. We showed that several important two-qubit quantum gates can be obtained using five or fewer mediated gates, and we proved that ten exchange gates is the maximum needed for generating an arbitrary two-qubit gate. We showed how the central ancilla qubit can be replaced with a spin bus, leading to significant improvements in scaling properties, for both the total gate time and the circuit depth. We also considered the mediated gates $\mathbb{U}_N$ with $N \geq 3$, and showed how mediated gate methods might be generalized to higher dimensions.

We find that mediated gates compare favorably with conventional, pairwise gating schemes, which make use of SWAP gates when qubits are not proximal. For each of the results reported in Table I, we compare the circuit depths based on mediated gates to those

involving conventional pairwise gates.

We thank Jun Zhang and Andrei Galiautdinov for helpful discussions. This work was supported by the DARPA QuEST program through a grant from AFOSR, by NSA/LPS through grants from ARO (W911NF-09-1-0393, W911NF-08-1-0482, and W911NF-12-1-0607), by NSF-PIF (PHY-1104672), and by the United States Department of Defense. The US government requires publication of the following disclaimer: the views and conclusions contained in this document are those of the authors and should not be interpreted as representing the official policies, either expressly or implied, of the US Government.

Chapter 3

Exchange Only Qubit

3.1 Introduction.

A great challenge in quantum computation is to perform prescribed operations with very small error rates. Logical qubits are important for achieving this [66], since they are fundamental for quantum error correction [67]. Moreover, logical qubits can have symmetries that give rise to so-called sweet spots, at which the effects of noise are suppressed [68]. Several logical spin qubits have been proposed for quantum dot architectures [8]. Here, we consider the exchange-only logical qubit [25], formed of three electrons in a triple dot [39, 40, 41], as illustrated in Fig. 3.1(d). This qubit has the advantage that it has the potential to be very fast, since all operations can be implemented without spatially varying magnetic fields.

The effects of charge noise can never be fully suppressed, even near a sweet spot [69]. In this paper, we quantify the effect of sweet spots on gate fidelities by performing theoretical simulations of pulsed gate operations in an exchange-only qubit. The sweet spot in this device occurs at the symmetry point shown in Fig. 3.1(b), where the detuning parameters $\varepsilon = \varepsilon_M = 0$, and the charge-induced fluctuations of the detuning [70] are suppressed, to leading order. (Charge noise in the tunnel coupling [71] is not suppressed at this point, but is not thought to be a dominant noise source [72].) As consistent with recent experiments [73], Z-rotations are performed at the sweet spot, while X-rotations are obtained by pulsing away

from this point. In principle, the different rotations can be turned on and off independently. However, in practice it may be necessary to turn on the exchange interactions and magnetic field at all times, to suppress leakage into the non-logical sector of the Hilbert space [74, 20].

The exchange-only qubit provides an ideal platform for assessing the effect of sweet spots, since all gate operations are generated by the same physical process (the exchange interaction [25, 75, 76]). The only difference between X and Z-rotations is their proximity to the sweet spot. The fidelities of these operations can therefore be used to quantify the effectiveness of the sweet spot for mitigating charge noise. This is in contrast with logical qubits where the different rotation axes correspond to different physical processes (e.g., exchange vs. magnetic couplings in singlet-triplet qubits [77, 9]).

In Ref. [20], we provided a detailed account of magnetic noise from nuclear spins on the decoherence of an exchange-only qubit. Here, we simulate realistic gate operations including quasistatic random Overhauser fields [78] and charge noise [74]. In certain regimes we find that the main limit on the gate fidelities arises from the Overhauser fields, as consistent with experimental observations [73]. However, when the gates are properly optimized, we predict that charge noise should determine the upper bound on gate fidelities. After optimization, we find that gate fidelities at the sweet spot are typically 20 times better than away from the sweet spot.

3.2 Theoretical Model.

We model the coherent evolution of the exchange-only qubit using a 3-electron, 3-site Hubbard model with the Hamiltonian B

$$\begin{aligned} H = & \sum_{\langle i,j\rangle\sigma} t_{ij}(c_{i\sigma}^{\dagger}c_{j\sigma} + c_{j\sigma}^{\dagger}c_{i\sigma}) + U\sum_{j} n_{j\uparrow}n_{j\downarrow} \\ & + \sum_{j} \varepsilon_j(n_{j\uparrow} + n_{j\downarrow}) - g\mu_B B\sum_{j}(n_{j\uparrow} - n_{j\downarrow}) \\ & + g\mu_B \sum_{j} \Delta B_j(n_{j\uparrow} - n_{j\downarrow}), \end{aligned} \tag{3.1}$$

where the labels $\{i, j\} = 1, 2, 3$ correspond to dot locations, $\uparrow, \downarrow$, and σ refer to individual spin s_z eigenstates, $c^\dagger_{j\sigma}$ and $c_{j\sigma}$ are electron creation and annihilation operators, and $n_{j\sigma}$ is the electron number operator. The first term in Eq. (3.1) describes the tunneling, with tunnel couplings t_{ij}. We assume a symmetric, linear triple dot geometry, as shown in Fig. 3.1(d), with $t_{12} = t_{23} \equiv t$ and $t_{13} = 0$. The second term describes the onsite Coulomb repulsion, with energies U that are the same at every site. The third term describes the local electrostatic potentials ε_j. The fourth term describes the Zeeman energy due to a uniform external magnetic field $\mathbf{B} = B\hat{\mathbf{z}}$, with the Landé g-factor and Bohr magneton μ_B. The fifth term describes the local variations of the Zeeman energy due to Overhauser field fluctuations $\Delta\mathbf{B}_j$. Here, we take $\Delta\mathbf{B}_j \| \mathbf{B}$ because the lateral components of $\Delta\mathbf{B}_j$ generate couplings between S_z manifolds that are highly suppressed in the regime of large Zeeman splittings, which we consider below. We also ignore Coulomb interactions between electrons in different dots. The detuning $\varepsilon = \varepsilon_1 - \varepsilon_3$ is defined in analogy with experiments [40, 73], and corresponds to the energy difference between the (2,0,1) and (1,0,2) charge configurations. For a triple dot, there is also a second, independent detuning parameter [79], which we define here as $\varepsilon_M = \varepsilon_2 - (\varepsilon_1 + \varepsilon_3)/2$. In experimental systems, the detunings ε and ε_M are controlled by voltages, including V_L and V_R, which are applied to the top-gates. A typical charge stability diagram is shown in Fig. 3.1(a) for a fixed value of ε_M.

The Hilbert space associated with Eq. (3.1) is large. For GaAs-based devices, most leakage channels can be suppressed by enforcing sizeable energy splittings [20]. As consistent with recent experiments [73], we therefore consider the energy hierarchy $g\mu_B B \gg J \gg g\mu_B \Delta B > 0$, where J is the exchange interaction generated by the tunnel couplings. (In B, we briefly consider ^{28}Si-based devices, which do not require such an energy heirarchy, due to the absence of nuclear spins.) Since $g\mu_B B$ is large, the energy spectrum splits into manifolds of constant total spin S_z. Our simulations focus on the seven states in the $S_z = 1/2$ manifold, where the two qubit states are defined in the decoherence free subspace with $S = S_z$ [25, 73]. For a basis set, we consider the seven eigenstates of Eq. (3.1) when $\varepsilon = \varepsilon_M = \Delta B_j = 0$, consisting of three singly-occupied $(1, 1, 1)$ states, $|0\rangle = \sqrt{1/3}|T_0\rangle_{13}|\uparrow\rangle_2 -$

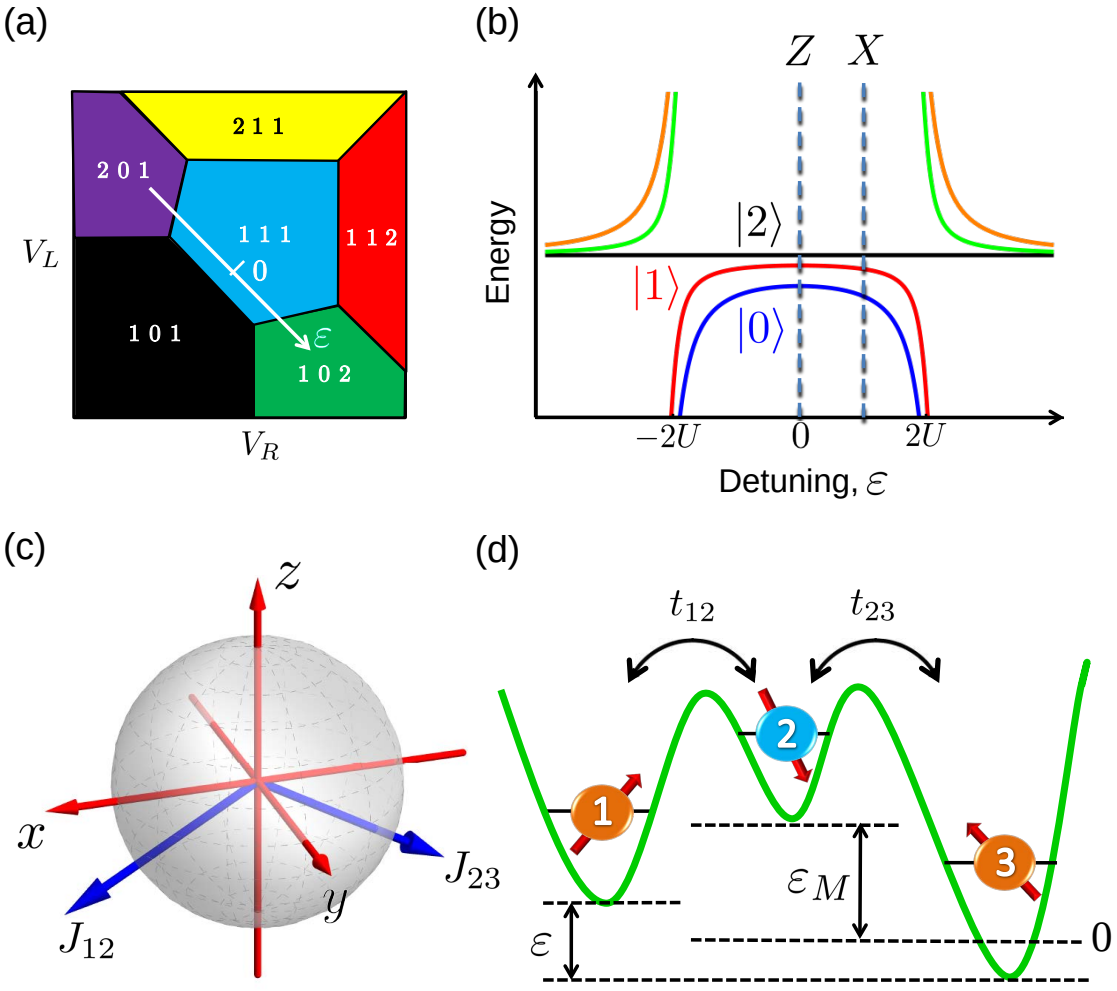

Figure 3.1: (a) A two-dimensional cut through the charge stability diagram of a triple quantum dot as a function of top-gate voltages, for a fixed value of the detuning parameter ε_M. (b) Energy level diagram of the $S_z = 1/2$ manifold as a function of the detuning parameter ε. In the central region, the low energy states $|0\rangle$-$|2\rangle$ are in the (1,1,1) charge configuration, while the high energy states are doubly occupied. (c) Bloch sphere representation of the logical qubit, with the rotation axes corresponding to $J_{23} = 0$ (left) and $J_{12} = 0$ (right). (d) Hubbard model of a triple quantum dot containing three electrons.

$\sqrt{2/3}|T_+\rangle_{13}|\downarrow\rangle_2$, $|1\rangle = |S\rangle_{13}|\uparrow\rangle_2$, and $|2\rangle = \sqrt{2/3}|T_0\rangle_{13}|\uparrow\rangle_2 + \sqrt{1/3}|T_+\rangle_{13}|\downarrow\rangle_2$, and four doubly-occupied states, $|3\rangle = |S\rangle_1|\cdot\rangle_2|\uparrow\rangle_3$, $|4\rangle = |\cdot\rangle_1|S\rangle_2|\uparrow\rangle_3$, $|5\rangle = |\uparrow\rangle_1|S\rangle_2|\cdot\rangle_3$, and $|6\rangle = |\uparrow\rangle_1|\cdot\rangle_2|S\rangle_3$. Here, the subscript denotes the dot index, $|S\rangle = \frac{1}{\sqrt{2}}(|\uparrow\downarrow\rangle - |\downarrow\uparrow\rangle)$, $|T_0\rangle = \frac{1}{\sqrt{2}}(|\uparrow\downarrow\rangle + |\downarrow\uparrow\rangle)$, and $|T_+\rangle = |\uparrow\uparrow\rangle$ are the singlet and triplet states of two spins, and $|\cdot\rangle$ represents a dot with no electrons. $|0\rangle$ and $|1\rangle$ are the logical qubit states, $|2\rangle$ is the main leakage state, and the doubly occupied states mediate the exchange interaction.

The gate simulations described below include the full set of seven basis states, in order to address questions of leakage and decoherence. However it is instructive to consider the effective Hamiltonian in the $\{|0\rangle, |1\rangle\}$ logical subspace [74],

$$H = \frac{\sqrt{3}}{4}(J_{12} - J_{23})\sigma_x - \frac{1}{4}(J_{12} + J_{23})\sigma_z, \tag{3.2}$$

where J_{12} and J_{23} are exchange interactions. The latter may be tuned independently as a function of the control parameters ε and ε_M, yielding a continuous set of rotations in the x-z plane of the Bloch sphere. For example, we could independently set J_{12} or J_{23} to zero, yielding the pair of rotation axes shown in Fig. 3.1(c). From Eq. (3.2), we see that Z-rotations are obtained when $J_{12} = J_{23}$. In B, we show that this requirement is met when either $\varepsilon = 0$ or $\varepsilon_M = 0$. We also show that the special combination $\varepsilon = \varepsilon_M = 0$ corresponds to a detuning sweet spot, because $\partial E_{01}/\partial\varepsilon = \partial E_{01}/\partial\varepsilon_M = 0$, where E_{01} is the energy splitting between the qubit states. Since always-on exchange interactions are needed to prevent leakage, and since $J_{12}, J_{13} > 0$, Eq. (3.2) suggests that we cannot achieve pure X-rotations. We overcome this problem by implementing a three-step pulse sequence [80]. This procedure requires moving away from the sweet spot, with consequences for the decoherence and gate fidelity. Finally, we note that a complete set of single-qubit operations must include initialization and readout. The latter are accomplished in experiments by adiabatically tuning the device to the $(2, 0, 1)$ or $(1, 0, 2)$ charge configurations in the far-detuned regime of Fig. 3.1(b) [73]. In our simulations, we do not investigate readout and initialization; we consider only the unitary gate operations. Moreover, we assume instantaneous (diabatic) pulses and do not investigate pulse imperfections. We consider only the errors caused by charge and nuclear noise sources, and by leakage outside the logical qubit Hilbert space.

3.3 Gate Simulations.

We simulate the dynamics of the logical qubit gate operations by solving the master equation

$$\frac{d\rho(t)}{dt} = -\frac{i}{\hbar}[H, \rho(t)] - D \tag{3.3}$$

for the 7×7 density matrix, ρ. The first term on the right-hand side of Eq. (3.3) describes the unitary evolution, while the second term describes the decoherence.

We consider dephasing from charge noise and random Overhauser fields. The nuclear fluctuations occur at frequencies much lower than the relevant electronic time scales [81]; we take them to be quasistatic with a Gaussian distribution width $\sigma_B = 4$ mT, as appropriate for GaAs [82]. The charge fluctuations occur over a range of frequencies [72]. Here, we model them as either "fast" (compared to qubit gate frequencies), with a characteristic Markovian dephasing rate $\Gamma \sim 1$ GHz [83], or "slow" (quasistatic), with a Gaussian distribution width $\sigma_\varepsilon = 5$ μeV [84, 85].

We consider two types of fast charge noise. The virtually occupied states $|3\rangle$-$|7\rangle$ mediate exchange interactions, but they also contribute to double occupation dephasing errors of the form [86] $D_U = \sum_i \frac{\Gamma}{2}[n_{i\uparrow} + n_{i\downarrow}, [n_{i\uparrow} + n_{i\downarrow}, \rho]]$. We also consider direct dephasing D_ε of the singly occupied states $|0\rangle$-$|2\rangle$, with rates that depend on the derivative of the energy splitting E_{ij} between eigenstates $|i\rangle$ and $|j\rangle$ with respect to the detuning [81]. We assume that contributions from the individual detuning parameters contribute in quadrature, with the dephasing rates $\gamma_{ij} = \Gamma[(\partial E_{ij}/\partial\varepsilon)^2 + 2(\partial E_{ij}/\partial\varepsilon_M)^2]^{1/2}$. Here, the factor of 2 reflects the relative magnitudes of the ε and ε_M terms in the effective 2×2 Hamiltonian for the

logical qubit states B. The resulting dephasing matrix is given by

$$D = D_U + D_\varepsilon = \tag{3.4}$$

$$\begin{pmatrix} 0 & \gamma_{01}\rho_{01} & \gamma_{02}\rho_{02} & \Gamma\rho_{03} & \Gamma\rho_{04} & \Gamma\rho_{05} & \Gamma\rho_{06} \\ \gamma_{01}\rho_{01}^* & 0 & \gamma_{12}\rho_{12} & \Gamma\rho_{13} & \Gamma\rho_{14} & \Gamma\rho_{15} & \Gamma\rho_{16} \\ \gamma_{02}\rho_{02}^* & \gamma_{12}\rho_{12}^* & 0 & \Gamma\rho_{23} & \Gamma\rho_{24} & \Gamma\rho_{25} & \Gamma\rho_{26} \\ \Gamma\rho_{03}^* & \Gamma\rho_{13}^* & \Gamma\rho_{23}^* & 0 & 4\Gamma\rho_{34} & 3\Gamma\rho_{35} & \Gamma\rho_{36} \\ \Gamma\rho_{04}^* & \Gamma\rho_{14}^* & \Gamma\rho_{24}^* & 4\Gamma\rho_{34}^* & 0 & \Gamma\rho_{45} & 3\Gamma\rho_{46} \\ \Gamma\rho_{05}^* & \Gamma\rho_{15}^* & \Gamma\rho_{25}^* & 3\Gamma\rho_{35}^* & \Gamma\rho_{45}^* & 0 & 4\Gamma\rho_{56} \\ \Gamma\rho_{06}^* & \Gamma\rho_{16}^* & \Gamma\rho_{26}^* & \Gamma\rho_{36}^* & 3\Gamma\rho_{46}^* & 4\Gamma\rho_{56}^* & 0 \end{pmatrix}.$$

We treat the slow fluctuations of the detuning and Overhauser fields by numerically solving the 49 coupled real differential equations in Eq. (3.3) for a fixed noise realization B. We then repeat the calculations for 625 realizations of Overhauser field fluctuations and 961 realizations of detuning fluctuations, and perform the appropriate Gaussian averages. The simulations are performed on the Open Science Grid at the University of Wisconsin-Madison [87]. The results reported here represent > 23 compute years.

3.4 Gate Optimization.

We begin by considering $Z(\pi)$ rotations of the logical qubit. As described above, these operations are performed at the sweet spot $\varepsilon = \varepsilon_M = 0$. Fluctuations of the detuning and the Overhauser fields give rise to errors within the qubit subspace as well as leakage. We monitor these effects by performing quantum process tomography (QPT) B, beginning the simulations in four different initial states, and comparing the final results to the ideal final states for a fixed value of the tunnel coupling t. In this procedure, the evolution period τ is treated as a variable. The optimal value of τ is chosen by maximizing the fidelity F obtained from QPT, with results shown in Fig. 3.3. For small t, the rotations are slow, and the fidelity is strongly suppressed by the quasistatic random Overhauser fields. For large t, the rotations are fast, and the fidelity is determined by a combination of charge

noise and leakage. Since the leakage process is coherent, the projection of the full density matrix onto the logical qubit subspace undergoes oscillations, as seen in the lower inset of Fig. 3.3. These oscillations are severe for large tunnel couplings, causing a deterioration of the fidelity as seen in the main figure.

We also investigate $X(\pi)$ rotations of the logical qubit. As noted above, it is not possible to perform a direct rotation around $\hat{\mathbf{x}}$; accurate rotations require multi-pulse gate sequences. Here, we consider a three-step procedure [80] that can be visualized as shown in the lower inset of Fig. 3.4. The sequence consists of (i) a π-rotation around the $-(\hat{\mathbf{x}}+\hat{\mathbf{z}})/\sqrt{2}$ axis on the Bloch sphere, (ii) a $Z(\pi)$ rotation, and (iii) a final π-rotation around the $-(\hat{\mathbf{x}}+\hat{\mathbf{z}})/\sqrt{2}$ axis. For steps (i) and (iii), the values of ε and ε_M that determine the axis tilt are not known *a priori*; we find them by performing fidelity simulations for the desired gate operations in the absence of detuning and nuclear fluctuations. The results are shown in Fig. 3.2 for a fixed value of t, with the optimal values of ϵ and ϵ_M indicated by a red star. This calibration procedure is then repeated for other values of t. The three-step protocol is then optimized, step by step, by performing simulations to determine the evolution period τ that maximizes the fidelity of each step. The final fidelities of the three-step $X(\pi)$ protocol are shown in Fig. 3.4. We observe results similar to those in Fig. 3.3. However, the effects of leakage and charge noise are more severe because steps (i) and (iii) are not performed at sweet spots. The suppression of the fidelity due to leakage is most obvious at large t. The lower inset shows a typical evolution projected onto the logical qubit Bloch sphere.

3.5 Results and Discussion.

The X and Z-rotation protocols used in Fig. 3.3 3.4 are different. However, by comparing fidelities obtained using QPT, we can compare the final results effectively. We observe that maximal fidelities (or minimal infidelities, $1-F$) occur over a range of moderate to large tunnel couplings, $t \simeq$ 5-20 GHz, that depends on the Hubbard repulsion parameter U. Our results also depend on the local field gradients ΔB_j, which determine the leakage rate. The values of ΔB_j considered here are typical for GaAs triple dots. The optimal fidelities in

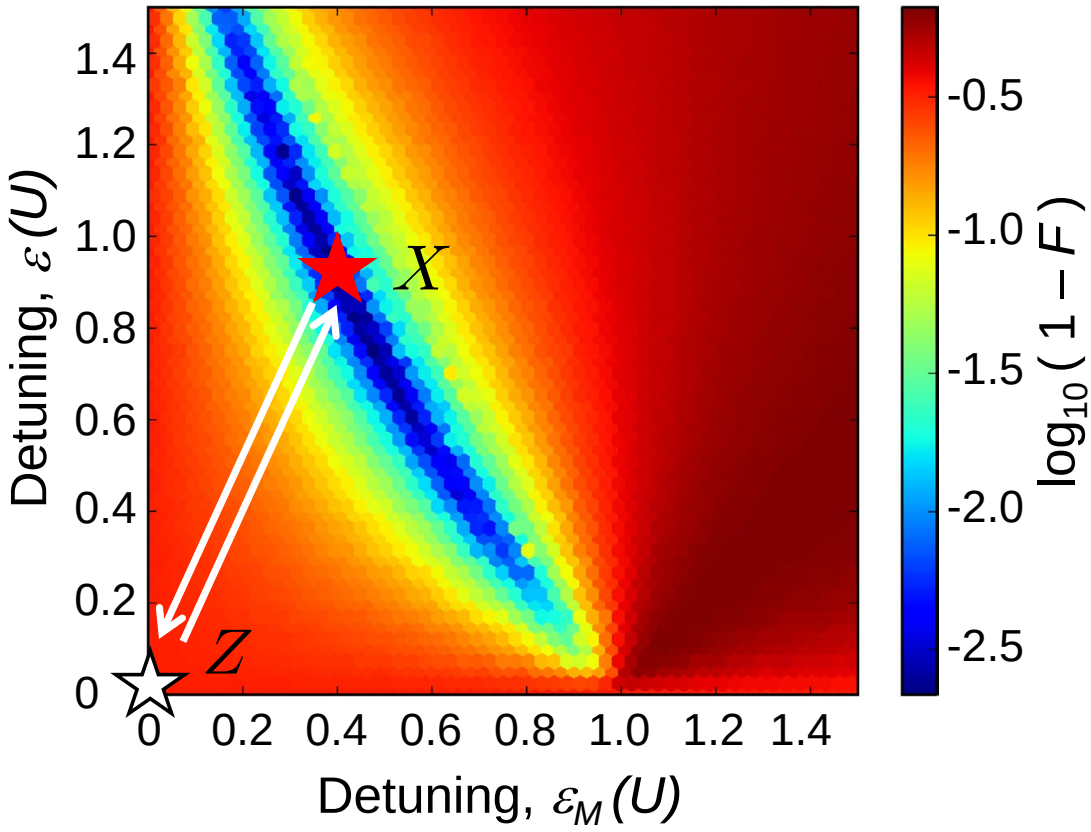

Figure 3.2: Fidelity of π-rotations around the axis $-(\hat{\mathbf{x}}+\hat{\mathbf{z}})/\sqrt{2}$, in the absence of noise, corresponding to step (i) of a three-step $X(\pi)$ rotation protocol [80], for $t = 5$ GHz. The red star indicates the optimal values of ε and ε_M.

Fig. 3.3 3.4 occur on a plateau, whose value is largely determined by the detuning noise. This is not the same conclusion reached in [73], where fidelity limits were attributed to nuclear noise. We speculate that those experiments were performed at lower t, below the plateau, where nuclear noise predominates. We emphasize that larger t should be used to achieve maximal fidelities.

Our most important results are obtained by comparing the maximal fidelities of $X(\pi)$ and $Z(\pi)$ rotations. We find that X-rotations have maximum fidelities ∼20 times worse than Z-rotations, which can be directly attributed to the fact that X-rotations occur away from the sweet spot, while Z-rotations occur at the sweet spot. The degradation of X-rotations is most noticeable for large t, where the fidelity is dominated by charge noise. Measurements

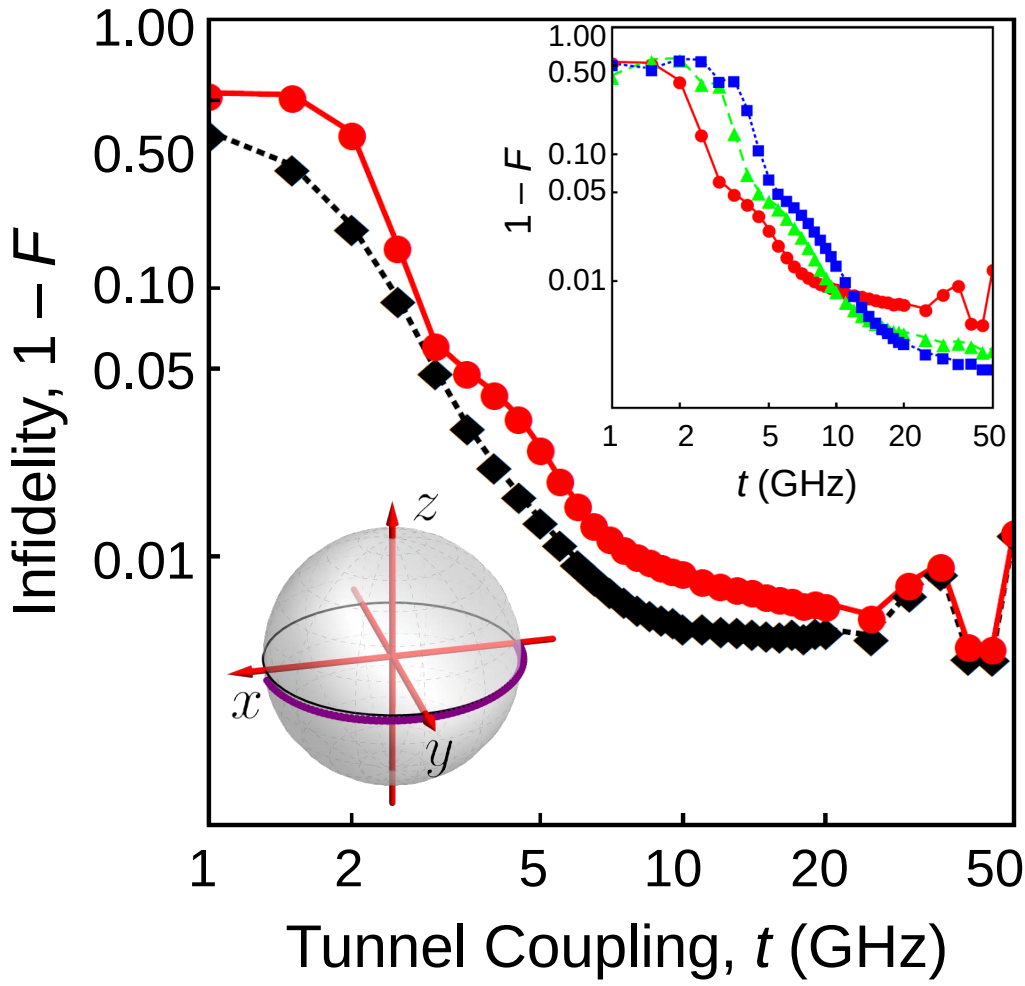

Figure 3.3: $Z(\pi)$ rotations. Circles include fast and slow detuning fluctuations, while the longitudinal magnetic field gradients are held fixed at $\Delta B_2^z - \Delta B_1^z = \Delta B_3^z - \Delta B_2^z = 3$ mT. Diamonds include quasistatic fluctuations of the Overhauser fields and fast detuning noise, but no slow detuning fluctuations. Both solutions assume an onsite Coulomb repulsion of $U = 1$ meV. For small t, the fidelity is mainly limited by nuclear noise and leakage into state $|2\rangle$, while for large t, the fidelity plateau is mainly limited by charge noise. For very large t, leakage into the excited charge states causes fidelity oscillations that are nearly independent of nuclear noise B. The lower inset shows the evolution of the density matrix projected onto the Bloch sphere of the logical qubit for the tunnel coupling $t = 10$ GHz; the small, rapid oscillations are caused by leakage. The upper inset shows results of averaging over detuning noise for $U = 1$ meV (circles, as in the main figure), $U = 2$ meV (triangles), and $U = 3$ meV (squares), with larger U yielding higher maximum fidelities.

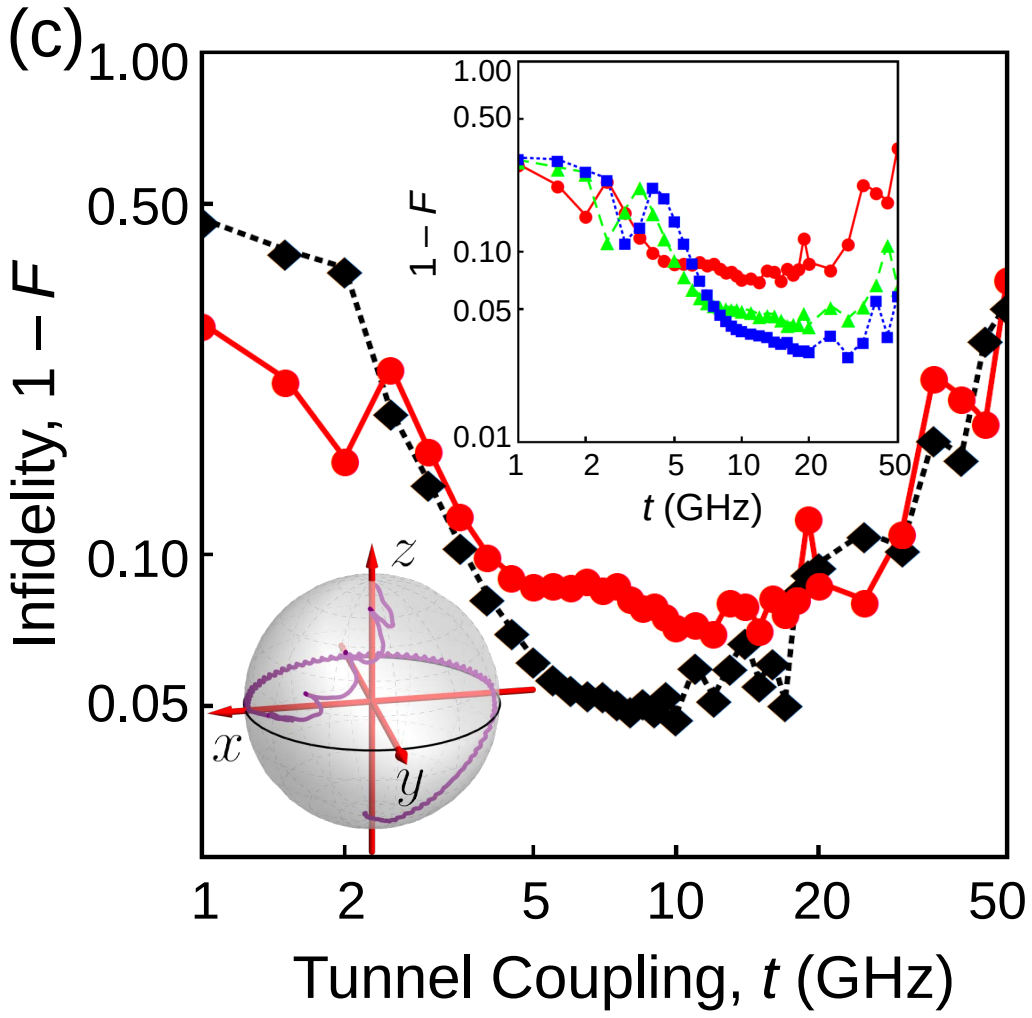

Figure 3.4: Final fidelity of $X(\pi)$ rotations, via the three-step protocol, where step (i) occurs at the red star in (b), step (ii) occurs at the white star ($\varepsilon = \varepsilon_M = 0$), and step (iii) occurs at the red star. The circles and diamonds have the same meaning as in 3.3. Here, the fidelity-limiting mechanisms are similar to 3.3, with a much stronger suppression of the fidelity at large t, due to leakage and charge noise. The insets are also defined as in 3.3. Note the large leakage oscillations during steps (i) and (iii) of the protocol.

of the quantum dot hybrid qubit show a similar degradation of coherence away from a sweet spot [88, 89]. This suggests that AC gating techniques could yield better fidelities than the DC pulsing techniques studied here, because the detuning is always centered at the sweet spot [74]. Indeed, recent experiments on the exchange-only qubit have employed such a strategy [90]. On the other hand, AC methods tend to produce somewhat slower gates, for which nuclear noise could be a problem.

Finally, we note that our analysis has focused on GaAs quantum dot devices, where nuclear noise is known to be important. For Si-based devices, especially isotopically purified ^{28}Si, the nuclear noise can be very small. As a result, Si devices should yield better fidelities for DC pulsed gates, especially in the low-t regime. (See B.) At higher t, where nuclear noise is not predominant, Si and GaAs exchange-only qubits should have similar fidelities.

We thank Z. Shi, X. Wu, K. Rudinger, J. Gamble, and C. Wong for helpful discussions. We also thank the HEP, Condor, and CHTC groups at UW-Madison for computational support. This work was supported in part by ARO (W911NF0910393), NSF (PHY-1104660 and PHY-1104672), UW-Madison (150 486700 4), and by the United States Department of Defense. The views and conclusions contained in this paper are those of the authors and should not be interpreted as representing the official policies, either expressed or implied, of the US Government.

Chapter 4

Separability Probability

4.1 Introduction

The surprising efficacy of complex numbers in describing the physical world has led to persistent speculation that quaternions might also serve as a fruitful foundation of physical theories. Quaternions resemble the complex numbers in forming a division ring: they are the richest such number system that has the very restrictive unique division property (Frobenius). Thus there is a natural mathematical progression from the real to the complex to the quaternionic numbers. We might ask if there is a corresponding natural progression also in physical theories that use these numbers.

Real numbers are sufficient to completely describe rebits, physical objects with two degrees of freedom whose 2×2 density matrices are symmetric real matrices. Complex numbers describe the usual qubits that have 2×2 complex Hermitian density matrices. Quaterbits are described by 2×2 density matrices with quaternionic entries. These matrices are Hermitian in the sense that the transpose is the quaternionic conjugate. The conjugate of a quaternion $h = a + i_h b + jc + kd$ is $\overline{h} = a - i_h b - jc - kd$. a, b, c, d are real and Hamilton's symbols i_h, j, k satisfy $i_h^2 = j^2 = k^2 = -1, i_h j = -j i_h = k$, etc. The density matrices are positive and have unit trace in all cases.

Recently, there has been some interesting mathematical work that gives some indication

of such a natural progression in the properties of these density matrices. This progression arises in the context of considering correlations in bipartite systems, i.e., in the 4×4 density matrices ρ that describe a pair of physical objects. Two objects A and B are said to be separable if ρ may be written as

$$\rho = \sum_i p_i \ \rho_i^A \otimes \rho_i^B \tag{4.1}$$

where the real numbers p_i satisfy $p_i \geq 0$ and $\sum_i p_i = 1$. ρ_i^A and ρ_i^B are 2×2 density matrices that refer to the 2 objects individually. Clearly this definition makes sense in all three number systems, as do the positivity and trace conditions.

Now there is a very fundamental question, first proposed in [91]: what proportion P of bipartite systems are separable? There is an intriguing conjecture that the formula

$$P(\alpha) = \sum_{i=0}^{\infty} f(\alpha + i), \tag{4.2}$$

where

$$f(\alpha) = \frac{q(\alpha)\, 2^{-4\alpha-6} \Gamma\left(3\alpha + \frac{5}{2}\right) \Gamma(5\alpha + 2)}{3\Gamma(\alpha + 1)\, \Gamma(2\alpha + 3)\, \Gamma\left(5\alpha + \frac{13}{2}\right)}, \tag{4.3}$$

with

$$\begin{aligned} q(\alpha) = {} & 185000\alpha^5 + 779750\alpha^4 + 1289125\alpha^3 \\ & + 1042015\alpha^2 + 410694\alpha + 63000, \end{aligned} \tag{4.4}$$

which for simple integral and half-odd-integral values of α gives results that are close to rational numbers with fairly small denominators, and that the rational numbers $P(1/2)$ gives the proportion of separable 2-rebit states, and $P(1)$ gives the proportion of separable 2-qubit states. This remarkable result [92, 93] comes from the computation of moments such as $\left\langle |\rho|^n \ \left|\rho^{PT}\right| \right\rangle$, an application of Zeilberger's algorithm [94], and numerical evaluation of Eq. 4.2 to thousands of decimal places. Here the angle brackets refer to an average over all physical states (i.e., those that satisfy positivity and have unit trace), and the straight brackets denote the determinant. The average is defined using the measure induced by the Hilbert-Schmidt metric on the space of density matrices. As we shall see, the $\alpha = 1$ and

$\alpha = 1/2$ conjectures are extremely well-supported. So it is natural to ask if higher values of α have a physical interpretation. In this paper, we shall focus on the possibility that $\alpha = 2$ corresponds to quaterbits (quaternion-based bits), though we also present computations for qubits and rebits. Our approach is to compute $P(\alpha)$ by a Monte Carlo method.

4.2 Qubits

For qubits, the conjecture based on Eq. 4.2 gives

$$P(1) = \frac{8}{33} = 0.\overline{24},$$

where the overbar indicates a repeating decimal.

This conjecture was also supported by numerical evidence [21], with Monte Carlo simulations yielding

$$P_{est}(1) = 0.2424 \pm 0.0002.$$

This earlier Monte Carlo work used the condition of zero concurrence for separability [47, 48]. This is equivalent to the Peres-Horodecki Criterion (PHC) [95, 96] which states that to be separable, it is necessary and sufficient for the partial transpose ρ^{PT} of the density matrix ρ to be positive. In the 2-qubit case, the 4×4 density matrix can be written as

$$\rho = \frac{1}{4} I_4 + \frac{1}{4} \sum_{i,j=0}^{3} n_{ij} (\sigma_i \otimes \sigma_j), \tag{4.5}$$

where I_n is the $n \times n$ identity matrix, $\sigma_0 = I_2$, and the σ_i are the Pauli matrices. The sum excludes the $i = j = 0$ term, and n_{ij} is thus a real 15-vector. We can use Euclidean measure to define probabilities in the space, which is equivalent to the Hilbert-Schmidt measure. The allowed values of n_{ij} form a compact and convex subset of R^{15} whose boundary is set by the condition thatρ is positive. This set is the generalization of the familiar Bloch sphere for spin 1/2. Its shape has been described in at least a partial fashion [21, 97], and its volume has been computed [98]. It lies within the sphere given by $\sum_{i,j=0}^{3} n_{ij}^2 = 3/4$. The 15-ball of radius $\sqrt{3/4}$ is sampled uniformly, testing both positivity and the PHC, which yields $P(1)$.

The sampling method is taken from [99]. In [21], 5×10^{12} points were sampled. We have now reproduced this calculation, sampling 5×10^{11} points. The new result is

$$P_{est}(1) = 0.24243 \pm 0.00001.$$

Thus the numerical results strongly support the conjecture $P(1) = 8/33$.

4.3 Rebits

The progression aspect of the problem arises already when we consider the same problem for rebits. Rebits are obtained by setting $n_{02} = n_{12} = n_{32} = n_{20} = n_{21} = n_{23} = 0$, *i.e.*, omitting the imaginary generators in Eq. 4.5. Positivity still requires that $\sum n_{ij}^2 \leq 3/4$ for the coefficients of the nonzero generators. The conjecture is that

$$P(1/2) = \frac{29}{64} = 0.453125.$$

What is remarkable is that $P(1)$ and $P\left(\frac{1}{2}\right)$ are given by the same formula, changing only the parameter α. We have performed the Monte Carlo sampling for this case, testing positivity and the PHC for points in the 9-ball. The result is

$$P(1/2) = 0.45313 \pm 0.00001, \text{ while}$$
$$\frac{29}{64} = 0.453125.$$

We tested 5×10^{11} points. Hence the unified formula is well-confirmed by the numerical computations for both $\alpha = 1/2$ and $\alpha = 1$.

4.4 Quaterbits

Now we consider quaterbits. It is reasonable to conjecture that $\alpha = 2$ formula should give the separability ratio for this 26-dimensional case. The conjecture is:

$$P(2) = \frac{26}{323} \approx 0.080495.$$

We first note that the PHC has not been proven for this case - it is not known whether positivity of the partial transpose is equivalent to separability. Thus it is very interesting to

repeat the above calculations for this case. The 2×2 matrix representation of quaternions in which $h = a + i_h b + ic + id \rightarrow I_2 a + ib\sigma_x + ic\sigma_y + id\sigma_z$ will be useful. I_n is the $n \times n$ identity.

Two quaterbits are described by 4×4 density matrices ρ with quaternionic entries. These matrices are self adjoint. Writing the quaternions themselves as matrices we find

$$\rho - \frac{I_8}{8} = \rho' = \begin{pmatrix} AI_2 & q_0 & q_1 & q_2 \\ \overline{q}_0 & BI_2 & q_3 & q_4 \\ \overline{q}_1 & \overline{q}_3 & CI_2 & q_5 \\ \overline{q}_2 & \overline{q}_4 & \overline{q}_5 & DI_2 \end{pmatrix},$$

with

$$q_i = \begin{pmatrix} a_i - id_i & ib_i + c_i \\ ib_i - c_i & a_i + id_i \end{pmatrix}, \quad \overline{q}_i = \begin{pmatrix} a_i + id_i & -ib_i - c_i \\ -ib_i + c_i & a_i - id_i \end{pmatrix}.$$

We must have that $A+B+C+D = 0$. Defining $u = 2A+2B, v = 2A+2C, w = -2B-2C$ and

$$\lambda_{ijk} = \sigma_i \otimes \sigma_j \otimes \sigma_k$$

so that $Tr\ \lambda_{ijk}\lambda_{i'j'k'} = 8\ \delta_{ii'}\delta_{jj'}\delta_{kk'}$, we find, after a lengthy calculation:

$$\begin{aligned} \rho' = & u\lambda_{300} + v\lambda_{030} + w\lambda_{330} \\ & + \frac{1}{2}a_0\left(\lambda_{010} + \lambda_{310}\right) + \frac{1}{2}b_0\left(\lambda_{021} + \lambda_{321}\right) - \frac{1}{2}c_0\left(\lambda_{022} + \lambda_{322}\right) \\ & - \frac{1}{2}d_0\left(\lambda_{023} + \lambda_{323}\right) + \frac{1}{2}a_1\left(\lambda_{100} + \lambda_{130}\right) - \frac{1}{2}b_1\left(\lambda_{201} + \lambda_{231}\right) \\ & - \frac{1}{2}c_1\left(\lambda_{202} + \lambda_{232}\right) - \frac{1}{2}d_1\left(\lambda_{203} + \lambda_{233}\right) + \frac{1}{2}a_2\left(\lambda_{110} - \lambda_{220}\right) \\ & - \frac{1}{2}b_2\left(\lambda_{121} + \lambda_{211}\right) - \frac{1}{2}c_2\left(\lambda_{122} + \lambda_{212}\right) - \frac{1}{2}d_2\left(\lambda_{123} + \lambda_{213}\right) \\ & + \frac{1}{2}a_3\left(\lambda_{110} + \lambda_{220}\right) + \frac{1}{2}b_3\left(\lambda_{121} - \lambda_{211}\right) - \frac{1}{2}c_3\left(\lambda_{122} - \lambda_{212}\right) \\ & + \frac{1}{2}d_3\left(\lambda_{123} - \lambda_{213}\right) + \frac{1}{2}a_4\left(\lambda_{100} - \lambda_{130}\right) - \frac{1}{2}b_4\left(\lambda_{201} - \lambda_{231}\right) \\ & + \frac{1}{2}c_4\left(\lambda_{202} - \lambda_{232}\right) - \frac{1}{2}d_4\left(\lambda_{023} - \lambda_{233}\right) + \frac{1}{2}a_5\left(\lambda_{010} - \lambda_{310}\right) \\ & - \frac{1}{2}b_5\left(\lambda_{021} - \lambda_{321}\right) + \frac{1}{2}c_5\left(\lambda_{022} - \lambda_{322}\right) - \frac{1}{2}d_5\left(\lambda_{023} - \lambda_{323}\right) \end{aligned}$$

Thus

$$\rho' = \sum_{ijk}{}' n_{ijk}\lambda_{ijk},$$

where the sum Σ' runs only over the combinations

$$\begin{aligned}\{ijk\} = &\{300\},\{030\},\{330\},\{010\},\{310\},\{021\},\\ &\{321\},\{022\},\{322\},\{023\},\{323\},\{100\},\\ &\{130\},\{201\},\{231\},\{202\},\{232\},\{203\},\\ &\{233\},\{110\},\{220\},\{121\},\{211\},\{122\},\\ &\{212\},\{123\},\{213\}.\end{aligned}$$

and positivity requires that

$$\sum_{ijk}{}' (n_{ijk})^2 \leq \frac{7}{64}.$$

To determine $P(2)$ numerically, we sample the 27-ball of radius $\sqrt{7/64}$ uniformly in the n_{ijk}, which, as stated above, is also uniform in the Hilbert-Schmidt metric. We test each point for PPT and positivity, giving an estimate $P_{est}(2)$. 5×10^{11} points are sampled in the Monte Carlo simulation. We find

$$P_{est}(2) = 0.08048 \pm 0.00005.$$

The numerical results give strong evidence in favor of the conjecture.

4.5 Conclusion

Quaternionic quantum mechanics has been investigated in detail. It can only describe the observed universe if some superselection rules are added [100]. Rebits do not have a rich enough mathematical structure to describe the real world - it would be very difficult to see how a rebit could display Ramsey fringes, for example, since the whole Bloch sphere is required for the dynamics. Qubits seem to be about right, of course. But it is remarkable that some mathematical structures overarch the three possibilities. The separability probability formula in Eq. 4.2 seems to be one of these.

We thank Dong Zhou for useful discussions. We thank P. B. Slater and K. Zyczkowski for helpful communications. We also thank the HEP, Condor, and CHTC groups at UW-Madison for computational support.

Chapter 5

Conclusion

In this thesis, we have investigated several different aspects of quantum computing problems, including applications, implementations and also the fundamentals. We provide some interesting results and new insights on each topic we've covered.

The first major topic we explored in detail is spin bus in chapter 2. We discussed the challenges need to be overcome in modern quantum computing when most practical implementations are already in a stage of scaling up. We extend the previous work on this subject and develop a new concept "mediated gates" using a spin bus to provide a viable solution to this problem. It usually improves the circuit efficiency significantly compared to conventional serial method when generating useful entanglement states, or arbitrary multi-qubit unitary gates. We discuss our method on how to approach and dissect such problems and build a complete toolbox dedicated for solving this type of problems. Specifically, we listed the "step-by-step recipes" for the generation of several resources of particular importance for quantum computing, like Bell state, W-state, GHZ-state, and CNOT, Toffoli gates. We show how much it improves upon conventional method in terms of circuit depth, which makes it more robust against noise and more likely to achieve high fidelity to meet practical needs.

Chapter 3 delves into issues in the effort of physically implementing accurate single qubit operations, which is the building block for all quantum computation schemes. We

primarily focus on the exchange-only logical qubit in a semiconductor triple quantum dot, inspired by the very active and fast developing experiments on this topic. We try to improve the overall quality of gate operations on such encoded qubit mainly by doing two things. First, tune the device and operate at the optimal working point, the "sweet spot". Second, optimize the pulse sequence in the parameter space to realize the rotation in an optimal way.

The idea of operating the qubit at its "sweet spot" of the energy level diagram has emerged as a widely used tool to provide protection for the encoded qubits against charge noise, such as in the context of singlet-triplet qubit [101, 102] and hybrid qubit [89]. Our work confirms that it works well for exchange-only qubit as well in a similar fashion. Compare to other implementations of logical encoded qubits, which has only one detuning parameter to operate on, there are two independent detuning parameters for exchange-only qubit. We discover that there's a "true sweet spot" for both detunings for exchange-only qubit, and it indeeds mitigate the effect of charge noise.

Due to the nature of the logical qubit rotation, for some operations, you have to operate away from the "sweet spot", such as in a DC pulsed gate sequence. We demonstrate how to optimize the tunable parameters to improve the fidelity in such cases. The optimization is conducted based on very practical estimation of the device, such as the strength of the nuclear bath and charge noise. And our calculation will point out the optimal fidelity we could anticipate when conducting such operations.

Finally, in chapter 4, we turn to the more fundamental questions in quantum computing, the entanglement properties of two partite systems. We investigate the geometrical structure of physical states, separable states and entangled states and compute the probability that a bipartite quantum state is separable by Monte Carlo sampling. We expand upon our previous work on two qubits [21], and calculate the separability probability for both two rebits and two quaterbits systems. Our numerical results match the analytical conjecture almost perfectly for such three different cases, which is surprisingly interesting and might indicate something more fundamental about entanglement space that we don't

quite understand yet.

Much effort has been devoted in the study of quaterbit system, in which case the Peres-Horodecki Criterion for separability has not been proven yet. So, we are actually testing a double-conjecture here by conducting similar separability probability calculation as in the two rebits and two qubits case. Our numerical results seems to support both. First, Peres-Horodecki Criterion is still a valid separability criterion for quaterbit. Second, the analytical conjecture for general separability probability formula still works for two quaterbits case.

Appendix A

Supplemental information for Chapter 2

A.1 Effective Hamiltonian of Odd Size Bus

Hamiltonian

Here we consider the Hamiltonian of the bus plus external qubits system

$$H = H_0 + H' = J_b \sum_{j=1}^{N-1} \mathbf{s}_j \cdot \mathbf{s}_{j+1} + \sum_{j=1}^{N} J_j \mathbf{s}_j \cdot \mathbf{S}_j, \tag{A.1}$$

where $\mathbf{s}_j$ represent bus internal spins, $\mathbf{S}_j$ represent external spins. J_b is the uniform bus internal coupling constant, and J_j is the coupling between the j^{th} bus internal node and the j^{th} external spin. We consider the case $J_j \ll J_b$, so that we could treat the 2^{nd} term as perturbation.

We use the eigenstates of H_0 as our basis states. Assume we have a subspace $\mathbb{D}_A$ spanned by a set of basis states with similar energies. Here $\mathbb{D}_A$ corresponds to the bus ground state manifold. The complementary subspace $\mathbb{D}_B$, excited states manifold, is spanned by basis states with energies well separated from the energies of the basis states of $\mathbb{D}_A$. The

Schrödinger equation for the eigenvalue problem is, in a matrix form,

$$\begin{pmatrix} \mathbf{H}_{AA} & \mathbf{H}_{AB} \\ \mathbf{H}_{BA} & \mathbf{H}_{BB} \end{pmatrix} \begin{pmatrix} \mathbf{a}_A \\ \mathbf{a}_B \end{pmatrix} = \varepsilon \begin{pmatrix} \mathbf{a}_A \\ \mathbf{a}_B \end{pmatrix}. \tag{A.2}$$

1^{st} order term

Up to the 2^{nd} order term, the effective Hamiltonian of the ground state manifold is given by

$$(\mathbf{H}_{\text{eff}})_{AA} = \overline{\mathbf{H}}^{(0)}_{AA} + \overline{\mathbf{H}}^{(1)}_{AA} + \overline{\mathbf{H}}^{(2)}_{AA} \tag{A.3}$$

$$= (\mathbf{H}_0)_{AA} + \mathbf{H'}_{AA} + \frac{i}{2}(\mathbf{H'}_{AB}\mathbf{S}^{(1)}_{BA} - \mathbf{S}^{(1)}_{AB}\mathbf{H'}_{BA}), \tag{A.4}$$

where $\mathbf{S}^{(1)}_{AB}$ and $\mathbf{S}^{(1)}_{BA}$ are

$$\mathbf{S}^{(1)}_{kl} = \frac{i\mathbf{H'}_{kl}}{\varepsilon^{(0)}_k - \varepsilon^{(0)}_l}, \qquad \forall k \in \mathbb{D}_A, \quad \forall l \in \mathbb{D}_B. \tag{A.5}$$

By the hermiticity of $\mathbf{S}$,

$$\mathbf{S}^{(1)}_{lk} = (\mathbf{S}^{(1)}_{lk})^* = \frac{i\mathbf{H'}_{lk}}{\varepsilon^{(0)}_l - \varepsilon^{(0)}_k}, \qquad \forall k \in \mathbb{D}_A, \quad \forall l \in \mathbb{D}_B. \tag{A.6}$$

We've already known that the 0^{th} order term $\overline{\mathbf{H}}^{(0)}_{AA}$ and the 1^{st} order term $\overline{\mathbf{H}}^{(1)}_{AA}$ [42],

$$\overline{\mathbf{H}}^{(0)}_{AA} = \varepsilon_0 \mathbb{1}_b = \varepsilon_0 |0_b\rangle\langle 0_b| = \varepsilon_0 |\Uparrow\rangle\langle\Uparrow|, \tag{A.7}$$

$$\overline{\mathbf{H}}^{(1)}_{AA} = \sum_{j=1}^{N} \tilde{J}^{(1)}_j \mathbf{S}_b \cdot \mathbf{S}_j, \tag{A.8}$$

where the subscript b means bus, and ε_0 is the bus ground state energy. The 1^{st} order effective coupling constant $\tilde{J}^{(1)}_j$ is

$$\tilde{J}^{(1)}_j = J_j \langle 0_b | s^z_j | 0_b \rangle = J_j \langle \Uparrow | s^z_j | \Uparrow \rangle. \tag{A.9}$$

2^{nd} order term

$$\overline{\mathbf{H}}^{(2)}_{AA} = \frac{i}{2}(\mathbf{H'}_{AB}\mathbf{S}^{(1)}_{BA} - \mathbf{S}^{(1)}_{AB}\mathbf{H'}_{BA}). \tag{A.10}$$

For $\forall k, k' \in \mathbb{D}_A, \forall l \in \mathbb{D}_B$, we have

$$\begin{aligned}
\overline{\mathbf{H}}^{(2)}_{kk'} &= \frac{i}{2}\langle k|\mathbf{H'}_{AB}\mathbf{S}^{(1)}_{BA} - \mathbf{S}^{(1)}_{AB}\mathbf{H'}_{BA}|k'\rangle && \text{(A.11)}\\
&= \frac{i}{2}\sum_l(\langle k|\mathbf{H'}_{AB}|l\rangle\langle l|\mathbf{S}^{(1)}_{BA}|k'\rangle - \langle k|\mathbf{S}^{(1)}_{AB}|l\rangle\langle l|\mathbf{H'}_{BA}|k'\rangle)\\
&= \frac{i}{2}\sum_l(\mathbf{H'}_{kl}\frac{i\mathbf{H'}_{lk'}}{\varepsilon^{(0)}_l - \varepsilon^{(0)}_{k'}} - \frac{i\mathbf{H'}_{kl}}{\varepsilon^{(0)}_k - \varepsilon^{(0)}_l}\mathbf{H'}_{lk'}) \qquad (\varepsilon^{(0)}_k = \varepsilon^{(0)}_{k'})\\
&= \sum_l \frac{\mathbf{H'}_{kl}\mathbf{H'}_{lk'}}{\varepsilon^{(0)}_k - \varepsilon^{(0)}_l}, \qquad \forall l \in \mathbb{D}_B. && \text{(A.12)}
\end{aligned}$$

We could always write the state k, k', l in terms of the bus spin state λ and external spin state $\{\sigma_j\}$,

$$|k\rangle = |\lambda_b; \{\sigma_j\}\rangle, \tag{A.13}$$

$$|k'\rangle = |\lambda'_b; \{\sigma'_j\}\rangle, \tag{A.14}$$

$$|l\rangle = |\lambda_l; \{\sigma''_j\}\rangle. \tag{A.15}$$

$$
\begin{aligned}
\overline{\mathbf{H}}^{(2)}_{kk'} &= \sum_{l} \frac{\mathbf{H'}_{kl}\mathbf{H'}_{lk'}}{\varepsilon^{(0)}_{k} - \varepsilon^{(0)}_{l}} \\
&= \sum_{\lambda_l;\{\sigma''_j\}} \frac{1}{\varepsilon^{(0)}_{k} - \varepsilon^{(0)}_{l}} \langle \lambda_b;\{\sigma_j\}|\mathbf{H'}|\lambda_l;\{\sigma''_j\}\rangle\langle\lambda_l;\{\sigma''_j\}|\mathbf{H'}|\lambda'_b;\{\sigma'_j\}\rangle \\
&= \sum_{jj'} \sum_{\lambda_l;\{\sigma''_j\}} \frac{J_j J_{j'}}{\varepsilon^{(0)}_{k} - \varepsilon^{(0)}_{l}} \langle \lambda_b;\{\sigma_j\}|\mathbf{s_j}\cdot\mathbf{S_j}|\lambda_l;\{\sigma''_j\}\rangle\langle\lambda_l;\{\sigma''_j\}|\mathbf{s_{j'}}\cdot\mathbf{S_{j'}}|\lambda'_b;\{\sigma'_j\}\rangle \\
&= \sum_{jj'} \sum_{\lambda_l;\{\sigma''_j\}} \frac{J_j J_{j'}}{\varepsilon^{(0)}_{k} - \varepsilon^{(0)}_{l}} \langle \lambda_b|\mathbf{s_j}|\lambda_l\rangle\cdot\langle\{\sigma_j\}|\mathbf{S_j}|\{\sigma''_j\}\rangle\langle\lambda_l|\mathbf{s_{j'}}|\lambda'_b\rangle\cdot\langle\{\sigma''_j\}|\mathbf{S_{j'}}|\{\sigma'_j\}\rangle \\
&= \sum_{jj'} \sum_{\lambda_l;\{\sigma''_j\}} \frac{J_j J_{j'}}{\varepsilon^{(0)}_{k} - \varepsilon^{(0)}_{l}} \sum_{\alpha,\beta=x,y,z} \langle\lambda_b|\ s^{\alpha}_{j}|\lambda_l\rangle\langle\{\sigma_j\}|\ S^{\alpha}_{j}|\{\sigma''_j\}\rangle\langle\lambda_l|\ s^{\beta}_{j'}|\lambda'_b\rangle\langle\{\sigma''_j\}|\ S^{\beta}_{j'}|\{\sigma'_j\}\rangle \\
&= \sum_{jj'}\sum_{\lambda_l} \frac{J_j J_{j'}}{\varepsilon^{(0)}_{k} - \varepsilon^{(0)}_{l}} \sum_{\alpha,\beta=x,y,z} \langle\lambda_b|\ s^{\alpha}_{j}|\lambda_l\rangle\langle\lambda_l|\ s^{\beta}_{j'}|\lambda'_b\rangle\langle\{\sigma_j\}|\ S^{\alpha}_{j}S^{\beta}_{j'}|\{\sigma'_j\}\rangle. \qquad \text{(A.16)}
\end{aligned}
$$

$$
\overline{\mathbf{H}}^{(2)}_{AA} = \sum_{kk'} |k\rangle\overline{\mathbf{H}}^{(2)}_{kk'}\langle k'| \qquad \text{(A.17)}
$$

$$
\begin{aligned}
&= \sum_{\lambda_b;\{\sigma_j\}} \sum_{\lambda'_b;\{\sigma'_j\}} |\lambda_b;\{\sigma_j\}\rangle\overline{\mathbf{H}}^{(2)}_{kk'}\langle\lambda'_b;\{\sigma'_j\}| \\
&= \sum_{\lambda_b;\{\sigma_j\}} \sum_{\lambda'_b;\{\sigma'_j\}} |\lambda_b;\{\sigma_j\}\rangle \sum_{jj'}\sum_{\lambda_l} \frac{J_j J_{j'}}{\varepsilon^{(0)}_{k} - \varepsilon^{(0)}_{l}} \times \\
&\qquad\qquad \sum_{\alpha,\beta} \langle\lambda_b|\ s^{\alpha}_{j}|\lambda_l\rangle\langle\lambda_l|\ s^{\beta}_{j'}|\lambda'_b\rangle\langle\{\sigma_j\}|\ S^{\alpha}_{j}S^{\beta}_{j'}|\{\sigma'_j\}\rangle\langle\lambda'_b;\{\sigma'_j\}| \\
&= \sum_{\lambda_b\lambda'_b}\sum_{jj'}\sum_{\lambda_l} \frac{J_j J_{j'}}{\varepsilon^{(0)}_{k} - \varepsilon^{(0)}_{l}} \sum_{\alpha,\beta} \langle\lambda_b|\ s^{\alpha}_{j}|\lambda_l\rangle\langle\lambda_l|\ s^{\beta}_{j'}|\lambda'_b\rangle|\lambda_b\rangle\langle\lambda'_b|S^{\alpha}_{j}S^{\beta}_{j'} \\
&= \sum_{jj'}\sum_{\alpha,\beta}\sum_{\lambda_b\lambda'_b}\sum_{\lambda_l} \frac{J_j J_{j'}}{\varepsilon^{(0)}_{k} - \varepsilon^{(0)}_{l}} \langle\lambda_b|\ s^{\alpha}_{j}|\lambda_l\rangle\langle\lambda_l|\ s^{\beta}_{j'}|\lambda'_b\rangle|\lambda_b\rangle\langle\lambda'_b|S^{\alpha}_{j}S^{\beta}_{j'}. \qquad \text{(A.18)}
\end{aligned}
$$

Consider the state $|\lambda_b\rangle, |\lambda'_b\rangle$ could be $|\Uparrow\rangle$ or $|\Downarrow\rangle$, which gives 4 possible combinations. And α, β could be (x, y, z) or $(+, -, z)$, which gives 9 possible combinations. So in total, there will be 36 terms in the above summation. Here we expand those terms in terms of creation and annihilation operator $(+, -, z)$ by using

$$
\mathbf{s}_j \cdot \mathbf{S}_j = s^{\alpha}_{j} S^{\alpha}_{j} = \frac{1}{2}(s^{+}_{j}S^{-}_{j} + s^{-}_{j}S^{+}_{j}) + s^{z}_{j}S^{z}_{j}. \qquad \text{(A.19)}
$$

By carefully analyzing the total z component of angular momentum of each term, there are 10 non-zero terms,

$$\begin{aligned}\overline{\mathbf{H}}^{(2)}_{AA} = &\sum_{jj'} J_j J_{j'} \sum_{\lambda_l} \frac{1}{\varepsilon^{(0)}_k - \varepsilon^{(0)}_l} \times \\ &\Big(\frac{1}{4}\langle\Uparrow|s^+_j|\lambda_l\rangle\langle\lambda_l|s^-_{j'}|\Uparrow\rangle|\Uparrow\rangle\langle\Uparrow|S^-_j S^+_{j'} + \frac{1}{4}\langle\Downarrow|s^+_j|\lambda_l\rangle\langle\lambda_l|s^-_{j'}|\Downarrow\rangle|\Downarrow\rangle\langle\Downarrow|S^-_j S^+_{j'} \\ &+ \frac{1}{2}\langle\Uparrow|s^+_j|\lambda_l\rangle\langle\lambda_l|s^z_{j'}|\Downarrow\rangle|\Uparrow\rangle\langle\Downarrow|S^-_j S^z_{j'} + \frac{1}{4}\langle\Uparrow|s^-_j|\lambda_l\rangle\langle\lambda_l|s^+_{j'}|\Uparrow\rangle|\Uparrow\rangle\langle\Uparrow|S^+_j S^-_{j'} \\ &+ \frac{1}{4}\langle\Downarrow|s^-_j|\lambda_l\rangle\langle\lambda_l|s^+_{j'}|\Downarrow\rangle|\Downarrow\rangle\langle\Downarrow|S^+_j S^-_{j'} + \frac{1}{2}\langle\Downarrow|s^-_j|\lambda_l\rangle\langle\lambda_l|s^z_{j'}|\Uparrow\rangle|\Downarrow\rangle\langle\Uparrow|S^+_j S^z_{j'} \\ &+ \frac{1}{2}\langle\Uparrow|s^z_j|\lambda_l\rangle\langle\lambda_l|s^+_{j'}|\Downarrow\rangle|\Uparrow\rangle\langle\Downarrow|S^z_j S^-_{j'} + \frac{1}{2}\langle\Downarrow|s^z_j|\lambda_l\rangle\langle\lambda_l|s^-_{j'}|\Uparrow\rangle|\Downarrow\rangle\langle\Uparrow|S^z_j S^+_{j'} \\ &+ \langle\Uparrow|s^z_j|\lambda_l\rangle\langle\lambda_l|s^z_{j'}|\Uparrow\rangle|\Uparrow\rangle\langle\Uparrow|S^z_j S^z_{j'} + \langle\Downarrow|s^z_j|\lambda_l\rangle\langle\lambda_l|s^z_{j'}|\Downarrow\rangle|\Downarrow\rangle\langle\Downarrow|S^z_j S^z_{j'}\Big). \end{aligned} \tag{A.20}$$

Let's reorganize them into pairs as follows,

$$\begin{aligned}\overline{\mathbf{H}}^{(2)}_{AA} = &\sum_{jj'} J_j J_{j'} \sum_{\lambda_l} \frac{1}{\varepsilon^{(0)}_k - \varepsilon^{(0)}_l} \times \\ &\Big(\frac{1}{4}\langle\Uparrow|s^+_j|\lambda_l\rangle\langle\lambda_l|s^-_{j'}|\Uparrow\rangle|\Uparrow\rangle\langle\Uparrow|S^-_j S^+_{j'} + \frac{1}{4}\langle\Downarrow|s^-_j|\lambda_l\rangle\langle\lambda_l|s^+_{j'}|\Downarrow\rangle|\Downarrow\rangle\langle\Downarrow|S^+_j S^-_{j'} \\ &+ \frac{1}{4}\langle\Downarrow|s^+_j|\lambda_l\rangle\langle\lambda_l|s^-_{j'}|\Downarrow\rangle|\Downarrow\rangle\langle\Downarrow|S^-_j S^+_{j'} + \frac{1}{4}\langle\Uparrow|s^-_j|\lambda_l\rangle\langle\lambda_l|s^+_{j'}|\Uparrow\rangle|\Uparrow\rangle\langle\Uparrow|S^+_j S^-_{j'} \\ &+ \frac{1}{2}\langle\Uparrow|s^+_j|\lambda_l\rangle\langle\lambda_l|s^z_{j'}|\Downarrow\rangle|\Uparrow\rangle\langle\Downarrow|S^-_j S^z_{j'} + \frac{1}{2}\langle\Uparrow|s^z_j|\lambda_l\rangle\langle\lambda_l|s^+_{j'}|\Downarrow\rangle|\Uparrow\rangle\langle\Downarrow|S^z_j S^-_{j'} \\ &+ \frac{1}{2}\langle\Downarrow|s^-_j|\lambda_l\rangle\langle\lambda_l|s^z_{j'}|\Uparrow\rangle|\Downarrow\rangle\langle\Uparrow|S^+_j S^z_{j'} + \frac{1}{2}\langle\Downarrow|s^z_j|\lambda_l\rangle\langle\lambda_l|s^-_{j'}|\Uparrow\rangle|\Downarrow\rangle\langle\Uparrow|S^z_j S^+_{j'} \\ &+ \langle\Uparrow|s^z_j|\lambda_l\rangle\langle\lambda_l|s^z_{j'}|\Uparrow\rangle|\Uparrow\rangle\langle\Uparrow|S^z_j S^z_{j'} + \langle\Downarrow|s^z_j|\lambda_l\rangle\langle\lambda_l|s^z_{j'}|\Downarrow\rangle|\Downarrow\rangle\langle\Downarrow|S^z_j S^z_{j'}\Big). \end{aligned} \tag{A.21}$$

We could further simplify this expression by considering the following quantitative properties of the summation:

1. All the matrix elements, such as $\langle\Uparrow|s^+_j|\lambda_l\rangle$, are real numbers. The bus Hamiltonian is a real matrix. Under the spin configuration basis, we could always express the bus eigenstates, such as $|\Uparrow\rangle$, $|\Downarrow\rangle$, and $|\lambda_l\rangle$, in real vector form. Also, all the spin operators s^+_j, s^-_j, and s^z_j, can also be expressed in real matrix form under the same basis,

$$s^+ = \begin{pmatrix} 0 & 1 \\ 0 & 0 \end{pmatrix}, \quad s^- = \begin{pmatrix} 0 & 0 \\ 1 & 0 \end{pmatrix}, \quad s^z = \begin{pmatrix} 1 & 0 \\ 0 & -1 \end{pmatrix}. \tag{A.22}$$

so we have $\langle \Uparrow |s_j^+|\lambda_l\rangle = \langle \lambda_l|s_j^-|\Uparrow\rangle^* = \langle \lambda_l|s_j^-|\Uparrow\rangle$, etc.

2. We could exchange indices j and j' if needed, since they are dummy indices in the sum.

Sum over term 1 and term 2,

$$\begin{aligned}
&\sum_{jj'} J_j J_{j'} \sum_{\lambda_l} \frac{1}{\varepsilon_k^{(0)} - \varepsilon_l^{(0)}} \times \\
&\Big(\frac{1}{4}\langle \Uparrow |s_j^+|\lambda_l\rangle\langle\lambda_l|s_{j'}^-|\Uparrow\rangle|\Uparrow\rangle\langle\Uparrow|S_j^- S_{j'}^+ + \frac{1}{4}\langle\Downarrow|s_j^-|\lambda_l\rangle\langle\lambda_l|s_{j'}^+|\Downarrow\rangle|\Downarrow\rangle\langle\Downarrow|S_j^+ S_{j'}^-\Big) \\
=&\sum_{jj'} J_j J_{j'} \sum_{\lambda_l} \frac{1}{\varepsilon_k^{(0)} - \varepsilon_l^{(0)}} \times \\
&\Big(\frac{1}{4}\langle \Uparrow |s_j^+|\lambda_l\rangle\langle\lambda_l|s_{j'}^-|\Uparrow\rangle|\Uparrow\rangle\langle\Uparrow|S_j^- S_{j'}^+ + \frac{1}{4}\langle\Downarrow|s_j^-|\lambda_l\rangle\langle\lambda_l|s_{j'}^+|\Downarrow\rangle|\Downarrow\rangle\langle\Downarrow|S_j^- S_{j'}^+\Big) \\
=&\sum_{jj'} J_j J_{j'} \sum_{\lambda_l} \frac{1}{\varepsilon_k^{(0)} - \varepsilon_l^{(0)}} \frac{1}{4}\langle \Uparrow |s_j^+|\lambda_l\rangle\langle\lambda_l|s_{j'}^-|\Uparrow\rangle\Big(|\Uparrow\rangle\langle\Uparrow| + |\Downarrow\rangle\langle\Downarrow|\Big) S_j^- S_{j'}^+ \\
=&\sum_{jj'} J_j J_{j'} \sum_{\lambda_l} \frac{\langle \Uparrow |s_j^+|\lambda_l\rangle\langle\lambda_l|s_{j'}^-|\Uparrow\rangle}{4(\varepsilon_k^{(0)} - \varepsilon_l^{(0)})} \mathbb{1}_b S_j^- S_{j'}^+.
\end{aligned} \tag{A.23}$$

Notice that,

$$\langle \Uparrow |s_j^+|\lambda_l; s_z^{tot} = -\frac{1}{2}\rangle = \langle \Downarrow |s_j^-|\lambda_l; s_z^{tot} = \frac{1}{2}\rangle, \tag{A.24}$$

$$\langle \lambda_l; s_z^{tot} = -\frac{1}{2}|s_{j'}^-|\Uparrow\rangle = \langle \lambda_l; s_z^{tot} = \frac{1}{2}|s_{j'}^+|\Downarrow\rangle. \tag{A.25}$$

Sum over term 3 and term 4,

$$\begin{aligned}
&\sum_{jj'} J_j J_{j'} \sum_{\lambda_l} \frac{1}{\varepsilon_k^{(0)} - \varepsilon_l^{(0)}} \times \\
&\Big(\frac{1}{4}\langle \Downarrow |s_j^+|\lambda_l\rangle\langle\lambda_l|s_{j'}^-|\Downarrow\rangle|\Downarrow\rangle\langle\Downarrow|S_j^- S_{j'}^+ + \frac{1}{4}\langle\Uparrow|s_j^-|\lambda_l\rangle\langle\lambda_l|s_{j'}^+|\Uparrow\rangle|\Uparrow\rangle\langle\Uparrow|S_j^+ S_{j'}^-\Big) \\
=&\sum_{jj'} J_j J_{j'} \sum_{\lambda_l} \frac{1}{\varepsilon_k^{(0)} - \varepsilon_l^{(0)}} \times \\
&\Big(\frac{1}{4}\langle \Downarrow |s_j^+|\lambda_l\rangle\langle\lambda_l|s_{j'}^-|\Downarrow\rangle|\Downarrow\rangle\langle\Downarrow|S_j^- S_{j'}^+ + \frac{1}{4}\langle\Uparrow|s_j^-|\lambda_l\rangle\langle\lambda_l|s_{j'}^+|\Uparrow\rangle|\Uparrow\rangle\langle\Uparrow|S_j^- S_{j'}^+\Big) \\
=&\sum_{jj'} J_j J_{j'} \sum_{\lambda_l} \frac{1}{\varepsilon_k^{(0)} - \varepsilon_l^{(0)}} \frac{1}{4}\langle \Uparrow |s_j^-|\lambda_l\rangle\langle\lambda_l|s_{j'}^+|\Uparrow\rangle\Big(|\Downarrow\rangle\langle\Downarrow| + |\Uparrow\rangle\langle\Uparrow|\Big) S_j^- S_{j'}^+ \\
=&\sum_{jj'} J_j J_{j'} \sum_{\lambda_l} \frac{\langle \Uparrow |s_j^-|\lambda_l\rangle\langle\lambda_l|s_{j'}^+|\Uparrow\rangle}{4(\varepsilon_k^{(0)} - \varepsilon_l^{(0)})} \mathbb{1}_b S_j^- S_{j'}^+.
\end{aligned} \tag{A.26}$$

Notice that,

$$\langle \Downarrow |s_j^+|\lambda_l; s_z^{tot} = -\frac{3}{2}\rangle = \langle \Uparrow |s_j^-|\lambda_l; s_z^{tot} = \frac{3}{2}\rangle, \tag{A.27}$$

$$\langle\lambda_l; s_z^{tot} = -\frac{3}{2}|s_{j'}^-|\Downarrow\rangle = \langle\lambda_l; s_z^{tot} = \frac{3}{2}|s_{j'}^+|\Uparrow\rangle. \tag{A.28}$$

Sum over term 5 and term 6,

$$\begin{aligned}
&\sum_{jj'} J_j J_{j'} \sum_{\lambda_l} \frac{1}{\varepsilon_k^{(0)} - \varepsilon_l^{(0)}} \times \\
&\Big(\frac{1}{2}\langle\Uparrow|s_j^+|\lambda_l\rangle\langle\lambda_l|s_{j'}^z|\Downarrow\rangle|\Uparrow\rangle\langle\Downarrow|S_j^- S_{j'}^z + \frac{1}{2}\langle\Uparrow|s_j^z|\lambda_l\rangle\langle\lambda_l|s_{j'}^+|\Downarrow\rangle|\Uparrow\rangle\langle\Downarrow|S_j^z S_{j'}^-\Big) \\
=&\sum_{jj'} J_j J_{j'} \sum_{\lambda_l} \frac{1}{\varepsilon_k^{(0)} - \varepsilon_l^{(0)}} \times \\
&\Big(\frac{1}{2}\langle\Uparrow|s_j^+|\lambda_l\rangle\langle\lambda_l|s_{j'}^z|\Downarrow\rangle|\Uparrow\rangle\langle\Downarrow|S_j^- S_{j'}^z + \frac{1}{2}\langle\Downarrow|s_j^-|\lambda_l\rangle\langle\lambda_l|s_{j'}^z|\Uparrow\rangle|\Uparrow\rangle\langle\Downarrow|S_j^- S_{j'}^z\Big) \\
=&\sum_{jj'} J_j J_{j'} \sum_{\lambda_l} \frac{1}{\varepsilon_k^{(0)} - \varepsilon_l^{(0)}} \times \\
&\frac{1}{2}\Big(\langle\Uparrow|s_j^+|\lambda_l\rangle\langle\lambda_l|s_{j'}^z|\Downarrow\rangle + \langle\Downarrow|s_j^-|\lambda_l\rangle\langle\lambda_l|s_{j'}^z|\Uparrow\rangle\Big)|\Uparrow\rangle\langle\Downarrow|S_j^- S_{j'}^z \\
=&0.
\end{aligned} \tag{A.29}$$

Notice that,

$$\langle\Uparrow|s_j^+|\lambda_l; s_z^{tot} = -\frac{1}{2}\rangle = \langle\Downarrow|s_j^-|\lambda_l; s_z^{tot} = \frac{1}{2}\rangle, \tag{A.30}$$

$$\langle\lambda_l; s_z^{tot} = -\frac{1}{2}|s_{j'}^z|\Downarrow\rangle = -\langle\lambda_l; s_z^{tot} = \frac{1}{2}|s_{j'}^z|\Uparrow\rangle. \tag{A.31}$$

Sum over term 7 and term 8,

$$\begin{aligned}
&\sum_{jj'} J_j J_{j'} \sum_{\lambda_l} \frac{1}{\varepsilon_k^{(0)} - \varepsilon_l^{(0)}} \times \\
&\Big(\frac{1}{2}\langle\Downarrow|s_j^-|\lambda_l\rangle\langle\lambda_l|s_{j'}^z|\Uparrow\rangle|\Downarrow\rangle\langle\Uparrow|S_j^+ S_{j'}^z + \frac{1}{2}\langle\Downarrow|s_j^z|\lambda_l\rangle\langle\lambda_l|s_{j'}^-|\Uparrow\rangle|\Downarrow\rangle\langle\Uparrow|S_j^z S_{j'}^+\Big) \\
=&\sum_{jj'} J_j J_{j'} \sum_{\lambda_l} \frac{1}{\varepsilon_k^{(0)} - \varepsilon_l^{(0)}} \times \\
&\Big(\frac{1}{2}\langle\Downarrow|s_j^-|\lambda_l\rangle\langle\lambda_l|s_{j'}^z|\Uparrow\rangle|\Downarrow\rangle\langle\Uparrow|S_j^+ S_{j'}^z + \frac{1}{2}\langle\Uparrow|s_j^+|\lambda_l\rangle\langle\lambda_l|s_{j'}^z|\Downarrow\rangle|\Downarrow\rangle\langle\Uparrow|S_j^+ S_{j'}^z\Big) \\
=&\sum_{jj'} J_j J_{j'} \sum_{\lambda_l} \frac{1}{\varepsilon_k^{(0)} - \varepsilon_l^{(0)}} \times \\
&\frac{1}{2}\Big(\langle\Downarrow|s_j^-|\lambda_l\rangle\langle\lambda_l|s_{j'}^z|\Uparrow\rangle + \langle\Uparrow|s_j^+|\lambda_l\rangle\langle\lambda_l|s_{j'}^z|\Downarrow\rangle\Big)|\Downarrow\rangle\langle\Uparrow|S_j^+ S_{j'}^z \\
=&0.
\end{aligned} \tag{A.32}$$

Notice that,

$$\langle \Downarrow |s_j^-|\lambda_l; s_z^{tot} = \frac{1}{2}\rangle = \langle \Uparrow |s_j^+|\lambda_l; s_z^{tot} = -\frac{1}{2}\rangle, \tag{A.33}$$

$$\langle \lambda_l; s_z^{tot} = \frac{1}{2}|s_{j'}^z| \Uparrow\rangle = -\langle \lambda_l; s_z^{tot} = -\frac{1}{2}|s_{j'}^z| \Downarrow\rangle. \tag{A.34}$$

Sum over term 9 and term 10,

$$\begin{aligned}
&\sum_{jj'} J_j J_{j'} \sum_{\lambda_l} \frac{1}{\varepsilon_k^{(0)} - \varepsilon_l^{(0)}} \times \\
&\Big(\langle \Uparrow |s_j^z|\lambda_l\rangle\langle\lambda_l|s_{j'}^z| \Uparrow\rangle| \Uparrow\rangle\langle \Uparrow |S_j^z S_{j'}^z + \langle \Downarrow |s_j^z|\lambda_l\rangle\langle\lambda_l|s_{j'}^z| \Downarrow\rangle| \Downarrow\rangle\langle \Downarrow |S_j^z S_{j'}^z\Big) \\
=&\sum_{jj'} J_j J_{j'} \sum_{\lambda_l} \frac{\langle \Uparrow |s_j^z|\lambda_l\rangle\langle\lambda_l|s_{j'}^z| \Uparrow\rangle}{\varepsilon_k^{(0)} - \varepsilon_l^{(0)}} \Big(| \Uparrow\rangle\langle \Uparrow | + | \Downarrow\rangle\langle \Downarrow |\Big) S_j^z S_{j'}^z \\
=&\sum_{jj'} J_j J_{j'} \sum_{\lambda_l} \frac{\langle \Uparrow |s_j^z|\lambda_l\rangle\langle\lambda_l|s_{j'}^z| \Uparrow\rangle}{\varepsilon_k^{(0)} - \varepsilon_l^{(0)}} \mathbb{1}_b S_j^z S_{j'}^z \\
=&\sum_{jj'} \tilde{J}_{j,j'}^{zz} S_j^z S_{j'}^z,
\end{aligned} \tag{A.35}$$

where

$$\tilde{J}_{j,j'}^{zz} = J_j J_{j'} \sum_{\lambda_l} \frac{\langle \Uparrow |s_j^z|\lambda_l\rangle\langle\lambda_l|s_{j'}^z| \Uparrow\rangle}{\varepsilon_k^{(0)} - \varepsilon_l^{(0)}}. \tag{A.36}$$

We used the fact that,

$$\langle \Uparrow |s_j^z|\lambda_l; s_z^{tot} = \frac{1}{2}\rangle = -\langle \Downarrow |s_j^z|\lambda_l; s_z^{tot} = -\frac{1}{2}\rangle, \tag{A.37}$$

$$\langle \lambda_l; s_z^{tot} = \frac{1}{2}|s_{j'}^z| \Uparrow\rangle = -\langle \lambda_l; s_z^{tot} = -\frac{1}{2}|s_{j'}^z| \Downarrow\rangle. \tag{A.38}$$

Put all the calculations above together, we get

$$\overline{\mathbf{H}}_{AA}^{(2)} = \sum_{jj'} J_j J_{j'} \sum_{\lambda_l} \frac{\langle \Uparrow |s_j^+|\lambda_l\rangle\langle\lambda_l|s_{j'}^-| \Uparrow\rangle + \langle \Uparrow |s_j^-|\lambda_l\rangle\langle\lambda_l|s_{j'}^+| \Uparrow\rangle}{4(\varepsilon_k^{(0)} - \varepsilon_l^{(0)})} S_j^- S_{j'}^+ + \sum_{jj'} \tilde{J}_{j,j'}^{zz} S_j^z S_{j'}^z. \tag{A.39}$$

Let's define

$$I_{j,j'} = \frac{\langle \Uparrow |s_j^+|\lambda_l\rangle\langle\lambda_l|s_{j'}^-| \Uparrow\rangle + \langle \Uparrow |s_j^-|\lambda_l\rangle\langle\lambda_l|s_{j'}^+| \Uparrow\rangle}{4(\varepsilon_k^{(0)} - \varepsilon_l^{(0)})}. \tag{A.40}$$

We could easily show that

$$I_{j,j'} = I_{j',j} = I(j, j', \lambda_l), \tag{A.41}$$

$$\overline{\mathbf{H}}_{AA}^{(2)} = \sum_{jj'} J_j J_{j'} \sum_{\lambda_l} I(j, j', \lambda_l) S_j^- S_{j'}^+ + \sum_{jj'} \tilde{J}_{j,j'}^{zz} S_j^z S_{j'}^z. \tag{A.42}$$

Recall that,

$$S^+ = S^x + iS^y, \tag{A.43}$$

$$S^- = S^x - iS^y. \tag{A.44}$$

So,

$$S_j^- S_{j'}^+ = S_j^x S_{j'}^x + S_j^y S_{j'}^y + i(S_j^x S_{j'}^y - S_j^y S_{j'}^x). \tag{A.45}$$

$$\overline{\mathbf{H}}_{AA}^{(2)} = \sum_{jj'} J_j J_{j'} \sum_{\lambda_l} I(j, j', \lambda_l)(S_j^x S_{j'}^x + S_j^y S_{j'}^y + i(S_j^x S_{j'}^y - S_j^y S_{j'}^x)) + \sum_{jj'} \tilde{J}_{j,j'}^{zz} S_j^z S_{j'}^z. \tag{A.46}$$

The cross term $i(S_j^x S_{j'}^y - S_j^y S_{j'}^x)$ will be gone after the sum over j and j',

$$\overline{\mathbf{H}}_{AA}^{(2)} = \sum_{jj'} J_j J_{j'} \sum_{\lambda_l} I(j, j', \lambda_l)(S_j^x S_{j'}^x + S_j^y S_{j'}^y) + \sum_{jj'} \tilde{J}_{j,j'}^{zz} S_j^z S_{j'}^z. \tag{A.47}$$

Let's define

$$\tilde{J}_{j,j'}^{xx} = \tilde{J}_{j,j'}^{yy} = J_j J_{j'} \sum_{\lambda_l} I(j, j', \lambda_l). \tag{A.48}$$

$$\overline{\mathbf{H}}_{AA}^{(2)} = \sum_{jj'} \tilde{J}_{j,j'}^{xx} (S_j^x S_{j'}^x + S_j^y S_{j'}^y) + \sum_{jj'} \tilde{J}_{j,j'}^{zz} S_j^z S_{j'}^z. \tag{A.49}$$

We are not breaking any symmetry here. So we could expect,

$$\tilde{J}_{j,j'}^{xx} = \tilde{J}_{j,j'}^{yy} = \tilde{J}_{j,j'}^{zz} = \tilde{J}_{j,j'}^{(2)}. \tag{A.50}$$

Then we get the final form of the 2^{nd} order effective Hamiltonian of odd size bus, which is just spin-spin interaction,

$$\overline{\mathbf{H}}_{AA}^{(2)} = \sum_{j \neq j'} \tilde{J}_{j,j'}^{(2)} \mathbf{S_j} \cdot \mathbf{S_{j'}}, \tag{A.51}$$

where the 2^{nd} order effective coupling constant $\tilde{J}_{j,j'}^{(2)}$,

$$\tilde{J}_{j,j'}^{(2)} = J_j J_{j'} \sum_{\lambda_l} \frac{\langle \Uparrow | s_j^z | \lambda_l \rangle \langle \lambda_l | s_{j'}^z | \Uparrow \rangle}{\varepsilon_k^{(0)} - \varepsilon_l^{(0)}} \tag{A.52}$$

$$= -J_j J_{j'} \sum_{\lambda_l} \frac{\langle \Uparrow | s_j^z | \lambda_l \rangle \langle \lambda_l | s_{j'}^z | \Uparrow \rangle}{\varepsilon_l^{(0)} - \varepsilon_k^{(0)}}. \tag{A.53}$$

All the above calculations are supported by numerical simulations.

A.2 EXISTENCE PROOF FOR $\mathbb{U}_2$

Here, we prove that the gate $\mathbb{U}_2$, presented in Eq. (2.3) of the main text (and its family), represents the only solutions to the mediated gate problem for two qubits. For convenience, we adopt slightly different notation than in the main text, as indicated in Fig. A.1. Spins 1 and 3 are the two nonproximal qubits, while spin 2 is the central ancilla qubit.

Figure A.1: Two-qubit mediated gate geometry. Here, ancilla qubit 2 mediates gate $\mathbb{U}_2$, which acts on qubits 1 and 3.

We consider the following Hamiltonian for a linear three-qubit array:

$$H = J_a\, \mathbf{s}_1 \cdot \mathbf{s}_2 + J_b\, \mathbf{s}_2 \cdot \mathbf{s}_3, \tag{A.54}$$

where $\mathbf{s}_j$ is the spin operator for qubit j. In principle, J_a and J_b may take any value. However, we limit our search to the case where the couplings are turned on and off simultaneously. J_a and J_b are therefore constant throughout the gate operation. The goal of this Appendix is to identify specific relations between J_a and J_b that lead to mediated gates.

We make use of the identity [103, 104]

$$4\, \mathbf{s}_i \cdot \mathbf{s}_j = 2p^{ij} - I, \tag{A.55}$$

where p^{ij} is the SWAP (i.e., transposition) operator between spin i and spin j, and I is the two-qubit identity operator. Hamiltonian (A.54) can then be rewritten as

$$H = \frac{1}{2}(J_a p^{12} + J_b p^{23}) - \frac{1}{4}(J_a + J_b). \tag{A.56}$$

The time evolution operator is given by

$$\begin{aligned} U(t) &= e^{-iHt} \\ &= e^{i(J_a+J_b)t/4} e^{-iQJ_bt/2} \\ &= e^{i(J_a+J_b)t/4} \sum_{n=0}^{\infty} \frac{(-iJ_bt/2)^n}{n!} Q^n, \end{aligned} \tag{A.57}$$

where $\hbar = 1$ and we have defined

$$Q \equiv p^{23} + Jp^{12}, \tag{A.58}$$

with $J = J_a/J_b$. Since p^{23} and p^{12} are generators of the symmetric group S_3, we may expand Q^n in terms of the S_3 group elements:

$$Q^n = a_n p^{231} + b_n p^{312} + c_n p^{12} + d_n p^{13} + e_n p^{23} + f_n I. \tag{A.59}$$

Here, p^{ijk} is the tripartite, cyclic permutation operator.

Table A.1: Cayley table for the symmetric group S_3.

	I	p^{12}	p^{13}	p^{23}	p^{231}	p^{312}
I	I	p^{12}	p^{13}	p^{23}	p^{231}	p^{312}
p^{12}	p^{12}	I	p^{231}	p^{312}	p^{13}	p^{23}
p^{13}	p^{13}	p^{312}	I	p^{231}	p^{23}	p^{12}
p^{23}	p^{23}	p^{231}	p^{312}	I	p^{12}	p^{13}
p^{231}	p^{231}	p^{23}	p^{12}	p^{13}	p^{312}	I
p^{312}	p^{312}	p^{13}	p^{23}	p^{12}	I	p^{231}

The full set of S_3 group operations is listed in Table. A.1. We then deduce the recursion relations for $Q^{n+1} = QQ^n$:

$$a_{n+1} = c_n + Jd_n, \tag{A.60}$$

$$b_{n+1} = d_n + Je_n, \tag{A.61}$$

$$c_{n+1} = a_n + Jf_n, \tag{A.62}$$

$$d_{n+1} = b_n + Ja_n, \tag{A.63}$$

$$e_{n+1} = f_n + Jb_n, \tag{A.64}$$

$$f_{n+1} = e_n + Jc_n. \tag{A.65}$$

These relations can be expressed compactly as

$$\mathbf{v_{n+1}} = T\mathbf{v_n}, \tag{A.66}$$

where

$$\mathbf{v_n} = [f_n\ c_n\ e_n\ a_n\ b_n\ d_n]^T, \tag{A.67}$$

and

$$T = \begin{pmatrix} 0 & J & 1 & 0 & 0 & 0 \\ J & 0 & 0 & 1 & 0 & 0 \\ 1 & 0 & 0 & 0 & J & 0 \\ 0 & 1 & 0 & 0 & 0 & J \\ 0 & 0 & J & 0 & 0 & 1 \\ 0 & 0 & 0 & J & 1 & 0 \end{pmatrix}. \tag{A.68}$$

We now solve the recursion problem analytically. The $n = 0$ term of the summation in Eq. (A.57) corresponds to the initial condition $\mathbf{v_0} = [1\ 0\ 0\ 0\ 0\ 0]^T$. Equation (A.66) then leads to

$$a_n = \frac{1}{3}[(1+J)^n - (1-J+J^2)^{\frac{n}{2}}], \tag{A.69}$$

$$b_n = \frac{1}{3}[(1+J)^n - (1-J+J^2)^{\frac{n}{2}}], \tag{A.70}$$

$$f_n = \frac{1}{3}[(1+J)^n + 2(1-J+J^2)^{\frac{n}{2}}], \tag{A.71}$$

$$c_n = d_n = e_n = 0, \tag{A.72}$$

when n is even, and

$$c_n = \frac{1}{3}[(1+J)^n + (2J-1)(1-J+J^2)^{\frac{n-1}{2}}], \tag{A.73}$$

$$d_n = \frac{1}{3}[(1+J)^n - (1+J)(1-J+J^2)^{\frac{n-1}{2}}], \tag{A.74}$$

$$e_n = \frac{1}{3}[(1+J)^n + (2-J)(1-J+J^2)^{\frac{n-1}{2}}], \tag{A.75}$$

$$a_n = b_n = f_n = 0, \tag{A.76}$$

when n is odd. Performing the sum over n, the time evolution operator can finally be written as

$$\begin{aligned} U(t) = \frac{e^{iJ_b t(1+J)/4}}{3}\Bigg(& p^{231}\left\{\cos[J_b t(1+J)/2] - \cos(J_b t\sqrt{1-J+J^2}/2)\right\} \\ & + p^{312}\left\{\cos[J_b t(1+J)/2] - \cos(J_b t\sqrt{1-J+J^2}/2)\right\} \\ & + I\left\{\cos[J_b t(1+J)/2] + 2\cos(J_b t\sqrt{1-J+J^2}/2)\right\} \\ & - ip^{12}\left\{\sin[J_b t(1+J)/2] + \frac{2J-1}{\sqrt{1-J+J^2}}\sin(J_b t\sqrt{1-J+J^2}/2)\right\} \\ & - ip^{13}\left\{\sin[J_b t(1+J)/2] - \frac{1+J}{\sqrt{1-J+J^2}}\sin(J_b t\sqrt{1-J+J^2}/2)\right\} \\ & - ip^{23}\left\{\sin[J_b t(1+J)/2] + \frac{2-J}{\sqrt{1-J+J^2}}\sin(J_b t\sqrt{1-J+J^2}/2)\right\}\Bigg). \end{aligned} \tag{A.77}$$

The mediated gates we search for can be decomposed as

$$U = \mathbb{U}_2 \otimes I, \tag{A.78}$$

where $\mathbb{U}_2$ acts on qubits 1 and 3, while I is the single-qubit identity operator acting on spin 2. Condition (A.78) is satisfied when the coefficients of p^{231}, p^{312}, p^{12}, and p^{23} in Eq. (A.77) all vanish. The solution is given by

$$J = \frac{J_a}{J_b} = 1, \tag{A.79}$$

with

$$\cos(J_b t/2) = \cos(J_b t), \tag{A.80}$$

$$\sin(J_b t/2) = -\sin(J_b t). \tag{A.81}$$

We then solve Eqs. (A.80) and (A.81) to obtain the mediated gate periods, $t = T_g$:

$$J_b T_g = 0, \frac{4\pi}{3}, \frac{8\pi}{3}, 4\pi, \ldots. \tag{A.82}$$

The time evolution operator obtained from Eqs. (A.79)–(A.81) is given by

$$U(T_g) = e^{iJ_b T_g/2}[I\cos(J_b t) - ip^{13}\sin(J_b T_g)]. \tag{A.83}$$

Equation (A.82) then leads to three distinct types of gate operations. When $J_b T_g = (4m)\pi$, with m an integer, we obtain the trivial gate, $U(T_g) = I$. When $J_b T_g = (4m + \frac{4}{3})\pi$, we obtain the nontrivial result

$$U(T_g) = e^{-i\frac{\pi}{3}}(\frac{1}{2}I - i\frac{\sqrt{3}}{2}p^{1,3}). \tag{A.84}$$

The decomposition of Eq. (A.78) leads to the identification of the mediated gate $\mathbb{U}_2$, given in Eq. (2.3). When $J_b T_g = (4m + \frac{8}{3})\pi$, we obtain the complementary gate $U(T_g) = \mathbb{U}_2^2 \otimes I$. Finally, we note that $\mathbb{U}_2^3 = I$. Thus, $\mathbb{U}_2$, $\mathbb{U}_2^2 = \mathbb{U}_2^{-1}$, and I comprise the full set of two-qubit mediated gates.

A.3 GLOBAL OPTIMIZATION TECHNIQUES FOR CONSTRUCTING QUANTUM STATES AND GATES

In this Appendix, we outline the global optimization methods used to solve Eqs. (2.4) and (2.5), which act on two qubits. Identical methods can also be used to generate states and construct gates involving more than two qubits.

Equations (2.4) and (2.5) can be summarized as follows. An arbitrary two-qubit quantum circuit is formed of units comprised of one entangling gate, $\mathbb{U}_2$, sandwiched between single-qubit unitary rotations. One or more of these units can be combined, sequentially, to form a circuit. The single-qubit rotations in this protocol are arbitrary. However, the entangling gate $\mathbb{U}_2$ is fixed, with the form shown in Eq. (2.3).

Three scalar parameters are required, to fully specify an arbitrary single-qubit rotation, up to a global phase factor (*e.g.*, the Euler angle construction). Here, we adopt the ZYZ decomposition [50]:

$$U_1(\alpha, \beta, \gamma) = e^{-i\alpha\sigma_z/2} e^{-i\beta\sigma_y/2} e^{-i\gamma\sigma_z/2}. \tag{A.85}$$

In the most general case, the rotations will be applied to both qubits, before and after each exchange gate. The construction can be further simplified by noting that terms such as

$(U_1 \otimes U_1)(U_1 \otimes U_1)$ are redundant and can be collapsed into the form $U_1 \otimes U_1$. Thus, up to $6(n+1)$ rotation angles are required, to specify an arbitrary gate sequence of circuit depth n.

Here, we employ global optimization techniques, to search through this large parameter space. We have found that multistart clustering algorithms [105, 106] are particularly effective for solving this problem. We first define an appropriate objective function to be minimized. For generating arbitrary states, as in Eq. (2.4), we use the infidelity $(1-f)$ of the desired final state $|\psi_{\rm des}\rangle$ as the objective function, where

$$\begin{aligned} f &= |\langle\psi_{\rm des}|\psi_{\rm actual}\rangle|^2 \\ &= |\langle\psi_{\rm des}|(U_1 \otimes U_1)[\mathbb{U}_2(U_1 \otimes U_1)]^n|00\rangle|^2. \end{aligned} \tag{A.86}$$

For generating arbitrary gates, as in Eq. (2.5), we use the operator error norm ϵ as the objective function, where

$$\epsilon = ||U_{2,\rm des} - U_{2,\rm actual}||. \tag{A.87}$$

The global optimization is performed in two steps. In the first step, we use the multistart algorithm to identify potential candidate solutions. Then, we use these solutions as a first guess in a local Nelder-Mead downhill simplex search [107]. The final outcome generally provides results with very low or very high accuracy. The latter are accepted as valid solutions. We begin our searches using the minimal exchange gate sequence ($n = 1$). If no valid solutions are obtained for a given sequence length, we increment n by 1 and repeat the procedure. Once an optimal, numerical solution has been obtained, it is sometimes possible to work backwards, to determine the exact rotation angles, as in Figs. 2.3, 2.4, and 2.6. These identifications can then be confirmed analytically.

Appendix B

Supplemental information for Chapter 3

In these Supplementary Materials, we provide details about the calculations and simulations discussed in the main text. Section B.1 describes the Hamiltonian for the $S_z = 1/2$ spin manifold. Section B.2 provides analytical estimates for the exchange interactions in certain operating regimes of interest. Section B.3 provides details of the quantum process tomography methods. Section B.4 describes our statistical averaging procedure for treating quasistatic charge and nuclear noise. Section B.5 describes some additional results for simulations with averages over Overhauser field gradients. Section B.6 describes results with no Overhauser field gradients, consistent with pure, isotopically purified ^{28}Si.

B.1 Calculation Details

In this section, we describe our Hubbard model Hamiltonian. We evaluate each individual term of Eq. 3.2 in the main text using the 7D basis set defined by

$$|0\rangle = \frac{1}{\sqrt{6}}\left(|\uparrow\uparrow\downarrow\rangle + |\downarrow\uparrow\uparrow\rangle\right) - \sqrt{\frac{2}{3}}|\uparrow\downarrow\uparrow\rangle, \tag{B.1}$$

$$|1\rangle = \frac{1}{\sqrt{2}}\left(|\uparrow\uparrow\downarrow\rangle - |\downarrow\uparrow\uparrow\rangle\right), \tag{B.2}$$

$$|2\rangle = \frac{1}{\sqrt{3}}\left(|\uparrow\uparrow\downarrow\rangle + |\downarrow\uparrow\uparrow\rangle\right) + \sqrt{\frac{1}{3}}|\uparrow\downarrow\uparrow\rangle, \tag{B.3}$$

$$|3\rangle = \frac{1}{\sqrt{2}}\left(|\uparrow\downarrow\rangle_1 - |\downarrow\uparrow\rangle_1\right)|\cdot\rangle_2|\uparrow\rangle_3, \tag{B.4}$$

$$|4\rangle = \frac{1}{\sqrt{2}}|\cdot\rangle_1\left(|\uparrow\downarrow\rangle_2 - |\downarrow\uparrow\rangle_2\right)|\uparrow\rangle_3, \tag{B.5}$$

$$|5\rangle = \frac{1}{\sqrt{2}}|\uparrow\rangle_1\left(|\uparrow\downarrow\rangle_2 - |\downarrow\uparrow\rangle_2\right)|\cdot\rangle_3, \tag{B.6}$$

$$|6\rangle = \frac{1}{\sqrt{2}}|\uparrow\rangle_1|\cdot\rangle_2\left(|\uparrow\downarrow\rangle_3 - |\downarrow\uparrow\rangle_3\right), \tag{B.7}$$

where the notation $|\uparrow\downarrow\rangle_j$ (or $|\downarrow\uparrow\rangle_j$) indicates that both electrons are in the same dot, labelled $j = 1, 2, 3$, and $|\cdot\rangle_j$ indicates an empty dot. The creation-annihilation operator combinations, $c^\dagger_{i\sigma}c_{j\sigma}$, are then readily evaluated, as are the particle number operators $n_{i\sigma} = c^\dagger_{i\sigma}c_{i\sigma}$, for dots i, j, and spins $\sigma = \uparrow, \downarrow$.

We then obtain the following expressions for the individual terms in the Hubbard Hamiltonian, Eq. 3.2 in the main text. The tunnel coupling term is given by

$$H_t = \begin{pmatrix} 0 & 0 & 0 & \sqrt{\frac{3}{2}}t & -\sqrt{\frac{3}{2}}t & -\sqrt{\frac{3}{2}}t & \sqrt{\frac{3}{2}}t \\ 0 & 0 & 0 & -\frac{1}{\sqrt{2}}t & \frac{1}{\sqrt{2}}t & -\frac{1}{\sqrt{2}}t & \frac{1}{\sqrt{2}}t \\ 0 & 0 & 0 & 0 & 0 & 0 & 0 \\ \sqrt{\frac{3}{2}}t & -\frac{1}{\sqrt{2}}t & 0 & 0 & 0 & 0 & 0 \\ -\sqrt{\frac{3}{2}}t & \frac{1}{\sqrt{2}}t & 0 & 0 & 0 & 0 & 0 \\ -\sqrt{\frac{3}{2}}t & -\frac{1}{\sqrt{2}}t & 0 & 0 & 0 & 0 & 0 \\ \sqrt{\frac{3}{2}}t & \frac{1}{\sqrt{2}}t & 0 & 0 & 0 & 0 & 0 \end{pmatrix}. \tag{B.8}$$

The onsite Coulomb repulsion term describes the double-occupation energy cost for a single dot. It is given by

$$H_U = \begin{pmatrix} 0 & 0 & 0 & 0 & 0 & 0 & 0 \\ 0 & 0 & 0 & 0 & 0 & 0 & 0 \\ 0 & 0 & 0 & 0 & 0 & 0 & 0 \\ 0 & 0 & 0 & U & 0 & 0 & 0 \\ 0 & 0 & 0 & 0 & U & 0 & 0 \\ 0 & 0 & 0 & 0 & 0 & U & 0 \\ 0 & 0 & 0 & 0 & 0 & 0 & U \end{pmatrix}. \tag{B.9}$$

The detuning energies are given by

$$H_\varepsilon = \begin{pmatrix} \varepsilon_M & 0 & 0 & 0 & 0 & 0 & 0 \\ 0 & \varepsilon_M & 0 & 0 & 0 & 0 & 0 \\ 0 & 0 & \varepsilon_M & 0 & 0 & 0 & 0 \\ 0 & 0 & 0 & \frac{\varepsilon}{2} & 0 & 0 & 0 \\ 0 & 0 & 0 & 0 & 2\varepsilon_M - \frac{\varepsilon}{2} & 0 & 0 \\ 0 & 0 & 0 & 0 & 0 & 2\varepsilon_M + \frac{\varepsilon}{2} & 0 \\ 0 & 0 & 0 & 0 & 0 & 0 & -\frac{\varepsilon}{2} \end{pmatrix}. \tag{B.10}$$

Since the basis states all belong to the same $S_z = 1/2$ spin manifold, they all have the same Zeeman energy, which we ignore here. The local Overhauser field energies due to nuclear fluctuations are given by

$$H_{\Delta B} = g\mu_B \begin{pmatrix} \frac{2}{3}(\Delta B_l - \Delta B_r) & \frac{1}{\sqrt{3}}(\Delta B_l + \Delta B_r) & -\frac{\sqrt{2}}{3}(\Delta B_l - \Delta B_r) & 0 & 0 & 0 & 0 \\ \frac{1}{\sqrt{3}}(\Delta B_l + \Delta B_r) & 0 & \sqrt{\frac{2}{3}}(\Delta B_l + \Delta B_r) & 0 & 0 & 0 & 0 \\ -\frac{\sqrt{2}}{3}(\Delta B_l - \Delta B_r) & \sqrt{\frac{2}{3}}(\Delta B_l + \Delta B_r) & \frac{1}{3}(\Delta B_l - \Delta B_r) & 0 & 0 & 0 & 0 \\ 0 & 0 & 0 & -\Delta B_r & 0 & 0 & 0 \\ 0 & 0 & 0 & 0 & -\Delta B_r & 0 & 0 \\ 0 & 0 & 0 & 0 & 0 & \Delta B_l & 0 \\ 0 & 0 & 0 & 0 & 0 & 0 & \Delta B_l \end{pmatrix}, \tag{B.11}$$

where we define $\Delta B_l = B_1^z - B_2^z$ and $\Delta B_r = B_2^z - B_3^z$ to be the differences in local magnetic fields in the $\hat{\mathbf{z}}$ direction. As explained in the main text, we only consider longitudinal ($\hat{\mathbf{z}}$) components of the Overhauser fields, defined by $\mathbf{B} = B\hat{\mathbf{z}}$, as consistent with [81].

Equation 3.3 of the main text then represents a set of 49 real coupled differential equations. We solve these equations numerically and check that the trace-preserving condition is satisfied for the final density matrix, when the calculation is complete.

B.2 Exchange Interactions and the Sweet Spot

In this section, we estimate the effective exchange interactions J_{ij} that generate rotations. We can use the results to provide initial estimates for the evolution periods for gate operations; we use these estimates to optimize the gates, as discussed in the main text.

We now reduce the full 7×7 Hamiltonian, $H = H_t + H_U + H_\varepsilon$, to an effective 2×2 Hamiltonian for the logical qubit states. We consider the ideal case with no nuclear fields, so $\Delta B_j = 0$ and there is no coupling between the qubit states $\{|0\rangle, |1\rangle\}$ and the leakage state $|2\rangle$. A Schrieffer-Wolff transformation [108] to order t^2 in the small parameter t/U yields the well-known Heisenberg Hamiltonian

$$H_{\text{eff}} = J_{12}\, \mathbf{s}_1 \cdot \mathbf{s}_2 + J_{23}\, \mathbf{s}_2 \cdot \mathbf{s}_3, \tag{B.12}$$

for the 3×3 subspace of $(1,1,1)$ charge states. Here, $J_{12}, J_{23} \sim \mathcal{O}[t^2]$. In the absence of any coupling to the leakage state, we can immediately project H_{eff} onto the 2×2 logical qubit subspace, yielding

$$H_{\text{eff}} = (\text{const}) + \frac{\sqrt{3}}{4}(J_{12} - J_{23})\sigma_x - \frac{1}{4}(J_{12} + J_{23})\sigma_z, \tag{B.13}$$

where σ_x and σ_z are Pauli matrices. Here, we may drop the constant term, giving Eq. (2) in the main text.

We can also obtain H_{eff} by directly performing a Schrieffer-Wolff transformation of H onto the 2×2 subspace, yielding

$$H_{\text{eff}} \simeq -\frac{2\sqrt{3}t^2 U \varepsilon_M \varepsilon}{D}\sigma_x - \frac{2t^2 U(U^2 - \varepsilon_M^2 - \varepsilon^2/4)}{D}\sigma_z, \tag{B.14}$$

where the denominator is given by

$$D = U^4 - 2(\varepsilon_M^2 + \varepsilon^2/4)U^2 + (\varepsilon_M^2 - \varepsilon^2/4)^2. \tag{B.15}$$

By comparing Eqs. (B.13) and (B.14), we can identify the individual exchange interactions:

$$J_{12} = \frac{4t^2U(U^2 - (\varepsilon_M + \varepsilon/2)^2)}{D}, \tag{B.16}$$

$$J_{23} = \frac{4t^2U(U^2 - (\varepsilon_M - \varepsilon/2)^2)}{D}. \tag{B.17}$$

Diagonalizing Eq. (B.14), we obtain the energy splitting

$$E_{01} = \frac{4t^2U\sqrt{(U^2 - \varepsilon_M^2 - \varepsilon^2/4)^2 + 3\,\varepsilon_M^2\varepsilon^2}}{D}. \tag{B.18}$$

Since E_{01} is an even function in the variables ε and ε_M, we immediately find that

$$\frac{\partial E_{01}}{\partial \epsilon} = \frac{\partial E_{01}}{\partial \epsilon_M} = 0 \tag{B.19}$$

when $\epsilon = \epsilon_M = 0$, establishing this setting as a detuning sweet spot.

At the sweet spot, we find that

$$H_{\text{eff}} = -\frac{2t^2}{U}\sigma_z, \tag{B.20}$$

corresponding to a Z-rotation. Indeed, we see that Z-rotations are achieved when either $\varepsilon = 0$ or $\varepsilon_M = 0$. From Eq. (B.14), we see that rotations around the axis $-(\hat{\mathbf{x}} + \hat{\mathbf{z}})/\sqrt{2}$, used in the three-step $X(\pi)$ protocol described in the main text, are defined by the line

$$\varepsilon_M^2 + \varepsilon^2/4 + \sqrt{3}\,\varepsilon_M\varepsilon = U^2, \tag{B.21}$$

which correctly predicts the line of highest fidelities in Fig. 3.2 of the main text.

B.3 Quantum Process Tomography

Quantum process tomography (QPT) provides a means of characterizing quantum gates by comparing the ideal outcomes of gate operations with their actual outcomes. Here, we follow the QPT recipe given in [50]. We solve the master equation, Eq. (3) in the main

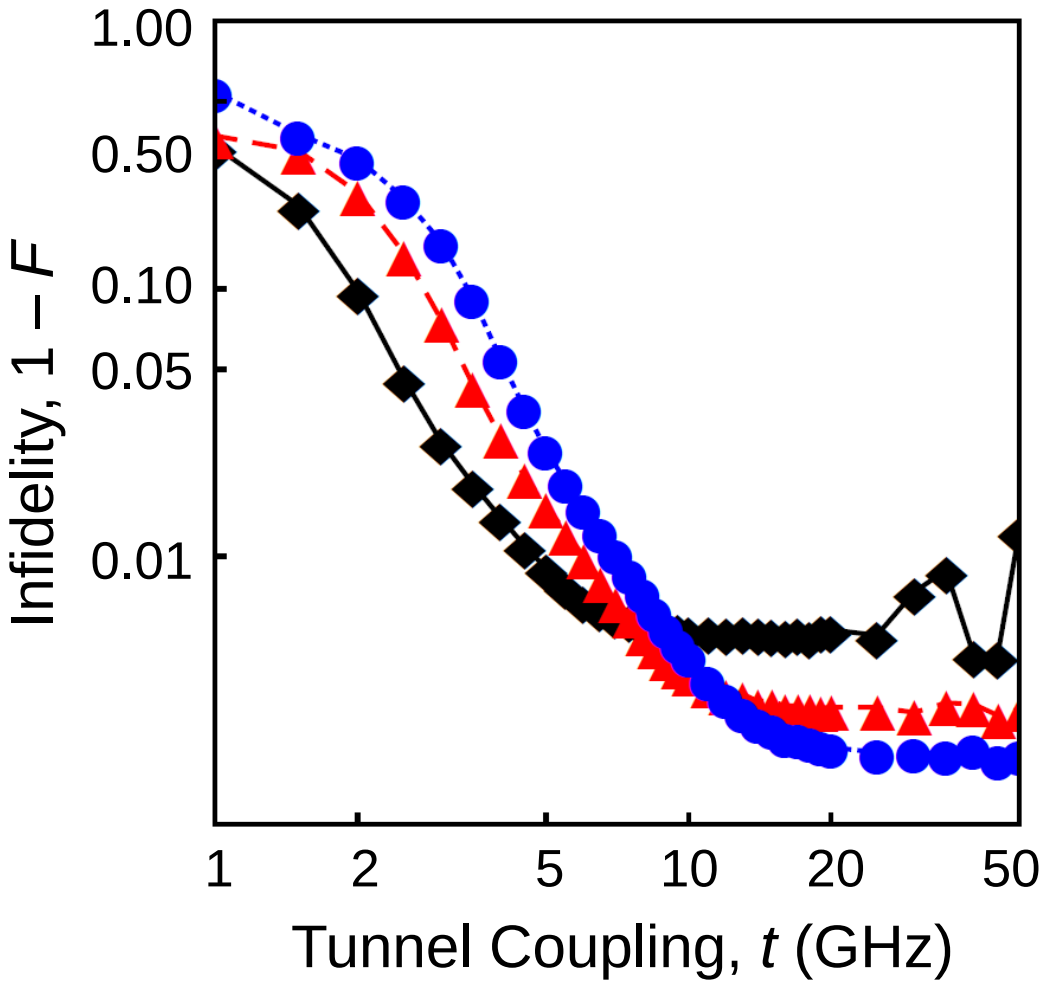

Figure B.1: Infidelity, $1 - F$, of a $Z(\pi)$ rotation, including quasistatic nuclear noise for three different values of the intradot Coulomb repulsion: $U = 1$ meV (black diamonds, as in the main panel of Fig. 3.3 in the main text), $U = 2$ meV (triangles), and $U = 3$ meV (circles), with larger U values yielding higher maximum fidelities.

text, for a specified pulse sequence for a given gate operation. For each simulation, the detuning parameters and the local magnetic fields are held constant. Using the simulation results, we calculate the final fidelity, as outlined below. In the following section, we describe our method for performing statistical averages of those fidelities, taking into account the fluctuations of the detuning parameters and the random magnetic fields. We now summarize the QPT method.

We consider a gate operation $\mathcal{E}(\rho)$ acting on an initial state described by the density

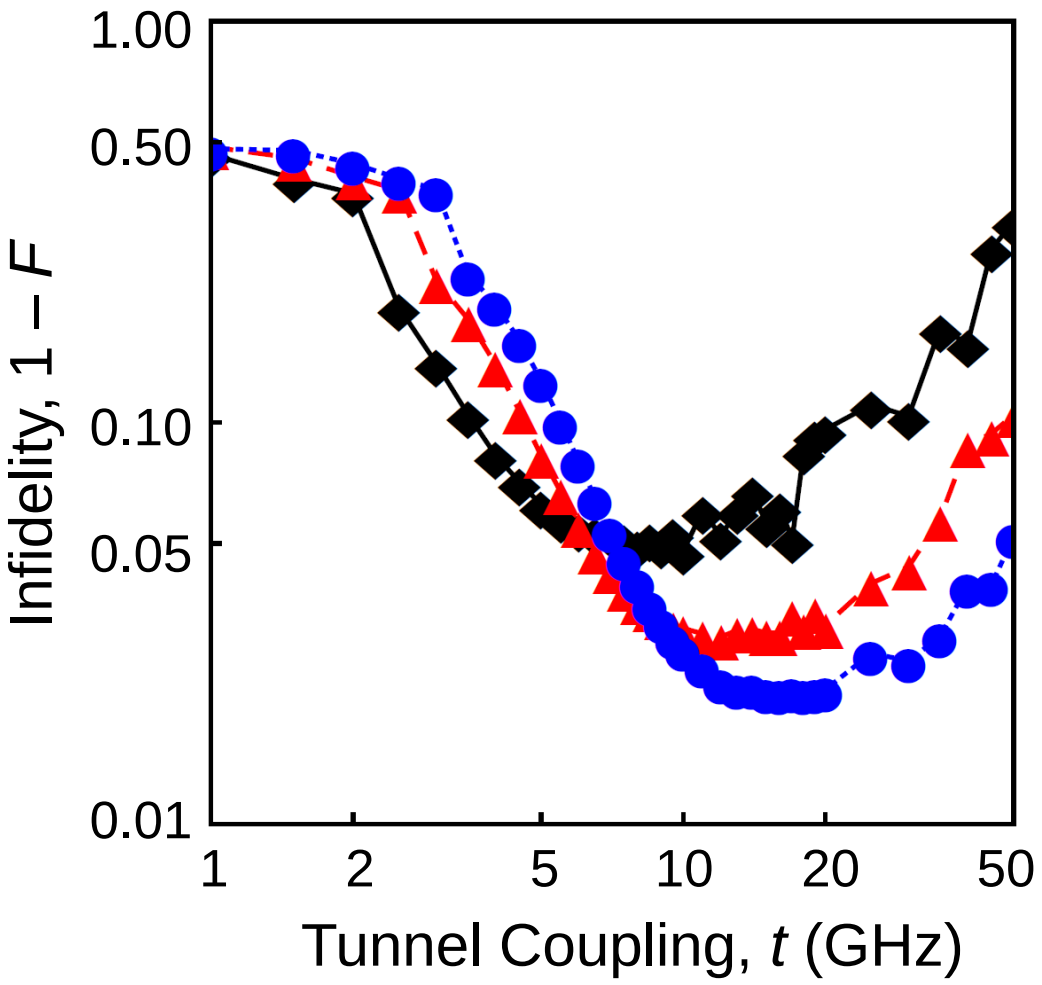

Figure B.2: Fidelity of a three-step $X(\pi)$ rotation, as described in the main text, including quasistatic nuclear noise for three different values of the Coulomb repulsion: $U = 1$ meV (black diamonds, as in the main panel of Fig. 3.4 in the main text), $U = 2$ meV (triangles), and $U = 3$ meV (circles). All fidelity averages are obtained assuming a Gaussian distribution of Overhauser field differences with standard deviation $\sigma_B = 4$ mT. Quasistatic noise in the detuning parameters are not included in this simulation.

matrix ρ. Here, $\mathcal{E}(\rho)$ represents the final density matrix, and has no relation to the detuning parameter. The $\mathcal{E}$ operation can be expressed in terms of operation elements E_i, such that

$$\mathcal{E}(\rho) = \sum_i E_i \rho E_i^\dagger. \tag{B.22}$$

The operation elements can be decomposed with respect to an orthogonal basis set of

operators $\tilde{E}_m$ for the state space, such that

$$E_i = \sum_m e_{im}\tilde{E}_m, \tag{B.23}$$

where e_{im} are complex numbers. If ρ describes a single qubit, then each $\tilde{E}_m$ is a 2×2 matrix. A convenient choice is the basis set

$$\tilde{E}_0 = I, \tag{B.24}$$

$$\tilde{E}_1 = \sigma_x, \tag{B.25}$$

$$\tilde{E}_2 = -i\sigma_y, \tag{B.26}$$

$$\tilde{E}_3 = \sigma_z, \tag{B.27}$$

where σ_α are Pauli matrices. We then have

$$\mathcal{E}(\rho) = \sum_{mn} \tilde{E}_m \rho \tilde{E}_n^\dagger \chi_{mn}, \tag{B.28}$$

where the process matrix χ is defined as

$$\chi_{mn} = \sum_i e_{im} e_{in}^*. \tag{B.29}$$

The process matrix can be fully characterized by initializing the system into linearly independent basis elements for the density matrix. A convenient choice of initial states is $|0\rangle$, $|1\rangle$, $|+\rangle = (|0\rangle + |1\rangle)/\sqrt{2}$, and $|-\rangle = (|0\rangle + i|1\rangle)/\sqrt{2}$. We then perform appropriate linear combinations of gate operations on the initial states, as described in [50]. Once the process matrix has been reconstructed, the process fidelity for a single-qubit rotation is given by [109]

$$\bar{F} = \frac{1}{3}\left(2\mathrm{Tr}[\chi\chi_{\mathrm{ideal}}] + 1\right), \tag{B.30}$$

where χ_{ideal} represents the ideal process matrix.

B.4 Averaging Procedure for Nuclear Field and Detuning Fluctuations

In the previous section, we described the calculation of QPT fidelities for individual simulations. Each simulation is performed for a constant value of the detuning parameters

and the local nuclear fields. However, these parameters are all quasistatic, and we should perform an average over these quantities, as described in the main text, to describe the inhomogeneous broadening.

There are two different fluctuation axes for the detuning parameters (ε and ε_M) and two different axes for the nuclear fields (ΔB_l and ΔB_r). While it is not computationally feasible to perform accurate, simultaneous averages over four different fluctuation axes, it is possible to perform simultaneous averages over two axes at a time. We choose to perform simultaneous averages over the detuning fluctuations and the random Overhauser fields separately, to distinguish the effects of charge and nuclear noise. These calculations are computationally intensive.

We first consider the quasistatic random Overhauser fields. When $B \gg \Delta B$, we only need to consider the longitudinal components of $\Delta B_{l,r}$ [81]. We model the probability distributions of these random fields as

$$P(\Delta B_l, \Delta B_r) = \frac{1}{2\pi\sigma_B^2} e^{-(\Delta B_l^2 + \Delta B_r^2)/(2\sigma_B^2)}, \tag{B.31}$$

where σ_B is the standard deviation of the random fields. The master equation is solved over a grid $(\Delta B_l, \Delta B_r)$ of size $N_g \times N_g$, with $N_g = 25$, while keeping ε and ε_M fixed. The noise-averaged fidelity is then given by

$$F = \int \frac{d\Delta B_l d\Delta B_r}{2\pi\sigma_B^2} \bar{F}(\Delta B_l, \Delta B_r, \varepsilon, \varepsilon_M) e^{-(\Delta B_l^2 + \Delta B_r^2)/(2\sigma_B^2)} \tag{B.32}$$

$$= \frac{(\Delta B_{\max} - \Delta B_{\min})^2}{2\pi\sigma_B^2 N_g^2} \sum_{\langle \Delta B_l, \Delta B_r \rangle} \bar{F}(\Delta B_l, \Delta B_r, \varepsilon, \varepsilon_M) e^{-(\Delta B_l^2 + \Delta B_r^2)/(2\sigma_B^2)}. \tag{B.33}$$

In our simulations, we choose ΔB_l and ΔB_r in the range (-12 mT,+12 mT), and σ_B=4 mT, as consistent with [82].

Similarly, we consider fluctuations of the detuning parameters keeping the local magnetic fields fixed. We model the fluctuation probability distribution as

$$P(\Delta\varepsilon, \Delta\varepsilon_M) = \frac{1}{2\pi\sigma_\varepsilon^2} e^{-(\Delta\varepsilon^2 + \Delta\varepsilon_M^2)/(2\sigma_\varepsilon^2)} \tag{B.34}$$

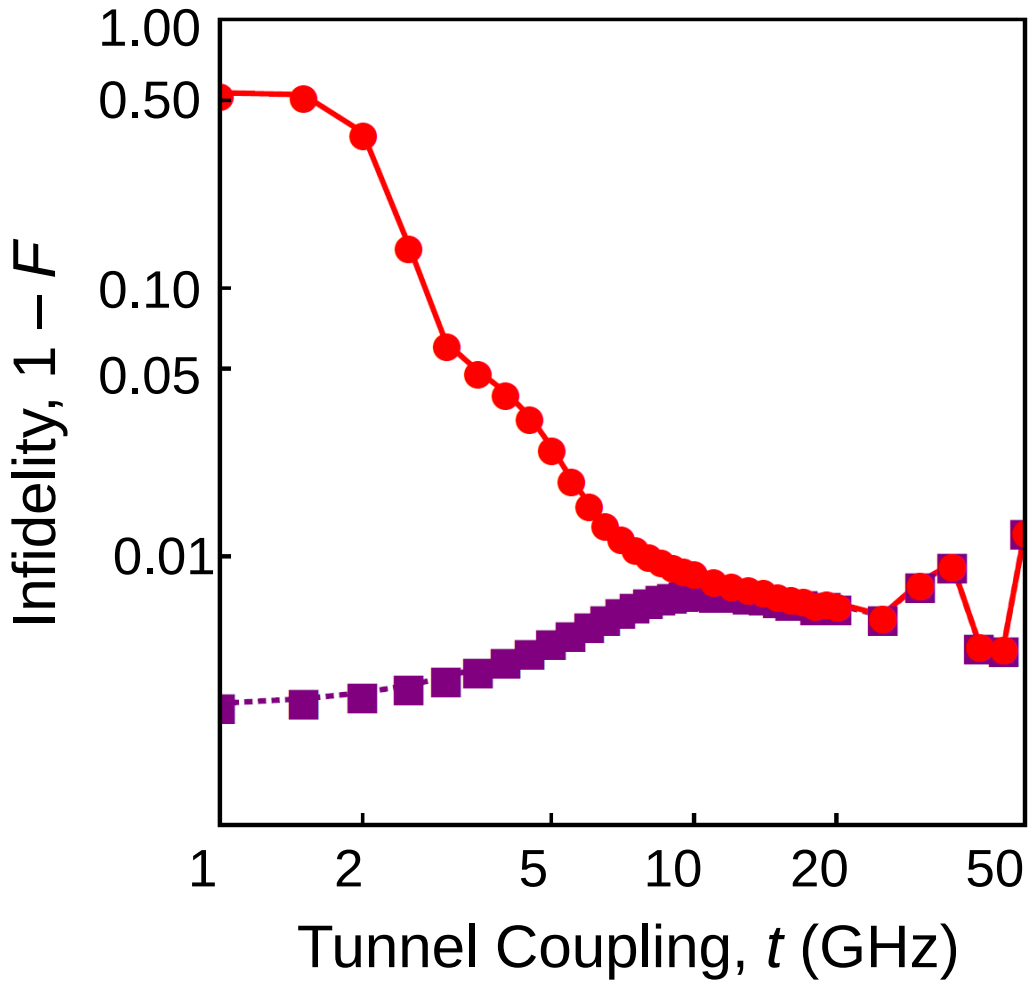

Figure B.3: Comparison of gate infidelities, $1 - F$, for perfect, isotopically purified ^{28}Si (purple squares) and GaAs (red circles) in the presence of detuning fluctuations. The GaAs results are identical to the red circles in Fig. 3.3 3.4 of the main text. For ^{28}Si, we assume no Overhauser fields in the dots, while for GaAs, we assume the fixed values $\Delta B_2^z - \Delta B_1^z = \Delta B_3^z - \Delta B_2^z = 3$ mT, as for the red circles in Fig. 3.3 3.4. We assume an intradot Coulomb repulsion of $U = 1$ meV. $Z(\pi)$-rotations, as described in the main text.

over a grid $(\Delta\varepsilon, \Delta\varepsilon_M)$ of $N_g \times N_g$ points, with $N_g = 31$. The noise-averaged fidelity is then

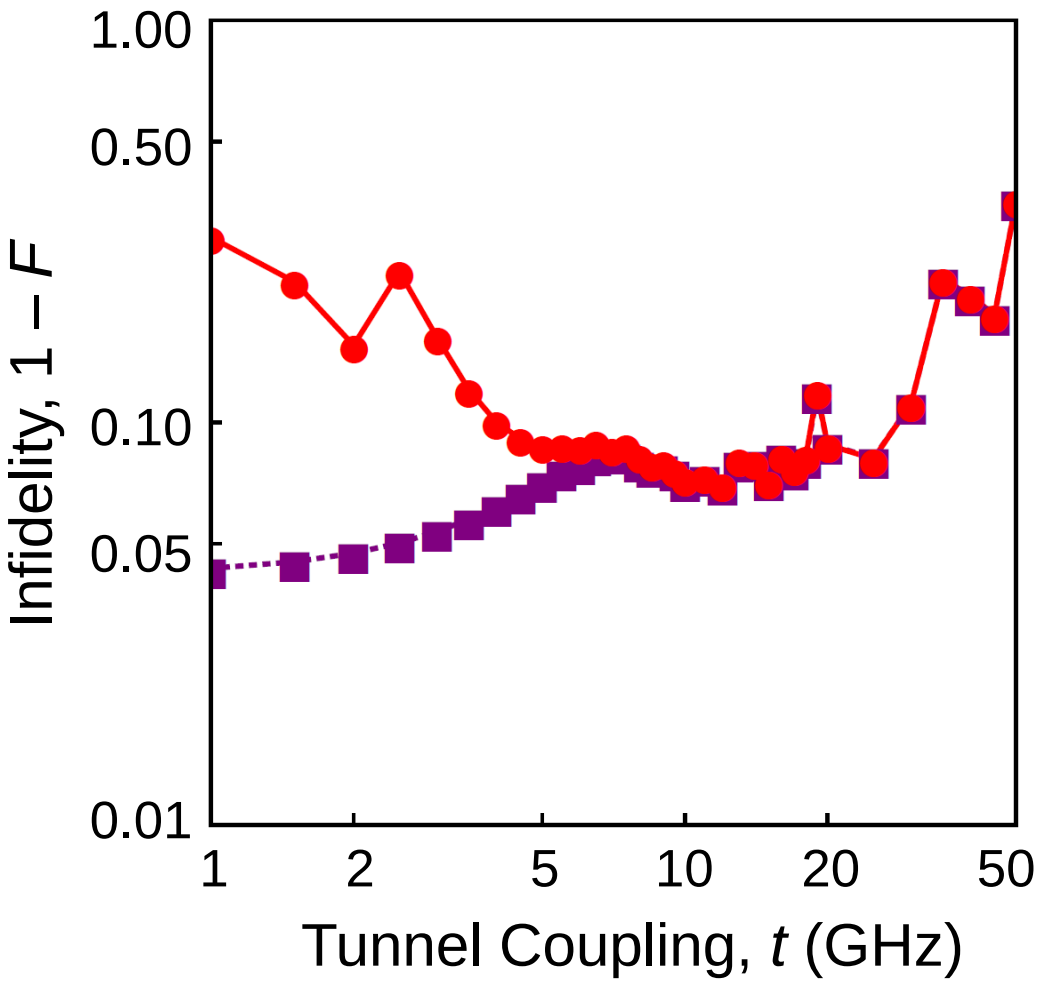

Figure B.4: Comparison of gate infidelities, $1-F$, for perfect, isotopically purified ^{28}Si (purple squares) and GaAs (red circles) in the presence of detuning fluctuations. The GaAs results are identical to the red circles in Fig. 3.3 3.4 of the main text. For ^{28}Si, we assume no Overhauser fields in the dots, while for GaAs, we assume the fixed values $\Delta B_2^z - \Delta B_1^z = \Delta B_3^z - \Delta B_2^z = 3$ mT, as for the red circles in Fig. 3.3 3.4. We assume an intradot Coulomb repulsion of $U = 1$ meV. Three-step $X(\pi)$ rotations, as described in the main text.

given by

$$F = \int \frac{d\Delta\varepsilon d\Delta\varepsilon_M}{2\pi\sigma_\varepsilon^2} \bar{F}(\varepsilon+\Delta\varepsilon, \varepsilon_M+\Delta\varepsilon_M, \Delta B_l, \Delta B_r) e^{-(\Delta\varepsilon^2+\Delta\varepsilon_M^2)/(2\sigma_\varepsilon^2)} \tag{B.35}$$

$$= \frac{(\Delta\varepsilon_{\max}-\Delta\varepsilon_{\min})^2}{2\pi\sigma_\varepsilon^2 N_g^2} \sum_{\langle\Delta\varepsilon,\Delta\varepsilon_M\rangle} \bar{F}(\varepsilon+\Delta\varepsilon, \varepsilon_M+\Delta\varepsilon_M, \Delta B_l, \Delta B_r) e^{-(\Delta\varepsilon^2+\Delta\varepsilon_M^2)/(2\sigma_\varepsilon^2)} \tag{B.36}$$

In our simulations, we choose $\Delta\varepsilon$ and $\Delta\varepsilon_M$ in the range (-15 μeV,+15 μeV), and σ_ε=5 μeV, as consistent with [84, 85].

B.5 Nuclear Noise Averages

Figures 3.3 and 3.4 of the main text show comparisons of nuclear and charge noise averaging results, while the insets show comparisons of charge noise averaging for three different values of U.

In this section, we extend these results by plotting nuclear noise-averaged results for three different values of U, as shown in Fig. B.1 B.2. As before, we find that $X(\pi)$ rotations have fidelities that are approximately 20 times worse than $Z(\pi)$ rotations, with optimal values that improve when U is larger.

B.6 ^{28}Si

In previous sections, particularly in Fig. 3.2 3.3 3.4 of the main text and Fig. B.1 B.2 of the Supplemental Materials, we compared the effects of random nuclear fields and detuning fluctuations. When we simulated detuning fluctuations, we adopted a fixed, characteristic magnetic field difference between the two dots. To complete this story, we perform the same simulation here, setting the static Overhauser fields to zero. This can be viewed as the ideal case for perfect, isotopically purified ^{28}Si devices, whereas the previous simulations corresponded to GaAs.

The results of our ^{28}Si simulation are shown in Fig. B.3 B.4, assuming only detuning fluctuations. We also show the equivalent GaAs simulation for comparison, with the same detuning fluctuations but setting $\Delta B_2^z - \Delta B_1^z = \Delta B_3^z - \Delta B_2^z = 3$ mT, as in Fig. 3.3 3.4 of the main text. We see that using ^{28}Si is highly beneficial in two ways. First, it yields an improvement in the maximum fidelity. Second, it lowers the optimal tunnel coupling, and therefore the gate speed, to a range that may be more convenient from a technological perspective. At even lower gate speeds, fast charge noise eventually degrades

the gate fidelity. At higher tunnel couplings, where the effects of quasistatic charge noise and leakage to doubly-occupied charge states dominate the fidelity, the presence of a magnetic field difference is irrelevant. Once again, we find the optimal fidelity for Z-rotations is approximately one order of magnitude better than for X-rotations, due to the presence of the sweet spot.

Appendix C

Supplemental information for Chapter 4

C.1 Quaternions

A quaternion is defined as $h = a + i_h b + jc + kd$ where a, b, c, d are real and Hamilton's symbols i_h, j, k satisfy $i_h^2 = j^2 = k^2 = -1, i_h j = -j i_h = k$, etc. The conjugate is defined as $\overline{h} = a - i_h b - jc - kd$. The magnitude squared is $h\overline{h} = \overline{h}h = a^2 + b^2 + c^2 + d^2$. Two quaternions do not commute in general: $gh \neq hg$. We define taking the real part by tr $h = a$.We will find it very convenient to write quaternions as 2×2 matrices using the identifications $i_h = i\sigma_x, j = i\sigma_y$ and $k = i\sigma_z$, so that

$$h = \begin{pmatrix} a + id & ib + c \\ ib - c & a - id \end{pmatrix}. \tag{C.1}$$

It is easy to see that this gives the right commutation relations.

Matrices with quaternionic entries can be defined and clearly do not commute. If we define the adjoint as

$$M^{\dagger}_{rs} = \overline{M}_{sr} \tag{C.2}$$

and the trace as

$$Tr\ M = \sum_r tr\ M_{rr} \tag{C.3}$$

then we have

$$(MN)^\dagger = N^\dagger M^\dagger \tag{C.4}$$

and

$$Tr\,(MN) = Tr\,(NM) \tag{C.5}$$

but in contrast to complex matrices

$$\overline{MN} \neq \overline{MN} \tag{C.6}$$

and

$$(MN)^T \neq N^T M^T \tag{C.7}$$

in general. If M is self-adjoint then $M^\dagger = M$, and for this case when $M\psi = \psi\lambda$ for some quaternionic vector ψ, then the eigenvalues λ are real.

C.2 Single Quaterbits

Quaterbits are described by 2×2 density matrices ρ with quaternionic entries. These matrices are self adjoint. Thus we have

$$\rho = \begin{pmatrix} a & q \\ \overline{q} & a' \end{pmatrix}, \tag{C.8}$$

where a is "real", i.e., $a = \overline{a}$. Using the matrix forms for the individual quaternions, this becomes a 4×4 matrix of the form

$$\rho = \frac{1}{4} I + \begin{pmatrix} A & 0 & a+id & ib+c \\ 0 & A & ib-c & a-id \\ a-id & -ib-c & -A & 0 \\ -ib+c & a+id & 0 & -A \end{pmatrix}, \tag{C.9}$$

which has 5 real parameters A, a, b, c, d. This is more than the 3 real parameters that characterize a qubit density matrix, but much less than the 15 that characterize a 4×4

2-qubit density matrix. This can be written as

$$\rho - \frac{1}{4}I = \begin{pmatrix} A & 0 & a+id & ib+c \\ 0 & A & ib-c & a-id \\ a-id & -ib-c & -A & 0 \\ -ib+c & a+id & 0 & -A \end{pmatrix}$$
$$= A\ \sigma_z \otimes \sigma_0 + a\ \sigma_x \otimes \sigma_0 - b\ \sigma_y \otimes \sigma_x - c\ \sigma_y \otimes \sigma_y - d\ \sigma_y \otimes \sigma_z. \quad \text{(C.10)}$$

C.3 Two Quaterbits

Quaterbits are described by 4×4 density matrices ρ with quaternionic entries. These matrices are self adjoint. So

$$\rho - \frac{I}{8} = \rho' = \begin{pmatrix} AI_2 & q_0 & q_1 & q_2 \\ \overline{q}_0 & BI_2 & q_3 & q_4 \\ \overline{q}_1 & \overline{q}_3 & CI_2 & q_5 \\ \overline{q}_2 & \overline{q}_4 & \overline{q}_5 & DI_2 \end{pmatrix}. \quad \text{(C.11)}$$

When the quaternions are rewritten as 2×2 matrices, we get an 8×8 matrix with

$$I_2 = \begin{pmatrix} 1 & 0 \\ 0 & 1 \end{pmatrix} \quad \text{(C.12)}$$

and

$$q_i = \begin{pmatrix} a_i - id_i & ib_i + c_i \\ ib_i - c_i & a_i + id_i \end{pmatrix} \quad \text{(C.13)}$$

$$q_i = \begin{pmatrix} a_i + id_i & -ib_i - c_i \\ -ib_i + c_i & a_i - id_i \end{pmatrix}. \quad \text{(C.14)}$$

We must have that $A+B+C+D = 0$. Defining $u = 2A+2B, v = 2A+2C, w = -2B-2C$ and

$$\lambda_{ijk} = \sigma_i \otimes \sigma_j \otimes \sigma_k \quad \text{(C.15)}$$

so that $Tr\ \lambda_{ijk}\lambda_{i'j'k'} = 8\ \delta_{ii'}\delta_{jj'}\delta_{kk'}$, we find, after a lengthy calculation:

$$\begin{aligned}
\rho' &= u\lambda_{300} + v\lambda_{030} + w\lambda_{330} \\
&+\frac{1}{2}a_0\left(\lambda_{010}+\lambda_{310}\right) + \frac{1}{2}b_0\left(\lambda_{021}+\lambda_{321}\right) - \frac{1}{2}c_0\left(\lambda_{022}+\lambda_{322}\right) - \frac{1}{2}d_0\left(\lambda_{023}+\lambda_{323}\right) \\
&+\frac{1}{2}a_1\left(\lambda_{100}+\lambda_{130}\right) - \frac{1}{2}b_1\left(\lambda_{201}+\lambda_{231}\right) - \frac{1}{2}c_1\left(\lambda_{202}+\lambda_{232}\right) - \frac{1}{2}d_1\left(\lambda_{203}+\lambda_{233}\right) \\
&+\frac{1}{2}a_2\left(\lambda_{110}-\lambda_{220}\right) - \frac{1}{2}b_2\left(\lambda_{121}+\lambda_{211}\right) - \frac{1}{2}c_2\left(\lambda_{122}+\lambda_{212}\right) - \frac{1}{2}d_2\left(\lambda_{123}+\lambda_{213}\right) \\
&+\frac{1}{2}a_3\left(\lambda_{110}+\lambda_{220}\right) + \frac{1}{2}b_3\left(\lambda_{121}-\lambda_{211}\right) - \frac{1}{2}c_3\left(\lambda_{122}-\lambda_{212}\right) + \frac{1}{2}d_3\left(\lambda_{123}-\lambda_{213}\right) \\
&+\frac{1}{2}a_4\left(\lambda_{100}-\lambda_{130}\right) - \frac{1}{2}b_4\left(\lambda_{201}-\lambda_{231}\right) + \frac{1}{2}c_4\left(\lambda_{202}-\lambda_{232}\right) - \frac{1}{2}d_4\left(\lambda_{023}-\lambda_{233}\right) \\
&+\frac{1}{2}a_5\left(\lambda_{010}-\lambda_{310}\right) - \frac{1}{2}b_5\left(\lambda_{021}-\lambda_{321}\right) + \frac{1}{2}c_5\left(\lambda_{022}-\lambda_{322}\right) - \frac{1}{2}d_5\left(\lambda_{023}-\lambda_{323}\right)
\end{aligned} \tag{C.16}$$

It is sufficient to write

$$\rho' = \sum_{ijk}{}' n_{ijk}\lambda_{ijk}, \tag{C.17}$$

where the sum Σ' runs only over the combinations

$$\begin{aligned}
\{ijk\} &= \{300\},\{030\},\{330\},\{010\},\{310\},\{021\},\{321\},\{022\},\{322\}, \\
&\quad \{023\},\{323\},\{100\},\{130\},\{201\},\{231\},\{202\},\{232\},\{203\}, \\
&\quad \{233\},\{110\},\{220\},\{121\},\{211\},\{122\},\{212\},\{123\},\{213\}.
\end{aligned}$$

We may use the condition that $Tr\ \rho^2 \leq 1$, together with

$$Tr\lambda_{ijk}\lambda_{i'j'k'} = \delta_{ii'}\delta_{jj'}\delta_{kk'} \tag{C.18}$$

to get

$$\begin{aligned}
Tr\rho^2 &= Tr\left(\rho' + \frac{1}{8}I\right)^2 \\
&= Tr\rho'^2 + Tr\frac{1}{64}I \\
&= Tr\left(\sum_{ijk}{}' n_{ijk}\lambda_{ijk}\right)^2 + \frac{1}{8} \\
&= \frac{1}{8} + 8\sum_{ijk}{}' \left(n_{ijk}\right)^2 \\
&\leq 1
\end{aligned}$$

so that

$$\sum_{ijk}^{'} (n_{ijk})^2 \leq \frac{7}{64}. \tag{C.19}$$

C.4 Computational Methods

Two Qubits

We wish to find the ratio of the total number of separable states to the total number of physical states. We write

$$\rho - \frac{1}{4} I = \sum_{i,j=0,3}^{'} n_{ij} \lambda_{ij}, \tag{C.20}$$

where the n_{ij} are real and the prime on the sum indicates that the term $i = j = 0$ is omitted. $\lambda_{ij} = \frac{1}{4} \sigma_i \otimes \sigma_j$. We have

$$\begin{aligned} Tr\ \rho^2 &= Tr\ \left[\frac{1}{4} I + \sum_{i,j=0,3}^{'} n_{ij} \lambda_{ij} \right]^2 \\ &= \frac{1}{4} + Tr \sum_{i,j=0,3}^{'} n_{ij} \lambda_{ij} \sum_{k,l=0,3}^{'} n_{kl} \lambda_{kl} \\ &= \frac{1}{4} + \sum_{i,j=0,3}^{'} n_{ij}^2\ Tr \lambda_{ij}^2 \\ &= \frac{1}{4} + 4 \sum_{i,j=0,3}^{'} n_{ij}^2 \\ &\leq 1 \end{aligned}$$

so

$$\sum_{ij}^{'} (n_{ij})^2 \leq \frac{3}{16}. \tag{C.21}$$

Hence we need to sample the 15-ball uniformly. Then we check for positivity, which may be done by computing the eigenvalues, and for separability, which may be done by checking the positivity of the partial transpose. To get the desired ratio, we discard those ρ that are not positive, and for the remaining ρ's just divide the separable ones by the total. The

partial transpose is given by

$$\left(n^T\right)_{ij} = -n_{ij} \quad \text{if } j = 2, \tag{C.22}$$

$$\left(n^T\right)_{ij} = n_{ij} \quad \text{if } j \neq 2. \tag{C.23}$$

This is because $\sigma_i^T = \sigma_i$ except when $i = 2$.

Two Rebits

We write the expansion for ρ using only the real generators:

$$\begin{aligned} \rho - \frac{1}{4}I &= n_{01}\lambda_{01} + n_{03}\lambda_{03} + n_{10}\lambda_{10} + n_{11}\lambda_{11} + n_{11}\lambda_{11} + n_{22}\lambda_{22} \\ &\quad + n_{30}\lambda_{30} + n_{31}\lambda_{31} + n_{33}\lambda_{33}. \end{aligned} \tag{C.24}$$

where the n_{ij} are again real. The constraint on the 9-vector $\overrightarrow{n}$ is that

$$\overrightarrow{n}^2 \leq \frac{3}{16}.$$

Now we sample the 9-ball and proceed exactly as we did for 2 qubits. The partial transpose is given by

$$\left(n^T\right)_{ij} = -n_{ij} \quad \text{if } j = 2, \tag{C.25}$$

$$\left(n^T\right)_{ij} = n_{ij} \quad \text{if } j \neq 2. \tag{C.26}$$

For this case, the only n_{ij} that is changed is n_{22}.

Two Quaterbits

We write the expansion for ρ using only the generators λ_{ijk} with

$$\begin{aligned} \{ijk\} &= \{300\}, \{030\}, \{330\}, \{010\}, \{310\}, \{021\}, \{321\}, \{022\}, \{322\}, \\ &\quad \{023\}, \{323\}, \{100\}, \{130\}, \{201\}, \{231\}, \{202\}, \{232\}, \{203\}, \\ &\quad \{233\}, \{110\}, \{220\}, \{121\}, \{211\}, \{122\}, \{212\}, \{123\}, \{213\}. \end{aligned}$$

$$\rho - \frac{1}{4}I = n_{01}\lambda_{01} + n_{03}\lambda_{03} + n_{10}\lambda_{10} + n_{11}\lambda_{11} + n_{11}\lambda_{11} + n_{22}\lambda_{22} + n_{30}\lambda_{30} + n_{31}\lambda_{31} + n_{33}\lambda_{33}. \quad \text{(C.27)}$$

where the n_{ij} are again real. The constraint on the 27-vector $\overrightarrow{n}$ is that

$$\overrightarrow{n}^2 \leq \frac{7}{64}.$$

Now we sample the 27-ball and proceed exactly as we did for 2 qubits. The partial transpose is given by

$$\left(n^T\right)_{ijk} = -n_{ijk} \quad \text{if } j = 2, \quad \text{(C.28)}$$

$$\left(n^T\right)_{ijk} = n_{ijk} \quad \text{if } j \neq 2. \quad \text{(C.29)}$$

Monte Carlo Sampling

To get an error estimate for the computation, we consider the volume V of physical states, each given by some $\vec{n}$. Let $p(\vec{n}) = 1/V$, so

$$\int_V p(\vec{n}) d\vec{n} = 1. \quad \text{(C.30)}$$

Now define the function $f(\vec{n}) = 1$, if $\vec{n}$ is separable, and $f(\vec{n}) = 0$, if not. The quantity we wish to estimate is

$$P = \langle f(\vec{n}) \rangle = \int_V f(\vec{n}) p(\vec{n}) d\vec{n}. \quad \text{(C.31)}$$

We do this by taking the finite sum

$$S_N = \frac{1}{N} \sum_{i=1}^{N} f(\vec{n}_i), \quad \text{(C.32)}$$

with the $\vec{n}_i$ each distributed uniformly, i.e., $p_i(\vec{n}_i) = p_(\vec{n}_i) 1/V$. Now note that

$$\langle S_N \rangle = \frac{1}{N} \sum_{i=1}^{N} \langle f(\vec{n}_i) \rangle = P, \quad \text{(C.33)}$$

and the variance is

$$\begin{aligned} Var(S_N) &= \left\langle (S_N - P)^2 \right\rangle \\ &= \left\langle \left[\frac{1}{N} \sum_{i=1}^{N} f(\vec{n}_i) - P \right]^2 \right\rangle \\ &= \frac{1}{N} \left(P - P^2 \right)^2 \leq \frac{1}{4N}, \end{aligned} \quad \text{(C.34)}$$

since $0 \leq P \leq 1$. Chebyshev's inequality is

$$\begin{aligned} Pr\left(|S_N - P| > a\right) &\leq \frac{1}{a^2}\left\langle (S_N - P)^2 \right\rangle \\ &\leq \frac{1}{4Na^2}. \end{aligned} \tag{C.35}$$

Setting $a = \frac{1}{2}\varepsilon^{-1/2}N^{-1/2}$, we find

$$Pr\left(|S_N - P| > \frac{1}{2}\varepsilon^{-1/2}N^{-1/2}\right) \leq \varepsilon. \tag{C.36}$$

Hence if we want the probability that we are off by more than $a = 0.01$ to be less than $\varepsilon = 0.1$, we need

$$N = \frac{1}{4\varepsilon a^2} = 2.5 \times 10^4 \text{ steps.}$$

Bibliography

[1] R. P. Feynman, "Simulating physics with computers," *International journal of theoretical physics*, vol. 21, no. 6, pp. 467–488, 1982.

[2] P. W. Shor, "Polynomial-time algorithms for prime factorization and discrete logarithms on a quantum computer," *SIAM journal on computing*, vol. 26, no. 5, pp. 1484–1509, 1997.

[3] T. D. Ladd, F. Jelezko, R. Laflamme, Y. Nakamura, C. Monroe, and J. L. OBrien, "Quantum computers," *Nature*, vol. 464, no. 7285, pp. 45–53, 2010.

[4] Z. Zhao, Y.-A. Chen, A.-N. Zhang, T. Yang, H. J. Briegel, and J.-W. Pan, "Experimental demonstration of five-photon entanglement and open-destination teleportation," *Nature*, vol. 430, no. 6995, pp. 54–58, 2004.

[5] N. K. Langford, S. Ramelow, R. Prevedel, W. J. Munro, G. J. Milburn, and A. Zeilinger, "Efficient quantum computing using coherent photon conversion," *Nature*, vol. 478, no. 7369, pp. 360–363, 2011.

[6] R. Blatt and D. Wineland, "Entangled states of trapped atomic ions," *Nature*, vol. 453, no. 7198, pp. 1008–1015, 2008.

[7] M. Neeley, R. C. Bialczak, M. Lenander, E. Lucero, M. Mariantoni, A. OConnell, D. Sank, H. Wang, M. Weides, J. Wenner, *et al.*, "Generation of three-qubit entangled states using superconducting phase qubits," *Nature*, vol. 467, no. 7315, pp. 570–573, 2010.

[8] D. Loss and D. P. DiVincenzo, "Quantum computation with quantum dots," *Phys. Rev. A*, vol. 57, pp. 120–126, Jan 1998.

[9] J. Petta, A. C. Johnson, J. Taylor, E. Laird, A. Yacoby, M. D. Lukin, C. Marcus, M. Hanson, and A. Gossard, "Coherent manipulation of coupled electron spins in semiconductor quantum dots," *Science*, vol. 309, no. 5744, pp. 2180–2184, 2005.

[10] L. K. Grover, "A fast quantum mechanical algorithm for database search," in *Proceedings of the twenty-eighth annual ACM symposium on Theory of computing*, pp. 212–219, ACM, 1996.

[11] J. K. Gamble, M. Friesen, D. Zhou, R. Joynt, and S. Coppersmith, "Two-particle quantum walks applied to the graph isomorphism problem," *Physical Review A*, vol. 81, no. 5, p. 052313, 2010.

[12] K. Rudinger, J. K. Gamble, M. Wellons, E. Bach, M. Friesen, R. Joynt, and S. Coppersmith, "Noninteracting multiparticle quantum random walks applied to the graph isomorphism problem for strongly regular graphs," *Physical Review A*, vol. 86, no. 2, p. 022334, 2012.

[13] A. Einstein, B. Podolsky, and N. Rosen, "Can quantum-mechanical description of physical reality be considered complete?," *Physical review*, vol. 47, no. 10, p. 777, 1935.

[14] J. Fei, D. Zhou, Y.-P. Shim, S. Oh, X. Hu, and M. Friesen, "Mediated gates between spin qubits," *Phys. Rev. A*, vol. 86, p. 062328, Dec 2012.

[15] S. Oh, L.-A. Wu, Y.-P. Shim, J. Fei, M. Friesen, and X. Hu, "Heisenberg spin bus as a robust transmission line for quantum-state transfer," *Phys. Rev. A*, vol. 84, p. 022330, Aug 2011.

[16] S. Oh, Y.-P. Shim, J. Fei, M. Friesen, and X. Hu, "Resonant adiabatic passage with three qubits," *Phys. Rev. A*, vol. 87, p. 022332, Feb 2013.

[17] S. Oh, Y.-P. Shim, J. Fei, M. Friesen, and X. Hu, "Effect of randomness on quantum data buses of heisenberg spin chains," *Phys. Rev. B*, vol. 85, p. 224418, Jun 2012.

[18] Y.-P. Shim, S. Oh, J. Fei, X. Hu, and M. Friesen, "Probing quantum phase transitions in a spin chain with a double quantum dot," *Phys. Rev. B*, vol. 87, p. 155405, Apr 2013.

[19] Y.-P. Shim, J. Fei, S. Oh, X. Hu, and M. Friesen, "Single-qubit gates in two steps with rotation axes in a single plane," *arXiv preprint arXiv:1303.0297*, 2013.

[20] J.-T. Hung, J. Fei, M. Friesen, and X. Hu, "Decoherence of an exchange qubit by hyperfine interaction," *Phys. Rev. B*, vol. 90, p. 045308, Jul 2014.

[21] D. Zhou, G.-W. Chern, J. Fei, and R. Joynt, "Topology of entanglement evolution of two qubits," *International Journal of Modern Physics B*, vol. 26, no. 07, 2012.

[22] R. Hanson, L. P. Kouwenhoven, J. R. Petta, S. Tarucha, and L. M. K. Vandersypen, "Spins in few-electron quantum dots," *Rev. Mod. Phys.*, vol. 79, pp. 1217–1265, Oct 2007.

[23] J. J. Morton, D. R. McCamey, M. A. Eriksson, and S. A. Lyon, "Embracing the quantum limit in silicon computing," *Nature*, vol. 479, no. 7373, pp. 345–353, 2011.

[24] J. Levy, "Universal quantum computation with spin-1/2 pairs and heisenberg exchange," *Phys. Rev. Lett.*, vol. 89, p. 147902, Sep 2002.

[25] D. P. DiVincenzo, D. Bacon, J. Kempe, G. Burkard, and K. B. Whaley, "Universal quantum computation with the exchange interaction," *Nature*, vol. 408, no. 6810, pp. 339–342, 2000.

[26] K. M. Svore, B. M. Terhal, and D. P. DiVincenzo, "Local fault-tolerant quantum computation," *Phys. Rev. A*, vol. 72, p. 022317, Aug 2005.

[27] N. Khaneja, S. J. Glaser, and R. Brockett, "Sub-riemannian geometry and time optimal control of three spin systems: Quantum gates and coherence transfer," *Phys. Rev. A*, vol. 65, p. 032301, Jan 2002.

[28] M.-H. Yung, D. W. Leung, and S. Bose, "An exact effective two-qubit gate in a chain of three spins," *Quantum Information and Computation*, vol. 4, no. 3, pp. 174–185, 2003.

[29] S. C. Benjamin and S. Bose, "Quantum computing with an always-on heisenberg interaction," *Phys. Rev. Lett.*, vol. 90, p. 247901, Jun 2003.

[30] M. A. Ruderman and C. Kittel, "Indirect exchange coupling of nuclear magnetic moments by conduction electrons," *Phys. Rev.*, vol. 96, pp. 99–102, Oct 1954.

[31] T. Kasuya, "A theory of metallic ferro-and antiferromagnetism on zener's model," *Progress of theoretical physics*, vol. 16, no. 1, pp. 45–57, 1956.

[32] K. Yosida, "Magnetic properties of cu-mn alloys," *Phys. Rev.*, vol. 106, pp. 893–898, Jun 1957.

[33] A. Mizel and D. A. Lidar, "Three- and four-body interactions in spin-based quantum computers," *Phys. Rev. Lett.*, vol. 92, p. 077903, Feb 2004.

[34] V. W. Scarola and S. Das Sarma, "Exchange gate in solid-state spin-quantum computation: The applicability of the heisenberg model," *Phys. Rev. A*, vol. 71, p. 032340, Mar 2005.

[35] C.-Y. Hsieh, A. Rene, and P. Hawrylak, "Herzberg circuit and berry's phase in chirality-based coded qubit in a triangular triple quantum dot," *Phys. Rev. B*, vol. 86, p. 115312, Sep 2012.

[36] M. D. Shulman, O. E. Dial, S. P. Harvey, H. Bluhm, V. Umansky, and A. Yacoby, "Demonstration of entanglement of electrostatically coupled singlet-triplet qubits," *Science*, vol. 336, no. 6078, pp. 202–205, 2012.

[37] R. Brunner, Y.-S. Shin, T. Obata, M. Pioro-Ladrière, T. Kubo, K. Yoshida, T. Taniyama, Y. Tokura, and S. Tarucha, "Two-qubit gate of combined single-spin rotation and interdot spin exchange in a double quantum dot," *Phys. Rev. Lett.*, vol. 107, p. 146801, Sep 2011.

[38] K. Nowack, M. Shafiei, M. Laforest, G. Prawiroatmodjo, L. Schreiber, C. Reichl, W. Wegscheider, and L. Vandersypen, "Single-shot correlations and two-qubit gate of solid-state spins," *Science*, vol. 333, no. 6047, pp. 1269–1272, 2011.

[39] L. Gaudreau, S. A. Studenikin, A. S. Sachrajda, P. Zawadzki, A. Kam, J. Lapointe, M. Korkusinski, and P. Hawrylak, "Stability diagram of a few-electron triple dot," *Phys. Rev. Lett.*, vol. 97, p. 036807, Jul 2006.

[40] E. A. Laird, J. M. Taylor, D. P. DiVincenzo, C. M. Marcus, M. P. Hanson, and A. C. Gossard, "Coherent spin manipulation in an exchange-only qubit," *Phys. Rev. B*, vol. 82, p. 075403, Aug 2010.

[41] L. Gaudreau, G. Granger, A. Kam, G. Aers, S. Studenikin, P. Zawadzki, M. Pioro-Ladriere, Z. Wasilewski, and A. Sachrajda, "Coherent control of three-spin states in a triple quantum dot," *Nature Physics*, vol. 8, no. 1, pp. 54–58, 2012.

[42] M. Friesen, A. Biswas, X. Hu, and D. Lidar, "Efficient multiqubit entanglement via a spin bus," *Phys. Rev. Lett.*, vol. 98, p. 230503, Jun 2007.

[43] C. D. Hill, "Robust controlled-not gates from almost any interaction," *Phys. Rev. Lett.*, vol. 98, p. 180501, May 2007.

[44] B. Kraus and J. I. Cirac, "Optimal creation of entanglement using a two-qubit gate," *Phys. Rev. A*, vol. 63, p. 062309, May 2001.

[45] J. Zhang, J. Vala, S. Sastry, and K. B. Whaley, "Geometric theory of nonlocal two-qubit operations," *Phys. Rev. A*, vol. 67, p. 042313, Apr 2003.

[46] Y. Makhlin, "Nonlocal properties of two-qubit gates and mixed states, and the optimization of quantum computations," *Quantum Information Processing*, vol. 1, no. 4, pp. 243–252, 2002.

[47] S. Hill and W. K. Wootters, "Entanglement of a pair of quantum bits," *Phys. Rev. Lett.*, vol. 78, pp. 5022–5025, Jun 1997.

[48] W. K. Wootters, "Entanglement of formation of an arbitrary state of two qubits," *Phys. Rev. Lett.*, vol. 80, pp. 2245–2248, Mar 1998.

[49] A. Barenco, C. H. Bennett, R. Cleve, D. P. DiVincenzo, N. Margolus, P. Shor, T. Sleator, J. A. Smolin, and H. Weinfurter, "Elementary gates for quantum computation," *Phys. Rev. A*, vol. 52, pp. 3457–3467, Nov 1995.

[50] M. A. Nielsen and I. L. Chuang, *Quantum computation and quantum information*. Cambridge university press, 2010.

[51] G. Vidal and C. M. Dawson, "Universal quantum circuit for two-qubit transformations with three controlled-not gates," *Phys. Rev. A*, vol. 69, p. 010301, Jan 2004.

[52] M. J. Bremner, C. M. Dawson, J. L. Dodd, A. Gilchrist, A. W. Harrow, D. Mortimer, M. A. Nielsen, and T. J. Osborne, "Practical scheme for quantum computation with any two-qubit entangling gate," *Phys. Rev. Lett.*, vol. 89, p. 247902, Nov 2002.

[53] M. A. Nielsen, "Conditions for a class of entanglement transformations," *Phys. Rev. Lett.*, vol. 83, pp. 436–439, Jul 1999.

[54] J. Elzerman, R. Hanson, L. W. Van Beveren, L. Vandersypen, and L. Kouwenhoven, "Excited-state spectroscopy on a nearly closed quantum dot via charge detection," *Applied physics letters*, vol. 84, no. 23, pp. 4617–4619, 2004.

[55] J. Zhang, J. Vala, S. Sastry, and K. B. Whaley, "Minimum construction of two-qubit quantum operations," *Phys. Rev. Lett.*, vol. 93, p. 020502, Jul 2004.

[56] Y.-P. Shim, S. Oh, X. Hu, and M. Friesen, "Controllable anisotropic exchange coupling between spin qubits in quantum dots," *Phys. Rev. Lett.*, vol. 106, p. 180503, May 2011.

[57] W. Dür, G. Vidal, and J. I. Cirac, "Three qubits can be entangled in two inequivalent ways," *Phys. Rev. A*, vol. 62, p. 062314, Nov 2000.

[58] D. M. Greenberger, M. A. Horne, A. Shimony, and A. Zeilinger, "Bells theorem without inequalities," *Am. J. Phys*, vol. 58, no. 12, pp. 1131–1143, 1990.

[59] N. D. Mermin, *Quantum computer science: an introduction.* Cambridge University Press, 2007.

[60] A. Galiautdinov and J. M. Martinis, "Maximally entangling tripartite protocols for josephson phase qubits," *Phys. Rev. A*, vol. 78, p. 010305, Jul 2008.

[61] H. J. Briegel and R. Raussendorf, "Persistent entanglement in arrays of interacting particles," *Phys. Rev. Lett.*, vol. 86, pp. 910–913, Jan 2001.

[62] R. Raussendorf and H. J. Briegel, "A one-way quantum computer," *Phys. Rev. Lett.*, vol. 86, pp. 5188–5191, May 2001.

[63] V. V. Shende and I. L. Markov, "On the cnot-cost of toffoli gates," *Quantum Information & Computation*, vol. 9, no. 5, pp. 461–486, 2009.

[64] D. P. DiVincenzo and J. Smolin, "Results on two-bit gate design for quantum computers," *arXiv preprint cond-mat/9409111*, 1994.

[65] F. Bodoky and M. Blaauboer, "Production of multipartite entanglement for electron spins in quantum dots," *Phys. Rev. A*, vol. 76, p. 052309, Nov 2007.

[66] R. Laflamme, C. Miquel, J. Paz, and W. Zurek, "Perfect quantum error correcting code," *Phys. Rev. Lett.*, vol. 77, pp. 198–201, Jul 1996.

[67] P. W. Shor, "Scheme for reducing decoherence in quantum computer memory," *Phys. Rev. A*, vol. 52, pp. R2493–R2496, Oct 1995.

[68] D. Vion, A. Aassime, A. Cottet, P. Joyez, H. Pothier, C. Urbina, D. Esteve, and M. H. Devoret, "Manipulating the quantum state of an electrical circuit," *Science*, vol. 296, no. 5569, pp. 886–889, 2002.

[69] Y. Makhlin and A. Shnirman, "Dephasing of solid-state qubits at optimal points," *Phys. Rev. Lett.*, vol. 92, p. 178301, Apr 2004.

[70] W. Coish and D. Loss, "Singlet-triplet decoherence due to nuclear spins in a double quantum dot," *Phys. Rev. B*, vol. 72, p. 125337, Sep 2005.

[71] X. Hu and S. Das Sarma, "Charge-fluctuation-induced dephasing of exchange-coupled spin qubits," *Phys. Rev. Lett.*, vol. 96, p. 100501, Mar 2006.

[72] O. E. Dial, M. D. Shulman, S. P. Harvey, H. Bluhm, V. Umansky, and A. Yacoby, "Charge noise spectroscopy using coherent exchange oscillations in a singlet-triplet qubit," *Phys. Rev. Lett.*, vol. 110, p. 146804, Apr 2013.

[73] J. Medford, J. Beil, J. Taylor, S. Bartlett, A. Doherty, E. Rashba, D. DiVincenzo, H. Lu, A. Gossard, and C. M. Marcus, "Self-consistent measurement and state tomography of an exchange-only spin qubit," *Nature nanotechnology*, vol. 8, no. 9, pp. 654–659, 2013.

[74] J. M. Taylor, V. Srinivasa, and J. Medford, "Electrically protected resonant exchange qubits in triple quantum dots," *Phys. Rev. Lett.*, vol. 111, p. 050502, Jul 2013.

[75] I. P. Gimenez, C.-Y. Hsieh, M. Korkusinski, and P. Hawrylak, "Charged-impurity-induced dephasing of a voltage-controlled coded qubit based on electron spin in a triple quantum dot," *Phys. Rev. B*, vol. 79, p. 205311, May 2009.

[76] C.-Y. Hsieh, Y.-P. Shim, and P. Hawrylak, "Theory of electronic properties and quantum spin blockade in a gated linear triple quantum dot with one electron spin each," *Phys. Rev. B*, vol. 85, p. 085309, Feb 2012.

[77] J. Taylor, H.-A. Engel, W. Dür, A. Yacoby, C. Marcus, P. Zoller, and M. Lukin, "Fault-tolerant architecture for quantum computation using electrically controlled semiconductor spins," *Nature Physics*, vol. 1, no. 3, pp. 177–183, 2005.

[78] S. Mehl and D. P. DiVincenzo, "Noise analysis of qubits implemented in triple quantum dot systems in a davies master equation approach," *Phys. Rev. B*, vol. 87, p. 195309, May 2013.

[79] G. T. Hickman, X. Wang, J. P. Kestner, and S. Das Sarma, "Dynamically corrected gates for an exchange-only qubit," *Phys. Rev. B*, vol. 88, p. 161303, Oct 2013.

[80] R. Hanson and G. Burkard, "Universal set of quantum gates for double-dot spin qubits with fixed interdot coupling," *Phys. Rev. Lett.*, vol. 98, p. 050502, Jan 2007.

[81] J. M. Taylor, J. R. Petta, A. C. Johnson, A. Yacoby, C. M. Marcus, and M. D. Lukin, "Relaxation, dephasing, and quantum control of electron spins in double quantum dots," *Phys. Rev. B*, vol. 76, p. 035315, Jul 2007.

[82] L. V. C. Assali, H. M. Petrilli, R. B. Capaz, B. Koiller, X. Hu, and S. Das Sarma, "Hyperfine interactions in silicon quantum dots," *Phys. Rev. B*, vol. 83, p. 165301, Apr 2011.

[83] T. Hayashi, T. Fujisawa, H. D. Cheong, Y. H. Jeong, and Y. Hirayama, "Coherent manipulation of electronic states in a double quantum dot," *Phys. Rev. Lett.*, vol. 91, p. 226804, Nov 2003.

[84] K. D. Petersson, J. R. Petta, H. Lu, and A. C. Gossard, "Quantum coherence in a one-electron semiconductor charge qubit," *Phys. Rev. Lett.*, vol. 105, p. 246804, Dec 2010.

[85] Z. Shi, C. B. Simmons, J. R. Prance, J. K. Gamble, T. S. Koh, Y.-P. Shim, X. Hu, D. E. Savage, M. G. Lagally, M. A. Eriksson, M. Friesen, and S. N. Coppersmith, "Fast hybrid silicon double-quantum-dot qubit," *Phys. Rev. Lett.*, vol. 108, p. 140503, Apr 2012.

[86] S. D. Barrett and C. H. W. Barnes, "Double-occupation errors induced by orbital dephasing in exchange-interaction quantum gates," *Phys. Rev. B*, vol. 66, p. 125318, Sep 2002.

[87] "Open science grid." `http://www.opensciencegrid.org`.

[88] Z. Shi, C. Simmons, D. R. Ward, J. Prance, X. Wu, T. S. Koh, J. K. Gamble, D. Savage, M. Lagally, M. Friesen, S. Coppersmith, and E. MA, "Fast coherent manipulation of three-electron states in a double quantum dot," *Nature communications*, vol. 5, 2014.

[89] D. Kim, Z. Shi, C. Simmons, D. Ward, J. Prance, T. S. Koh, J. K. Gamble, D. Savage, M. Lagally, M. Friesen, S. Coppersmith, and E. MA, "Quantum control and process tomography of a semiconductor quantum dot hybrid qubit," *Nature*, vol. 511, no. 13407, p. 7074, 2014.

[90] J. Medford, J. Beil, J. M. Taylor, E. I. Rashba, H. Lu, A. C. Gossard, and C. M. Marcus, "Quantum-dot-based resonant exchange qubit," *Phys. Rev. Lett.*, vol. 111, p. 050501, Jul 2013.

[91] K. Życzkowski, P. Horodecki, A. Sanpera, and M. Lewenstein, "Volume of the set of separable states," *Phys. Rev. A*, vol. 58, pp. 883–892, Aug 1998.

[92] P. B. Slater and C. F. Dunkl, "Moment-based evidence for simple rational-valued hilbert–schmidt generic 2× 2 separability probabilities," *Journal of Physics A: Mathematical and Theoretical*, vol. 45, no. 9, p. 095305, 2012.

[93] P. B. Slater, "A concise formula for generalized two-qubit hilbert–schmidt separability probabilities," *Journal of Physics A: Mathematical and Theoretical*, vol. 46, no. 44, p. 445302, 2013.

[94] W. Y. Chen, Q.-H. Hou, and Y.-P. Mu, "The extended zeilberger algorithm with parameters," *Journal of Symbolic Computation*, vol. 47, no. 6, pp. 643–654, 2012.

[95] A. Peres, "Separability criterion for density matrices," *Phys. Rev. Lett.*, vol. 77, pp. 1413–1415, Aug 1996.

[96] M. Horodecki, P. Horodecki, and R. Horodecki, "Separability of mixed states: necessary and sufficient conditions," *Physics Letters A*, vol. 223, no. 1, pp. 1–8, 1996.

[97] M. S. Byrd and N. Khaneja, "Characterization of the positivity of the density matrix in terms of the coherence vector representation," *Phys. Rev. A*, vol. 68, p. 062322, Dec 2003.

[98] A. Andai, "Volume of the quantum mechanical state space," *Journal of Physics A: Mathematical and General*, vol. 39, no. 44, p. 13641, 2006.

[99] G. S. Watson, G. S. Watson, M. Statistiker, G. S. Watson, P. Statisticien, and G. S. Watson, *Statistics on spheres*, vol. 6. Wiley New York, 1983.

[100] S. L. Adler, *Quaternionic quantum mechanics and quantum fields*. Oxford Univ. Press, 1995.

[101] K. M. Weiss, J. M. Elzerman, Y. L. Delley, J. Miguel-Sanchez, and A. Imamoğlu, "Coherent two-electron spin qubits in an optically active pair of coupled ingaas quantum dots," *Phys. Rev. Lett.*, vol. 109, p. 107401, Sep 2012.

[102] K. Weiss, J. Miguel-Sanchez, and J. Elzerman, "Magnetically tunable singlet-triplet spin qubit in a four-electron ingaas coupled quantum dot," *Scientific reports*, vol. 3, 2013.

[103] P. A. M. Dirac, "The principles of quantum mechanics," 1930.

[104] R. P. Feynman, *Statistical mechanics*. Westview Press, Boulder, CO, 1998.

[105] L. C. W. Dixon and G. P. Szegö, *Towards global optimisation 2*. North-Holland Amsterdam, 1978.

[106] R. Horst and P. M. Pardalos, *Handbook of global optimization*, vol. 1. Kluwer Academic, Dordrecht, 1995.

[107] J. A. Nelder and R. Mead, "A simplex method for function minimization," *The computer journal*, vol. 7, no. 4, pp. 308–313, 1965.

[108] J. Schrieffer and P. Wolff, "Relation between the anderson and kondo hamiltonians," *Phys. Rev.*, vol. 149, pp. 491–492, Sep 1966.

[109] M. A. Nielsen, "A simple formula for the average gate fidelity of a quantum dynamical operation," *Physics Letters A*, vol. 303, no. 4, pp. 249–252, 2002.